AN INVESTIGATION INTO THE ANTI-CANCER MECHANISM OF GARLIC-RELATED ORGANOSULFUR COMPOUNDS

Thesis presented by

MUNEERAH SMITH

In fulfilment of the requirements for the

MASTERS DEGREE

in

Medical Biochemistry

Supervisor: Prof. M. Iqbal Parker

Co-supervisor: Dr. Catherine H. Kaschula

Faculty of Health sciences, University of Cape Town

February 2014

DECALARATION

I, Muneerah Smith, hereby declare that the work on which this thesis is based is my original work (except where acknowledgements indicate otherwise) and that neither the whole work not any part of it has been, is being, or is to be submitted for another degree in this or any other university.

I empower the University of Cape Town to reproduce for the purpose of research either the whole or any portion of the contents in any manner whatsoever.

……

February 2014

Acknowledgements

I would like to acknowledge the following individuals:

My supervisor, Prof. M. Iqbal Parker, for his excellent supervision, guidance, support and critical proof reading my thesis.

My co-supervisor, Dr. Catherine H. Kaschula, for her excellent supervision, guidance, support and critical proof reading my thesis.

Prof. Roger Hunter for his contributions to the project, especially with regards to the Chemistry sections.

Dr. Andriy Garfov from Finland for developing the solubilisation formulation for the *in vivo* studies.

Ms. Zenaria Abbas and Ms. Arielle Rowe for their daily assistance and ensuring that all reagents and equipment were available for my experiments.

To all my colleagues and friends at ICGEB and in the Medical Biochemistry Department, for encouragement and support.

Prof. E. Sturrock for use of his laboratory equipment.

Thank you to my funders; the National Research Foundation (NRF) and UCT funding.

A special thanks to my loving and encouraging Mother, Father, brother and sister.

List of abbreviations:

AEC	-	Animal Ethics Committee
BSA	-	Bovine Serum Albumin
cCMP	-	2',3'-Cytidine Cyclic Monophosphate
CO_2	-	Carbon Dioxide
CV	-	Coefficient of Variance
DTNB	-	5'5'-dithio-bis(2-nitrobenzoic acid)
DMSO	-	Dimethyl Sulfoxide
DOX	-	Doxorubicin
DAS	-	Diallyl Sulfide
DADS	-	Diallyl Disulfide
DATS	-	Diallyl Trisulfide
DAS4	-	Diallyl Tetrasulfide
DCF	-	7'-Dichloroflouroscin
DCFH-DA	-	2',7'-Dichloroflouricin Diacetate
DMEM	-	Dulbecco's Minimal Eagles Media
DNA	-	Deoxyribonucleic Acid
DPDS	-	Diproyl Disulfide
DTT	-	Dithiothreitol
ELISA	-	Enzyme-Linked Immune Sorbent Assay
EtOAc	-	Ethyl Acetate
EDTA	-	Ethylene-diamine-tetra-acetic Acid
ER	-	Endoplasmic Reticulum

FACS	-	Fluorescence-Activated Cell Sorting
FCS	-	Foetal Calf Serum
FL	-	Femtoliters
Δ G	-	Gibb's Free Energy
g/dl	-	Grams Per Decilitre
GAPDH	-	Glyceraldehyde 3-Phosphate Dehydrogenase
GR	-	Glutathione Reductase
GSH	-	L-Glutathione
GSSG	-	L-Glutathione Oxidised Disodium Salt
GST	-	Glutathione *S*-Transferase
× g	-	Gravitation Force
H_2O_2	-	Hydrogen Peroxide
HRP	-	Horse Radish Peroxidase
hSOD	-	Human Superoxide Dismutase
IC_{50}	-	Concentration of Compound Required to Kill 50 % of Cells
IHC	-	Immunohistochemistry
IP	-	Intraperitoneal
JNK	-	c-Jun N-terminal Kinase
$kJ.mol^{-1}$	-	Kilojoules Per Mole
KRB	-	Kreb's Ringer Buffer
MALDI-TOF-MS	-	Matric-Assisted Laser Desorption Ionisation Time of Flight Mass Spectrometry
MAPK	-	Mitogen-Activated Protein Kinase

Mg	-	Milligrams
mg/kg	-	Milligrams per Kilogram
MHz	-	Megahertz
µg	-	Micrograms
µl	-	Microlitre
µM	-	Micromolar
ml	-	Millilitres
mm	-	Millimetres
mM	-	Millimolar
mmol	-	Millimole
MTT	-	Thaizolyl Blue Tetrazolium Bromide
mV	-	Millivolts
nm	-	Nanometers
NAC	-	*N*-Acetyl Cysteine
NADH	-	Nicotinamide Adenine Dinucleotide (Reduced)
NADPH	-	Nicotinamide Adenine Dinucleotide Phosphate (Reduced)
NCI	-	National Cancer Institiute
NFκB	-	Nuclear Factor Kappa-light-chain-enhancer of activated B cells
NMR	-	Nuclear Magnetic Resonance
NR	-	Native RNase A
NS	-	No Significance
OSC	-	Organosulfur Compound
QC	-	Quality control

PBS	-	Phosphate Buffer Saline
PDI	-	Protein Disulfide Isomerase
PEG	-	Polyethylene Glycol
PI	-	Propidium Iodide
POD	-	Peroxidase
Ppm	-	Parts Per Million
RNase	-	Ribonuclease
ROS	-	Reactive Oxygen Species
Rpm	-	Rotations Per Minute
R-PDI	-	Reduced RNase A in the presence of PDI
RR	-	Reduced RNase A
SAMC	-	*S*-allylmercaptocysteine
± SD	-	Standard Deviation
SDS	-	Sodium Dodecyl Sulfate
SLS	-	Sodium Lauryl Sulfate
S-MMTS	-	*S*-methylmethane Thiosulfonate
THF	-	Tetrahydrafuran
TLC	-	Thin Layer Chromatography
UPR	-	Unfolded Protein Response
V	-	Volts
VCR	-	Vincristine
VLB	-	Vinblastine
WHO	-	World Health Organisation

Table of contents:

Abstract

Crushed garlic contains organosulfur compounds (OSC), which are reported to have cancer chemotherapeutic properties both *in vitro* and *in vivo*. A library of 15 organosulfur analogues were obtained as mechanistic probes in WHCO1 oesophageal cancer cells. Structure-activity studies showed a positive correlation between the anti-proliferative-IC_{50} of disulfides and the relative stability of their anion leaving groups, as assessed through resonance and quantified by predictive pK_a-values.

Compounds **t-PMB** (IC_{50} = 15 μM), a thiosulfonate, and **200** (IC_{50} = 10 μM), a diallyl disulfide (DADS) analogue, were selected for further mechanistic evaluation and showed to induce both G_2/M cell-cycle arrest and apoptosis in WHCO1 cells. Although treatment with **t-PMB**, but not **200**, resulted in increased ROS levels, treatment with ROS inhibitors showed that ROS production was not important for **t-PMB**-induced WHCO1 cell-death.

In vivo studies showed that 30 mg/kg **t-PMB** daily and 20 mg/kg **200** every second day significantly reduced A375 human melanoma tumour growth in nude mice within the first 16 days only, although **t-PMB**-treated mice experienced abdominal swelling side effects. Nude mice with the WHCO1 oesophageal cancer xenograft treated with 10 mg/kg **200** daily showed a significant reduction in tumour size up to 7 days.

Using immunohistochemistry, we observed co-localisation of **DP** and protein disulfide isomerase (PDI) in KYSE-180 cells, and furthermore found that OSC inhibited PDIs enzymatic activity, suggesting that PDI may be a protein target for OSC in cancer cells.

Chapter 1

Introduction

1.1. Cancer

Cancer is a heterogenous disease that can form almost anywhere in the body. The disease has a complex nature, where a cell or cells require a number of insults before it can progress to a state of malignancy. There are several characteristics which mark a cell as one that is cancerous; these characteristics have been termed the six hallmarks of cancer by Hanahan *et al*. (2011). The hallmarks provide a logical framework for understanding the disease and include: sustained proliferative signalling, evasion of growth suppressors, activation of invasion and metastasis, enabled replicative immortality, angiogenesis and resistance to cell death (Figure 1.1) (Hanahan *et al*. 2000; Hanahan & Weinberg 2011).

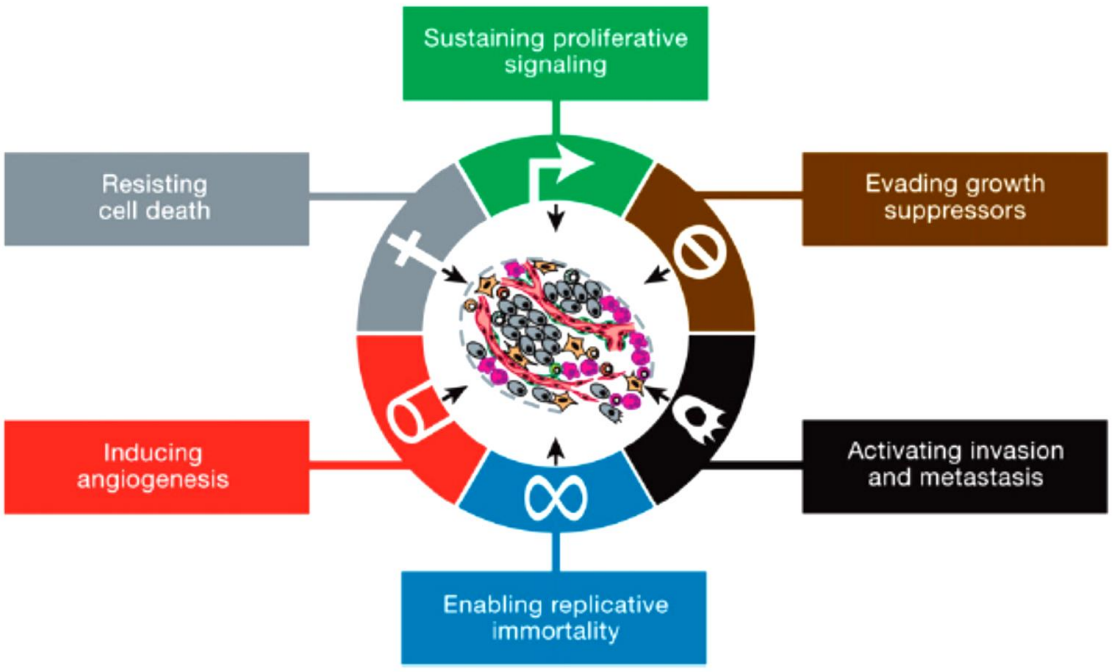

Figure 1.1. The Six Hallmarks of Cancer. The six hallmarks of cancer comprise of altered biological properties acquired by the cell during the development of human tumours. These six hallmarks include; resistance to cell death, sustained proliferative signalling, evasion of growth suppressors , evasion of metastasis, enabled replicative immortality and induction of angiogenesis (Hanahan & Weinberg 2011).

The prevalence of the disease is determined by both environmental and genetic factors affecting an individual (Fearnhead *et al*. 2002; Zbar *et al*. 1995), and furthermore, certain cancers have been shown to have gender specificity (Van Rensburg *et al*. 1985; Shaaban *et al*. 2012). In January 2013, the World Health Organisation (WHO) confirmed cancer to be the leading cause of human death world-wide (7.6 million deaths) and it is estimated that this number will rise to 13.1 million deaths by 2030.

1.1.1. Oesophageal cancer

In 2013, the WHO reported oesophageal cancer to be the 9th most commonly diagnosed cancer world-wide, and the 7th most lethal cancer. The two main types of oesophageal cancers include squamous cell carcinoma and adenocarcinoma. Squamous cell carcinoma usually occurs in the middle to upper third part of the oesophagus, and is associated with environmental insults such as alcohol intake and tobacco smoking, whilst adenocarcinoma, which occurs in the distal oesophagus, is usually associated with gastro-oesophageal reflux (Enzinger & Mayer 2003).

Since 1930, there has been an alarming increase in oesophageal cancer cases in the South African population, (Rose & McGlashan 1975; Jemal *et al*. 2011) (Figure 1.2). Squamous cell oesophageal cancer is most prevalent amongst South African black males, and mainly occurs in the sixth decade of life (Van Rensburg *et al*. 1985). Both environmental and genetic factors have been associated with squamous cell oesophageal cancer, where genetic profiling studies have shown that the deletion of GSTT2B, a polymorphic variant of the glutathione *S*-transferase gene, may have a protective effect on the risk of oesophageal squamous cell carcinoma in mixed ancestry South African populations (Matejcic *et al*. 2011). A number of environmental factors have been implicated in the increased risk of oesophageal cancer, which includes alcohol, tobacco smoking, carcinogenic exposure as well as diet. Previously, it was shown that in certain geographical regions where the staple diet includes sorghum, cassava, millet, yams, peanuts or a combination of these, the incidence of oesophageal cancer was significantly lower than in regions where corn or wheat was consumed (van Rensburg 1981). Other parts of the world with high incidences of squamous cell oesophageal cancer include Northern Iran, Soviet Central Russia, as well as China. Major risk factors for squamous cell oesophageal cancer in these areas are not well understood, but are thought to include poor nutrient intake as well as the drinking of beverages at high temperatures (Wu *et al*. 2009; F Islami *et al*. 2009a; F Islami *et al*. 2009b).

1.2. Cancer treatments

Due to its complex nature and an incomplete understanding of the disease, developing a cure for cancer is a great challenge. A number of therapies have been developed thus far which include various forms of chemotherapy, radiation, immunotherapy, surgery and combinations thereof (Miller *et al*. 1981). More recent approaches to cancer treatment is a targeted approach which includes nano-particles for drug delivery (Brigger *et al*. 2012; Peer *et al*. 2007) as well as those that target specific cell regulatory proteins (Lowe *et al*. 1994; Semenza 2003).

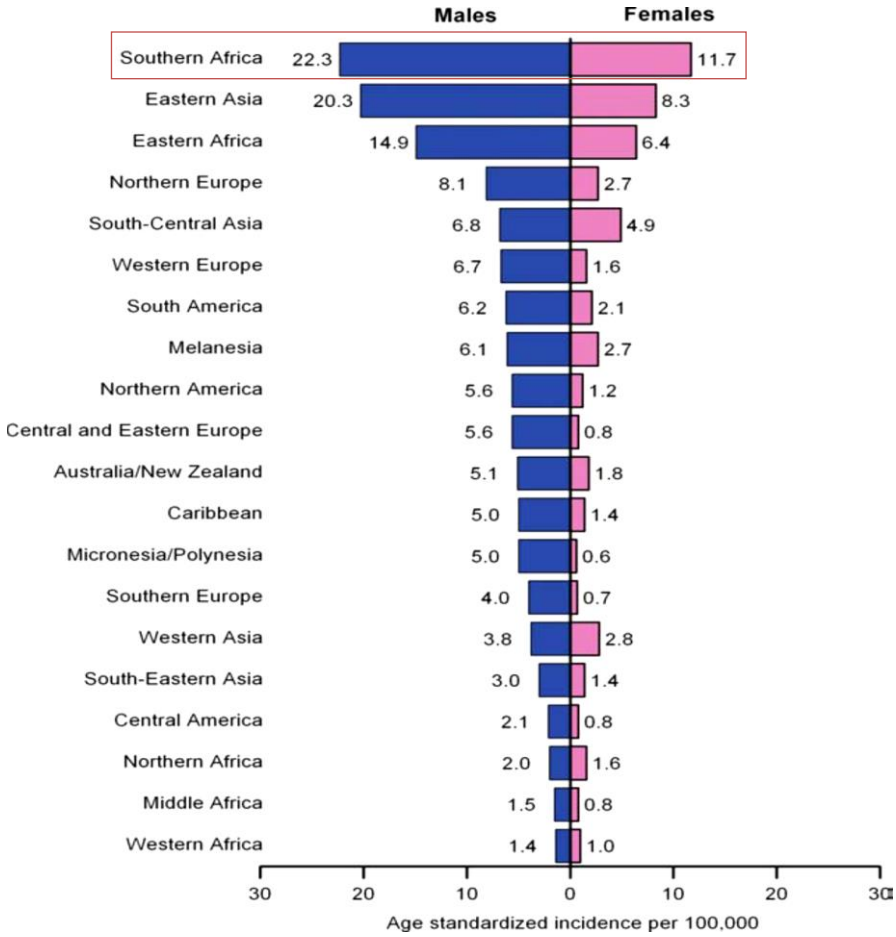

Figure 1.2. Aged standardised oesophageal cancer incidence rates by sex and world area, with the statistics for South African males and females boxed in red. Source: GLOBOCAN 2008.

Drugs currently used to inhibit oesophageal tumour growth include fluorouracil, the taxanes (Paclitaxel, Docetaxel), the natural alkaloid camptothecin from which irinotecan is derived, and cisplatin. It has been demonstrated that chemoresistance to 5-fluorouracil and cisplatin in oesophageal cancer patients may occur through the increased expression of miR-200

(Hamano *et al*. 2011). Furthermore, increased expression of the Multidrug Resistance Protein 2 (MRP2) has been shown in the tissue samples of patients resistant to neo-adjuvant chemotherapy including; 5-fluorouracil, doxorubicin and cisplatin (Vermorken *et al*. 2007). Combinations of chemotherapy and radiotherapy have also been shown to be effective, but side-effects of this treatment is high, particularly regarding cytotoxicity to non-cancer cells (Ilson & Kelson 1993). It is clear that new therapies with increased potency and reduced side-effects are needed.

1.3. Anti-cancer compounds from natural sources

Compounds derived from natural sources have been used in traditional medicines for many years (Nobili *et al*. 2009). Epidemiologic studies have shown that an inverse relationship exists between the prevalence of many cancer types and the consumption of fresh fruits and vegetables (Surh 2003). Furthermore, throughout history plant materials have been used in the treatment of many cancer types (Graham *et al*. 2000), indicating the potential importance of natural products as anti-cancer agents. The United States National Cancer institute (NCI) therefore initiated an extensive plant collection programme in 1960 in the hopes of finding plant materials that display anti-cancer activity, which resulted in the discovery of many novel chemotypes including the taxanes and camptothecins. Since then there have been numerous additional reports in the literature of the isolation and identification of novel anti-cancer agents from nature.

Natural compounds are the source of about 60 % of all new drugs that have been developed, and about 67 % of the drugs used for chemotherapy are natural products thereof (Cragg *et al*. 1997). The first natural anti-cancer agents to advance to clinical use were the vinca alkaloids; vinblastine (VLB) and vincristine (VCR) (Figure 1.3) isolated from a plant called the Madagascar periwinkle (*Catharanthus roseus*) (Cragg & Newman 2005). Another relatively potent anti-cancer agent is Paclitaxel (taxol®) (Figure 1.3) (Kingston *et al*. 2005), which was initially isolated from the bark of the Pacific yew, *Taxus brevifolia*, and is used in the treatment of breast, ovarian and non-small cell lung cancer. A great deal of research has gone into understanding the potential of natural compounds as anti-cancer agents. These compounds typically combat some of the hallmarks of cancer to induce cell-cycle arrest, apoptosis and inhibiting angiogenesis. Examples of such anti-cancer phytochemicals, and/or their relative natural source are shown in Figure 1.3 (Surh 2003).

Anti-cancer phytochemicals	Compound	Anti-cancer phytochemicals	Compound
Curcumin (Tumeric)	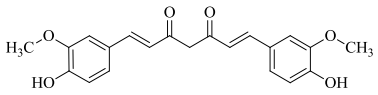	Resveratol (Grapes)	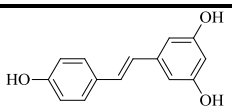
Capsaicin (Chilli peppers)	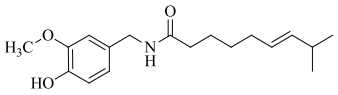	Caffeic acid phenethyl ester (Honey)	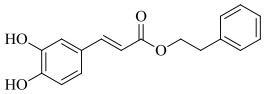
[6]-Gingerol (Ginger)	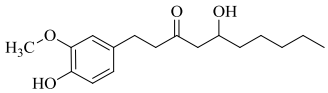	Diallyl Disulfide (Garlic)	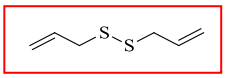
Epigallocatechin-3-gallate (Green Tea)	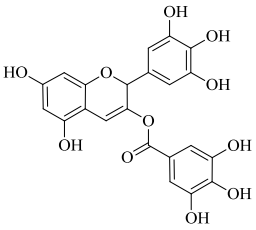	Indol-3-carbinol (Cabbage)	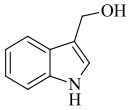
Genistein (Soybeans)	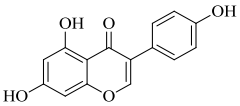	Sulphoraphane (Broccoli)	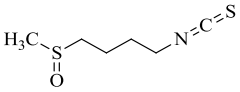
Paclitaxel (Bark of Pacific Yew)	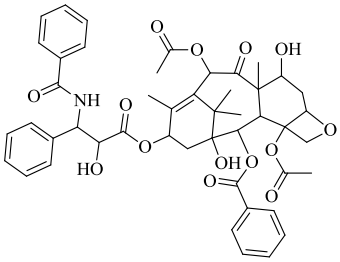	Vincristine (Madagascar Periwinkle)	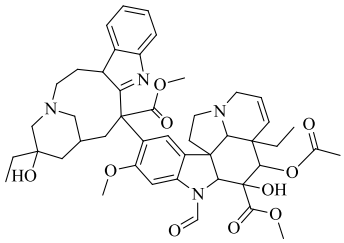
Honokiol (Magnolia)	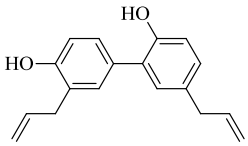	Zerumbone (Subtropical ginger)	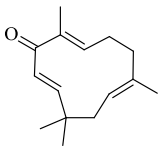
Withaferin A (Withania Somnifera)	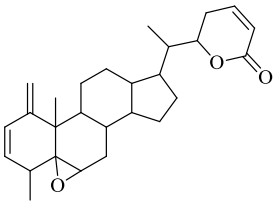		
Lycopene (Tomatoes)	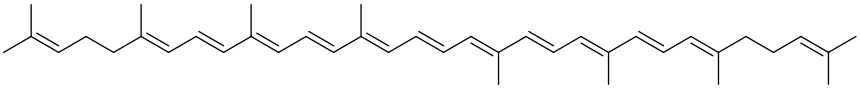		

Figure 1.3. The natural sources of anti-cancer phytochemicals shown with their respective chemical structures. The garlic-derived organosulfur compound, diallyl disulfide (DADS), is boxed in red (Surh 2003; Bai *et al.* 2003; Marukami *et al.* 2002; Bargagna-Mohan *et al.* 2007).

1.4. Garlic-derived anti-cancer compounds

Garlic (*Allium sativum*) has been used as a folk remedy for many centuries, for illnesses including heart disease, high blood pressure and cancer (Borek 2006; Ried *et al*. 2008; Reinhart *et al*. 2008). The active principles of garlic, which were shown to be lipophilic or hydrophillic, have previously been identified to be various organosulfur compounds (OSC) found in crushed cloves. Whole garlic contains alliin (*S*-allylcysteine sulfoxide), which is converted to allicin in the presence of an enzyme alliinase only when the clove is crushed or damaged (Figure 1.4A). Allicin, which is reported to be active as both an antimicrobial (Ankri & Mirelman 1999) and antifungal agent (Davis 2005), is unstable and rearranges readily to form an array of second generation OSCs, of which the major lipophilic components are diallyl sulfide (DAS), diallyl disulfide (DADS), diallyl trisulfide (DATS) and *E/Z* ajoene ((*E/Z*) 4,5,9-trithiododeca-1,6,11-triene 9 oxide) (Figure 1.4B) (Kaschula *et al*. 2011). The hydophillic second generation OSC's include *S*-allylmercaptocysteine (SAMC) Figure 1.6) and *S*-allyl cysteine (SAC) (Table 1.4). These second generation molecules as well as allicin, are reported to have both chemotherapeutic and chemopreventive properties (Taylor *et al*. 2006).

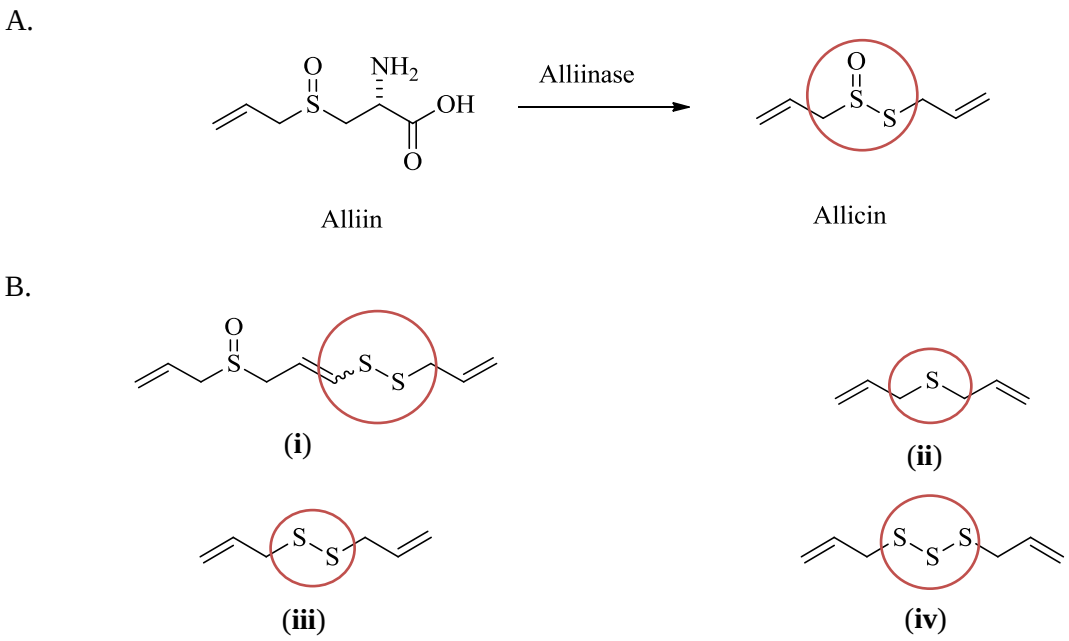

Figure 1.4. The chemical conversion of alliin to allicin by the enzyme alliinase (**A**) and the chemical structures of the secondary organosulfur compounds (**B**) as rearrangement products of allicin; (**i**) *E/Z* ajoene, (**ii**) diallyl sulfide (DAS), (**iii**) diallyl disulfide (DADS) and (**iv**) diallyl trisulfide (DATS) are presented. The sulfide or polysulfide pharmacophore (encircled in red) is proposed to be the key player involved in the anti-cancer activity of the OSC.

The composition and concentration of the various OSC from garlic differ depending on the type of garlic, as well as the preparation and the age of the extract. Allicin, which is found only in fresh extracts, is reported to at a concentration of 2.5-3.1 $mg.g^{-1}$ in garlic (Block *et al*., 1986; Kalra & Shukla, 2006). The composition and concentration of second generation OSC reported for extracts isolated through steam distillation and oil extraction varies, and is reported to be 20-240 $mg.g^{-1}$ for DAS, 280-900 $mg.g^{-1}$ for DADS, 40-200 $mg.g^{-1}$ for DATS and 130-480 for E/Z ajoene (Lee *et al*., 2003; Laakso *et al*. 1989; Kimbaris *et al*. 2006; Naznin *et al*. 2008). Other OSC, to include the water-soluble *S*-allyl cysteine and *S*-allylmercaptocysteine, are found to be at relatively low concentrations of $< 50\ \mu g.g^{-1}$.

1.4.1. Chemopreventative properties of garlic OSC

The inverse relationship between garlic consumption and occurrence of various cancers has been well documented over the last few decades, where the first case-control studies showed a negative correlation between the consumption of *Allium* vegetables and the occurrence of gastric cancer (You *et al*. 1989; Buiatti *et al*. 1989). Since then, additional documentations of case control studies were reported for Europe, the United States, South America and China (Fleischauer *et al*. 2001).

After having observed the inverse relationship between garlic consumption and occurrence of various cancers, a number of studies were performed to investigate the chemopreventative effects of garlic-derived OSCs. Initial studies by Wattenberg *et al*. (1989) showed a 90 % reduction in *N*-nitrosodiethylamine-induced forestomach tumor formation when 0.2 mmol DADS was administered 48- and 96-hours before *N*-nitrosodiethylamine. It was also observed that 200 mg/kg DADS and *S*-allyl cysteine administered via gavage 3 hours prior to 1,2-dimethylhydrazine (DMH) injection significantly inhibited colonic nuclear damage in female C57B1/6J mice (Sumiyoshi & Wargovich, 1990). More recent studies have shown that the garlic OSCs may induce their chemopreventative effects by modulating the concentration of metabolic enzymes. It is well known that many carcinogens require metabolic activation by the cytochrome P450 phase I enzymes, and that subsequent inactivation occurs through the phase II enzymes including glutathione transferases. The mechanism by which the OSC induce their chemopreventative activity has been shown to occur through competitive inhibition of the P450-dependent monooxygenases (phase I enzymes), as well as increasing the expression of phase II enzymes (Shukla *et al*. 2007;

Herman-Antosiewicz *et al*. 2007), which together not only prevents carcinogenic activation, but also increases its eradication.

1.4.2 Structure-activity insights into the *in vitro* anti-cancer activity of garlic OSC

OSC from garlic are reported to inhibit the proliferation of cancer cells both *in vitro* and *in vivo*, and this activity is proposed to be related to the presence of the disulfide or polysulfide functional group, encircled in red in Figure 1.4. All the OSCs displayed in Table 1.1 are reported to inhibit cancer cell proliferation with IC_{50}-values in the micro molar (μM) range.

Table 1.1. The IC_{50}'s of the garlic-derived OSC; *E/Z* ajoene, DATS, DADS and DAS, at inhibiting cell proliferation on various cancer cell-lines, where the IC_{50} is defined as the compound concentration required to inhibit the growth of 50 % of the cells.

Compound	Cell-line	Cell type	IC_{50} (μM)	Reference
***E/Z* Ajoene**	BJA-B	Burkitt lymphoma	12	Scharfenberg *et al*., 1990
	HL60	Pyromyeloleukemic cells	5.2	Li *et al*., 2002
	KB	Nasopharyngeal carcinoma	15.8	
	HT-2	Human colon	19	Taylor *et al*., 2006
	A549	Human lung	41	
	MDA-MB-231	Human mammary	7	
	SKBR-3	Human mammary	19	
	PANC-1	Human pancreatic	38	
DATS	HCT-15	Human colon	11.5	Hosono *et al*., 2005
	DLD-1	Human colon	13.3	
	PC3	Human Prostate	22	Dong Xiao *et al*., 2005
	PC3	Human Prostate	72	Chen *et al*., 2012
	H358	Human lung cancer	20	Xiao *et al*., 2008
DADS	COLO205	Human colon	22.47	Yang *et al*., 2009
	SW-480	Colon cancer	56	Danhua Xiao *et al*., 2005
	HL-60	Human leukaemia	25	Kwon *et al*., 2002
	PC3	Human prostate	35	Dong Xiao *et al*., 2005
	PC3	Human prostate	40	Arunkumar *et al*., 2006
DAS	SW-480	Colon cancer	inactive	Danhua Xiao *et al*., 2005
	PC3	Human prostate	inactive	Xiao *et al*., 2004

The *in vitro* anti-cancer mechanism of garlic OSC has been investigated, and although the mechanism is not empirically known, ROS production, cell-cycle arrest and apoptosis have been found to be important. Garlic OSC's to include ajoene (Li *et al*. 2002; Dirsch *et al*. 2002), DATS (Kim *et al*. 2007; Xiao *et al*. 2004), DADS (Filomeni *et al*. 2003; Das *et al*. 2007; Yang *et al*. 2009), and allicin (Kim *et al*. 2008) have been found to induce G_2/M cell-cycle arrest in a number of different cell-lines. Apoptosis induction through the mitochondrial (intrinsic) pathway has been observed in cancer cell-lines treated with ajoene (Li *et al*. 2002; Dirsch *et al*. 2002), DATS (Kim *et al*. 2007; Xiao *et al*. 2004), DADS (Filomeni *et al*. 2003; Das *et al*. 2007; Yang *et al*. 2009), and allicin (Kim *et al*. 2008). Although apoptosis through the death receptor (extrinsic) pathway has not been as extensively investigated, it has been found to not play a role in the case of ajoene-treated HL-60 leukemic cells (Dirsch *et al*. 2002), but was found to be activated in DADS-treated HCT-15 human colon cancer cells (Yang *et al*. 2009) and allicin treated PC-3 human prostate cancer cells (Kim *et al*. 2008). Furthermore, the activation of c-Jun N-terminal Kinase-1 (JNK1) has been shown in DADS-treated T98G and U87MG glioblastoma cells (Das *et al*. 2007) and in the SH-SY-5Y neuroblasoma cell-line (Filomeni *et al*. 2003). Protein thiolation and Reactive Oxygen Species (ROS) production also appear to be important for the *in vitro* anti-cancer activity of OSC; features discussed in greater detail in sections 1.6 and 1.7 respectively.

1.4.3. *In vivo* anti-cancer activity of OSC

In vivo studies have revealed that ajoene is effective in treating skin carcinomas in both rodents and humans. Topical application of ajoene to a chemically induced skin tumour in mice were found to almost completely inhibit tumour growth (Nishikawa *et al*. 2002), and application of ajoene to humans with basal cell carcinomas was found to reduce the tumour size in 81% of patients (Tilli *et al*. 2003). Another study on a melanoma tumour model in mice showed that intraperitoneal injection (IP) of ajoene (25 mg/kg) reduced tumour size three-fold and strongly inhibited metastasis to the lung (Taylor *et al*. 2006).

For DADS, there is data to demonstate that gastric intubation of 1 mg DADS thrice weekly causes a reduction in HCT-15 human colon tumour volume by 69%, which was found to be further enhanced with IP injection of 0.5 mg DADS. Furthermore, the mice experienced no notable side-effects when treating with DADS (Sundaram & Milner 1996b). In another study, leukemic mice treated with 25 μM/100 μl DADS via IP injection were found to experience a significant decrease in cancer cell-viability compared to untreated mice. The disease is

usually associated with an increase in the size of the liver and spleen of mice, although mice treated with DADS had a liver size similar to that of the controls (Yang *et al*, 2006).

DATS *in vivo* anti-cancer activity has been reported for the human colon cancer xenograft in a mouse model. Here, it was found that the mean tumour size, measured at 27 days after the transplantation of the xenograft, was 70 % larger in the control mice compared to the mice treated with 6 mg/kg DATS. DATS-treatment was found to not affect body weight or induce notable side-effects (Hosono *et al*, 2005).

Thiosulfonate compounds are not reported to be found in garlic extracts, although they are reported to be found in cauliflower (*Brassica oleracea* L). It has previously been shown that the cauliflower-derived thiosulfonate, *S*-methylmethane thiosulfonate (*S*-MMTS) (Figure 1.5), is able to significantly reduce colon cancers in both rat and mice animal models at 80 ppm either alone or in combination with sulindac, another experimental anti-cancer drug (Kawamori *et al*. 1995; Reddy *et al*. 1999).

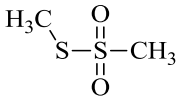

Figure 1.5. The chemical structure of *S*-methylmethane thiosulfonate (*S*-MMTS), an OSC anti-cancer compound isolated from cauliflower, which is reported to have *in vivo* anti-cancer activity against both mice and rat models with colon cancers (Kawamori *et al*. 1995; Reddy *et al*. 1999).

1.4.4. Structure-activity based OSC studies

Previous structure-activity based studies by Hunter *et al*. (2008) have shown that synthetic ajoene analogues, with substituted R^1 groups, display varying anti-cancer activities; as seen by the IC_{50}-values obtained against transformed CT-1 fibroblast cells (Table 1.2). Here it was observed that the *Z*-isomers were marginally more active than the corresponding *E*-isomers. Compound **13**, in which R^1 was substituted for *p*-methoxybenzyl, was found to be the most active compound in the series.

Table 1.2. The IC_{50}'s of ajoene analogues with substituted R^1 groups against CT-1 fibroblast cells (Hunter *et al*. 2008).

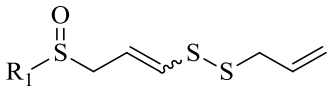

No.	Name	-R^1	CT-1 cell-line IC_{50} (μM)
1	*E*-ajoene	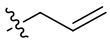	17.6
2	*Z*-ajoene		15.5
3	*E*-propyl	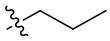	26.7
4	*Z*-propyl		17.0
5	*E/Z-tert*-butyl		33.1
6	*E*-OH	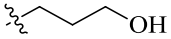	23.1
7	*Z*-OH		22.8
8	*E*-OPMB	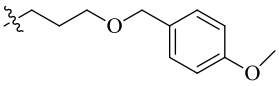	23.5
9	*Z*-OPMB		21.7
10	*E*-phthal	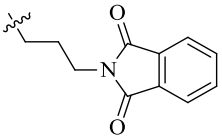	95.9
11	*Z*- phthal		34.6
12	*E/Z*-benzyl	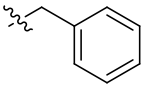	16.6
13	*E/Z*-PMB	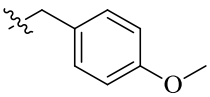	11.2

To further understand the structure/anti-cancer activity relationships in ajoene, Kaschula *et al*. (2012) synthesised a range of ajoene variants and tested them for their *in vitro* anti-cancer activity (Table 1.3). Here it was found that when at least one of the terminal allyl groups of

ajoene was varied for propyl and/or methyl, the anti-proliferative activity against WHCO1 oesophageal cancer cells was retained, indicating that the ajoene pharmacophore does not reside within the terminal allyl groups. In contrasts, Sundaram & Milner (1996a) observed that when the terminal allyl groups of DADS is substituted for propyl to yield dipropyl disulfide (DPDS) (Table 1.4), the compound is ineffective at inhibiting the growth of human colon, skin and lung cancer cells. It would therefore appear that there is an underlying difference between the anti-proliferative activity of ajoene and DADS with respect to side-group functionality. Furthermore, Kaschula *et al.* (2012) observed increased anti-proliferative activity against WHCO1 cells when the terminal allyl groups of ajoene were substituted with electron-rich end groups such as *p*-methoxybenzyl (*E/Z*-**4l**), resulting in a compound 12-fold more active than ajoene. The IC_{50} of *E/Z*-**4l**, which is 2.1 μM against WHCO1 cells, falls within the *in vitro* clinical range of two other oesophageal cancer chemotherapeutics namely cisplatin and 5-fluorouracil, whose IC_{50}'s are 9.2 μM and 7.9 μM respectively against the same cell-line. These findings indicate that although the terminal allyl groups of ajoene are not critical for their anti-proliferative activity against WHCO1 cells, they do appear to play an important modulating role. In support of the hypothesis that the ajoene pharmacophore resides within the disulfide functional group, it was shown that ajoene analogues, *E/Z*-**5**, *Z*-**6** and *E*-**6** (Table 1.3), that lack the disulfide bond, are inactive at inhibiting the proliferation of WHCO1 cells. This result is possibly supported by the literature report that DAS and *S*-allyl cysteine (Table 1.4), both monosulfides, are ineffective at inhibiting the growth of human colon, lung and skin cancer cells (Sundaram & Milner 1996a; Sundaram & Milner 1996c). Interestingly, the ajoene analogue *E/Z*-**3l**, containing an intact vinyl disulfide pharmacophore, but lacking the sulfoxide, was found to be three-fold more active than *E/Z*-**4l** returning an IC_{50} of 700 nM, implying that the sulfoxide group is not critical for the anti-cancer activity. Analogue **7**, which contains the disulfide pharmacophore, but lacks both the sulfoxide and vinyl group, was found to be inactive, implying some synergy between the two groups. Mechanistic studies revealed that *E/Z*-**4l**, like its garlic-derived parent compound, induces G_2/M cell-cycle arrest and apoptosis in WHCO1 oesophageal cancer cells (Kaschula *et al*. 2012).

Table 1.3. Chemical structures and IC_{50}'s of ajoene analogues against WHCO1 oesophageal cancer cell proliferation (Kaschula *et al*. 2011; Kaschula *et al*. 2012).

Ajoene and ajoene analogues			
Compound	Isomer	Chemical structure	IC_{50} (μM)
Ajoene	*Z*	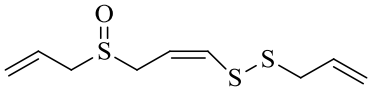	25
	E	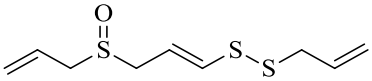	39
4a	*Z*	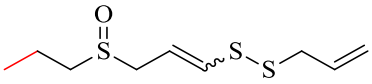	23
	E		37
4h	*Z*	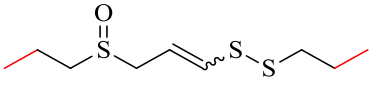	18
	E		24
4i	*Z*	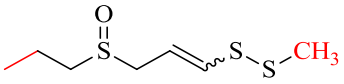	26
	E		28
E/Z-**4l**	-	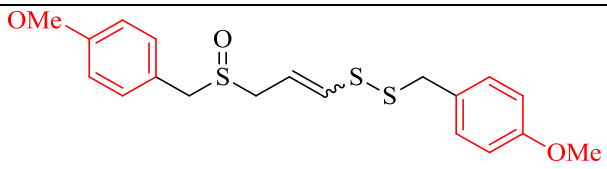	2.1
E/Z-**5**	-	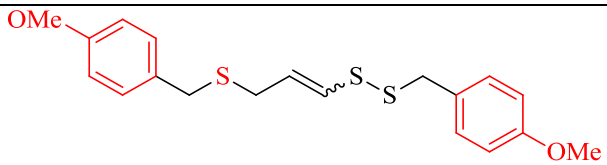	>200
Z-**6**	*Z*	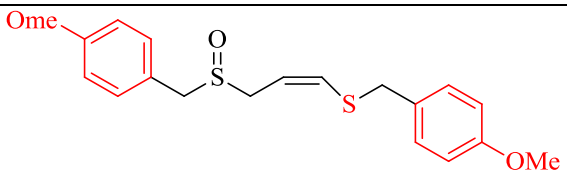	>200
E-**6**	*E*	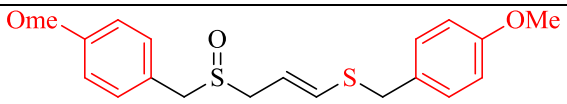	>200
7	-	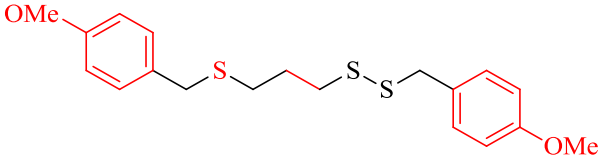	>200

The water soluble counterpart of DADS, *S*-allylmercaptocysteine (SAMC) (Figure 1.6) is reported to be three-fold less active than DADS on human colon and leukaemia cells, indicating that some hydrophobicity may be needed for effective anti-cancer activity (Yang *et al*. 2009; Kwon *et al*. 2002; Xiao *et al*. 2005).

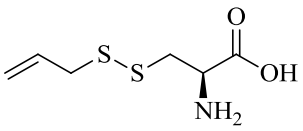

Figure 1.6. Chemical structure of water-soluble DADS analogue, *S*-allylmercaptocysteine (SAMC) which displays three-fold decreased anti-cancer activity compared to DADS (Kwon *et al*. 2002; Xiao *et al*. 2005; Yang *et al*. 2009).

In summary, it appears that the anti-proliferative activity of both ajoene and DADS relies on the presence of the disulfide functional group, and furthermore that the side groups at either end of the disulfide modulates the compounds anti-cancer activity. It seems likely therefore that the disulfide functional group may be the pharmacophore of the garlic-derived OSC.

Table 1.4. The chemical structures *S*-allyl cysteine, as well as the synthetic DADS analogue, DPDS. *S*-allyl cysteine is an inactive compound, whereas DPDS is three-fold less active than DADS on the HL-60 leukaemia cell-line (Sundaram & Milner 1996a).

Compound	Chemical structure
DPDS	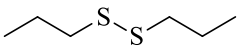
***S*-allyl cysteine**	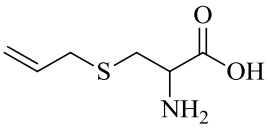

1.5. The chemical reactivity of the disulfide bond: thermostability and kinetics

Chemical reactivity between molecules is governed by both kinetic and thermodynamic parameters. In our study we propose that sulfenylation reactions and the generation of ROS may be important in the anti-cancer activity of OSC. We propose that the disulfide functional group of OSC may react with the cysteine nucleophile of a protein, resulting in the formation of an alkylated protein product and the expulsion of an anion leaving group. We further propose that the anion leaving group may react readily with free oxygen in the cell to generate ROS. During protein thiolation, activation energy is required to transform from its' primary state to a transition state, which in turn is related to the kinetics of the reaction (demonstrated in Figure 1.7 and 1.8). A strong nucleophile will increase the reaction rate,

however since the incoming nucleophile is the same in all cases (cysteine thiol of a protein); the rate of reaction is dependent only on the accessibility of the incoming nucleophile to the electrophilic sulfur.

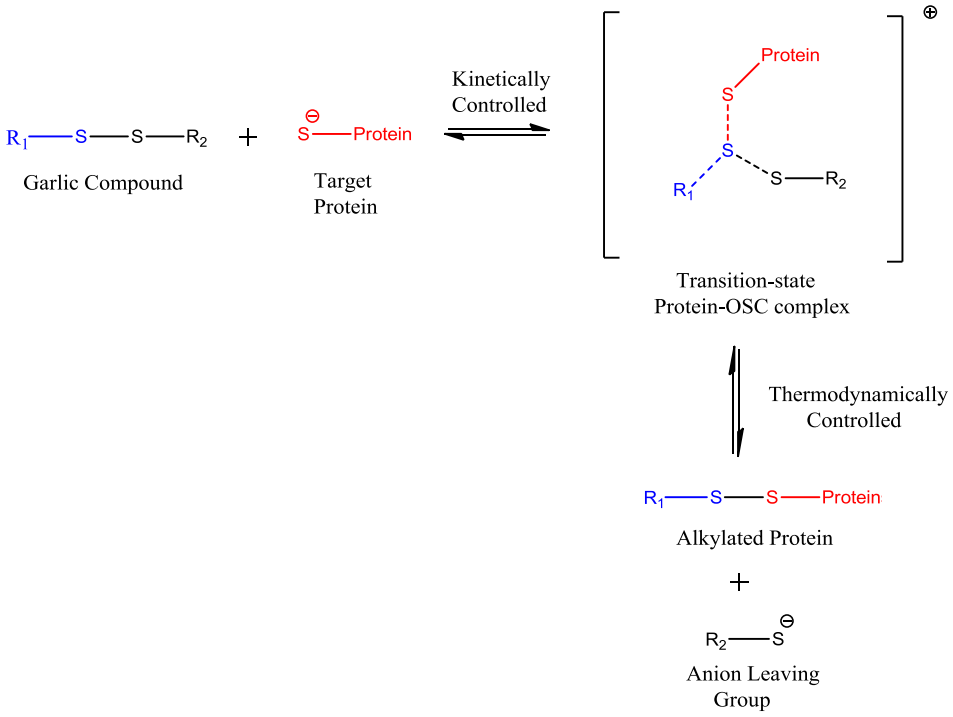

Figure 1.7. Schematic of the equilibrium reaction between an OSC and the cysteine nucleophile of a protein to form the transition state and final product. Here, an incoming cysteine nucleophile reacts with the more electropositive sulfur of the disulfide, thereby leading to a mixed disulfide product and the expulsion of an anion leaving group.

The thermodynamics of protein thiolation is driven by the stability of the products, which in our case, is largely governed by the stability of the negatively charged leaving group. The greater the ability of this leaving group to stabilise the anion, the greater the thermodynamic driving force and the more negative the ΔG (Gibbs free-energy) (Figure 1.8). Factors which increase stabilization of the leaving group include degree of conjugation, resonance and number of electronegative atoms. These effects are related to the theory that delocalised π-electron systems present in aromatic rings impart increased stability. The different localised structures attempt to depict the real structure and are called resonance forms. Therefore, the more resonance forms available, the more stable the leaving group anion.

In our thiolation hypothesis we propose that a free cysteine nucleophile reacts with the more electrophilic sulfur atom in the disulfide of the OSC to generate an alkylated protein product,

with the expulsion of an anion leaving group. We further propose that this anion leaving group may then react with free oxygen in the cell to generate ROS.

Although we can qualitatively assess the relative stability of the leaving group through its resonance, the extent of the leaving group stability can be quantitated through its pK_a-value. The pK_a-value is related to the acidity of the compound, whose strength is dependent on the stability of the conjugate base. This is highlighted in the examples of *p*-toluene sulfonic acid (Figure 1.9) and *p*-toluene sulfinic acid (Figure 1.10), where the former is a stronger acid than the later due to the increased stability of the sulfonic over the sulfinate anion. This is due to the superior resonance stabilisation of the negative charge acquired upon deprotonation by the sulfonic (pK_a = -2.8) versus the sulfinic (pK_a = 2.0) groups.

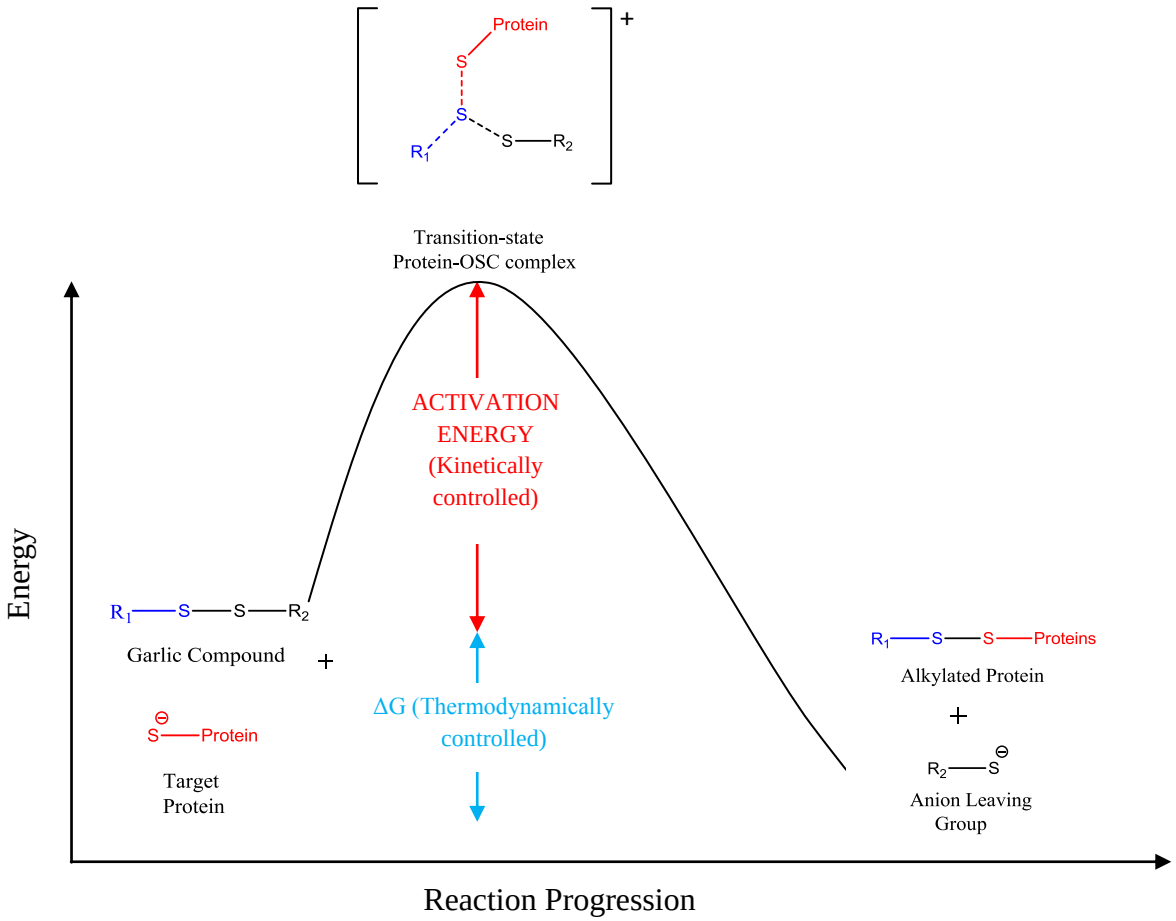

Figure 1.8. An exothermic energy diagram proposing the energy changes involved when an OSC reacts with a cysteine nucleophile in a protein to produce an alkylated protein and the expulsion of an anion leaving group. $\Delta G = \Delta H - T\Delta S$ (Gibbs free-energy equation).

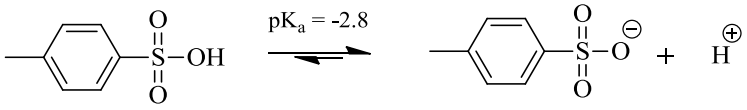

Figure 1.9. The deprotonation equilibrium reaction of *p*-toluene sulfonic acid.

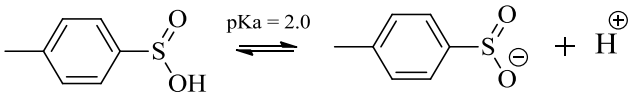

Figure 1.10. The deprotonation equilibrium reaction of *p*-toluene sulfinic acid.

1.6. Protein thiolation

Protein thiolation by OSC has been demonstrated in various cell-free systems. A study by Krauth-Siegel *et al*. (1996) revealed, by X-ray crystallography, that the vinyl sulfur of ajoene (Figure 1.12) is able to react with glutathione reductase (GR), at Cys58 to produce an alkylated protein within the active site of the form allylSOCH$_2$CH=CHSS(Cys$_{58}$)-GR. A rationale for this interaction was proposed by Kaschula *et al.* (2011) where the allyl sulfur of ajoene was found to be the more electrophilic sulfur in view of the greater leaving ability of the vinylthio moiety in the disulfur exchange (Figure 1.11). In the model reaction, *N*-Boc-L-cysteine ethyl was treated with the disubstituted *p*-methoxybenzyl ajoene derivative *E/Z*-**41** to give *p*-methoxybenzyl *N*-Boc cysteine ethyl ester disulfide (Figure 1.13), indicating that the preferred site of attack in solution is at the non-vinyl sulfur. It is therefore likely that in the reaction between glutathione reductase and ajoene as observed by Krauth-Siegel *et al*. (1996), the product may have been observed as a result of a secondary reaction between the expelled sulfoxide/vinyl sulfide fragment and GR (Kaschula *et al*. 2011). In support of this, Lawson & Gardner (2005) have reported a reaction between excess cysteine (2eq) and ajoene to form a mixed disulfide ajocysteine product, *S*-allylcysteine.

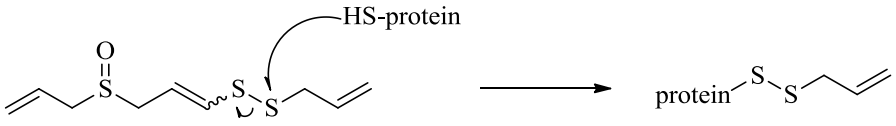

Figure 1.11. Proposed protein thiolation reaction between a yet to be identified protein target and *E/Z* ajoene, resulting in the formation of an alkylated protein product.

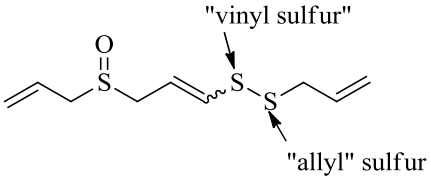

Figure 1.12. The allyl and vinyl sulfur of the disulfide of *E/Z*-ajoene, a garlic-derived OSC with anti-cancer properties.

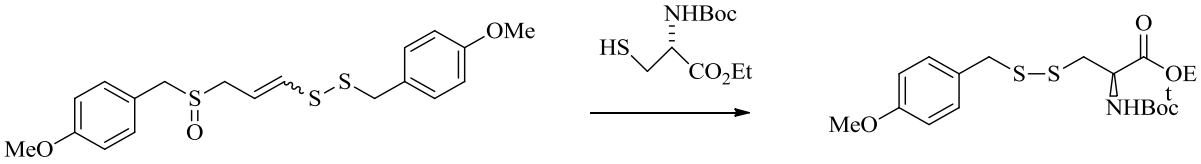

Figure 1.13. Reaction demonstrating the chemical reactivity of the disulfide bond between an ajoene analogue and *N*-Boc protected cysteine methyl ester (Kaschula *et al*. 2012).

Hosono *et al*. (2005) observed DATS-induced mitotic arrest and depolymerisation of microtubules in colon cancer cell-lines, which lead to them postulating that the protein, β-tubulin, may be a drug target of DATS. Using Liquid Chromatography-Tandem Mass Spectrometry, they found that DATS is able to oxidatively modify β-tubulin at Cys-12β and Cys-354β *in vitro* through a mass increase of 72,1 Da, corresponding to *S*-allylmercaptocysteine, a fragment molecule derived from DATS. It was thus concluded that DATS modification of β-tubulin may interfere with β-tubulin polymerisation, thereby leading to the observed delay in cell-cycle progression at the M-phase of the cell-cycle.

1.7. Reactive oxygen species

1.7.1. Evidence for ROS in the *in vitro* anti-cancer mechanism of OSC

Reactive oxygen species (ROS) are chemically reactive molecules containing oxygen, which usually have unpaired electrons or do not follow the octet rule. ROS form as a natural by-product of normal oxygen metabolism and are important in cell signalling and homeostasis. However, under deregulated conditions, ROS are toxic and give rise to a condition termed oxidative stress which may induce deleterious effects like cell dysfunction and cell death. Evidence suggests that cancer cells exhibit higher levels of oxidative stress than their normal counterparts (Coussens & Werb 2002), supported by reports that markers of constitutive oxidative stress are found within tumours of cancer patients (Wang *et al*. 1996; Toyokuni *et*

al. 1995). Increased levels of ROS production in cancer cells have been shown to arise through elevated levels of superoxide production, which is due to the low coupling efficiency of the mitochondrial electron transport with subsequent electron leakage. Here, excess superoxide has the potential to transform into more toxic ROS such as hydrogen peroxide (H_2O_2) and hydroxyl radicals (Pelicano *et al*. 2004) which may result in significant damage to cell structures. The highly oxidative state of cancer cells renders them vulnerable to agents that may increase their ROS levels further, resulting in a cascade of events leading to cancer-cell death. Examples of cancer chemotherapeutics employing a ROS-generating mechanism include doxorubicin (Wang *et al*. 2004; Tsang *et al*. 2003), as well as garlic-derived OSC.

OSC-induced cancer cell-death through increased ROS production and apoptosis has been extensively investigated in the family of garlic-derived OSCs. *In vitro* studies of ajoene-induced apoptosis in HL-60 human leukaemia cells revealed that the anti-cancer mechanism involved ROS generation with the subsequent activation of nuclear factor kappa-light-chain-enhancer of activated B cells (NFκB). Permeabilisation of the mitochondrial membrane, and the subsequent release of cytochrome c from the mitochondria was found to occur downstream of ROS production and NFκB activation, and was confirmed when pre-treating with the ROS scavenger *N*-acetyl cysteine (NAC), but not when pre-treating with the ROS inhibitor, catalase (Dirsch *et al*. 1998). This result appears to imply that either H_2O_2 is not one of the ROS species produced as a result of ajoene treatment or that though ROS is produced, it is not involved in the anti-cancer mechanism leading to cell death, and that NAC may be interfering with ajoene-induced cancer cell-death through a mechanism other than ROS production, a possibility discussed later in the Discussion section.

A number of studies suggest that DAS either has minimal or no anti-cancer activity on most cell-lines (Hosono *et al*., 2005; Xiao *et al*, 2004; Xiao *et al*, 2005). Although, DAS, as well as DADS, has been shown to decrease cell viability in the glioblastoma cell-line; T98G and U87MG, with a significant increase in the levels of ROS production and subsequent p38 mitogen-activated protein kinase (MAPK) activation, c-Jun N-terminal kinase-1 (JNK1) phosphorylation and apoptosis through the mitochondrial pathway, features which were abrogated when pre-treating cells with the ROS scavenger, ascorbate (Das *et al*. 2007).

Kwon *et al*. (2002) observed a time-dependent increase in the levels of ROS production in the HL-60 leukemic cell-line treated with DADS. Here, ROS production peaked at 30 minutes post-treatment, indicating that if ROS is important; it may be an early event leading to

cancer-cell death. DADS treatment resulted in caspase-3 activation and PARP cleavage, indicative of apoptosis, which were all blocked when pre-treating the HL-60 cells with catalase, indicating that increased levels of H_2O_2 is important in the anti-cancer mechanism of DADS in HL-60 cells (Kwon *et al*. 2002). When treating the A549 lung cancer cell-line with DADS, an early dose-dependent ROS event was also observed where ROS levels peaked 4 hours post-treatment. Pre-treatment with NAC completely abrogated the DADS-induced apoptosis and cell-cycle arrest, indicating that ROS production occurs upstream of these events (Wu *et al*. 2005). Filomeni *et al*. (2003) evaluated the potential damaging effects of ROS production to macromolecules within the SH-SY5Y neuroblastoma cell-line. Here they observed increased lipid peroxidation subsequent to observing increased ROS production, which was significantly decreased in cells transfected with the anti-oxidant enzyme, human superoxide dismutase (hSOD), confirming a strict relationship between oxidative burst and the apoptotic response. Although, a G_2/M cell-cycle arrest was still observed in the DADS-treated hSOD transfected cells, indicating that mechanisms other than ROS production may affect cell-proliferation in DADS treated SH-SY5Y cells.

DATS, an OSC containing three sulfur atoms, also induces cancer-cell death through apoptosis. It was previously shown that when the LNCaP prostate cancer cell-line is treated with DATS, a dose-dependent increase in the levels of ROS was observed for up to 8 hours. Moreover, the non-cancer control prostate epithelial cell-line, PrEC, treated with relatively high levels of DATS, was found to display a significant delay in ROS production for 16 hours. DATS treatment also caused apoptosis via the mitochondrial pathway with increased levels of cleaved caspase-9, disruption of the cristae in the mitochondria, elevated levels of cytosolic cytochrome c as well as decreased levels of the anti-apoptotic proteins; Bcl-2 and Bcl-xL. Lastly, pre-treating the LNCaP cells with NAC was found to almost completely protect against disruption of the mitochondrial membrane potential as well as cytoplasmic histone associated deoxyribonucleic acid (DNA) fragmentation. The authors therefore concluded that DATS-induced apoptosis in LNCaP cells correlated with ROS production (Kim *et al*. 2007).

Diallyl tetrasulfide (DAS4) (Figure 1.14), a garlic-derived OSC with four sulfur atoms, is only present in low abundance in crushed garlic preparations and is therefore not as extensively studied for its anti-cancer properties as the OSC discussed previously, but has increased *in vitro* anti-cancer activity compared DATS, DADS and DAS (Kelkel *et al*. 2012). Furthermore, the authors determined through an *in vitro* β-tubulin turbidity assay that

incubation of β-tubulin with DAS4 caused a significant increase in β-tubulin depolymerisation compared to the DMSO control. They also observed a correlation between β-tubulin depolymerisation and the number of sulfur atoms of the tested diallyl polysulfide: DAS4 exerts the strongest effects, followed by DATS, whereas DADS and DAS only barely affected β-tubulin depolymerisation. When treating the U937 histiocytic lymphoma cancer cell-line with DAS4, no changes in ROS levels were observed. Also, NAC, but not TROLOX was found to inhibit the anti-cancer activity of DAS4. In order to understand why NAC prevented DAS4-induced anti-cancer activity, the authors used a tubulin assay to test whether NAC interfered with DAS4-induced tubulin polymerisation. The authors showed that when the β-tubulin protein was co-incubated with DAS4 and NAC, the activity of DAS4 was inhibited, implying that NAC interferes with DAS4-induced tubulin depolymerisation, and not ROS per se (Kelkel *et al*. 2012).

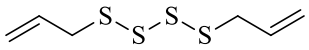

Figure 1.14. The chemical structure of diallyl tetrasulfide (DAS4), a garlic-derived OSC with four sulfur atoms, which has been shown to induce β-tubulin polymerisation in a cell-free system, and whose anti-cancer mechanism was shown to not involve ROS production in the U937 histiocytic lymphoma cell-line (Kelkel *et al*. 2012).

In vitro anti-cancer mechanistic investigations of garlic-derived OSC provide evidence that although ajoene, DATS, DADS, DAS and allicin fall into different compound classes, there is much evidence to suggest that they act via a similar anti-cancer mechanism by inducing increased levels of ROS, cell-cycle arrest and eventually apoptosis. These findings therefore imply that these compounds may have similar targets in cancer cells, and we propose that this reactivity is linked to the presence of the disulfide/polysulfide/thiosulfinate functional group.

1.7.2. ROS production mechanism

Although ROS production has been implicated in the anti-cancer mechanism of garlic-derived OSC, the cellular mechanism leading to ROS production is still unclear, although a number of hypotheses have been proposed. In a study by Gallwitz *et al*. (1999), it was shown that ajoene modification of glutathione reductase (GR) leads to the functional inactivation of the protein. Essentially, glutathione reductase is responsible for replenishing the concentrations of glutathione from glutathione disulfide within the cell, and it is proposed that glutathione reductase inactivation, and the subsequent decrease in the ratio of glutathione

to glutathione disulfide may result in an imbalance in the redox state of the cell towards ROS burden (Gallwitz *et al*. 1999). This finding could support the anti-cancer mechanism in which a synergy exists between protein thiolation and increased ROS levels.

Although one common explanation for the biological activity of OSC is their ability to react with protein thiols, the biochemical importance of the leaving group in the thiol-polysulfide reaction may also be important. Some consider the leaving group to be the actual active form of the polysulfide. The leaving group thiol or perthiol are reducing agents that may react rapidly with oxidants like dioxygen and oxyhaemoglobin to form ROS. A mixture of oxy-/methaemoglobin in the presence of disulfides or polysulfides may convert dioxygen to H_2O_2. If the disulfide bond is flanked by at least one side-group that is electron withdrawing, *i.e.* the side-group weakens the disulfide bond, the disulfide compound will react more readily with potential protein targets, and furthermore, may also result in an increased ROS response.

Another possibility is that OSC-induced ROS production may occur through the homolytic cleavage of the disulfide bond within polysulfides to generate a thiyl or perthiol radical. Antosiewics *et al.*(2006) has shown that DATS-induced ROS generation in DU145 and PC-3 cells is caused by an increase in labile iron pool due to the degradation of ferritin mediated by JNK signalling. Labile iron is considered an important determinant of ROS generation in cells as even low concentrations of labile iron, and can cause oxidative stress through Fenton/Haber-Weiss reactions.

1.8. Protein Disulfide Isomerase

We propose that garlic-derived OSC induce their anti-cancer effects by forming mixed disulfides with protein targets within cancer cells, with the resultant generation of ROS. Mixed disulfide formation may lead to protein inhibition, which may affect cancer cell viability, possibility leading to apoptosis and cancer cell death. The proposed target protein should therefore have a free cysteine residue available for nucleophilic attack on the OSC, and the chemistry of the cysteine environment should also facilitate this reaction. Previous work in our laboratory has found co-localisation of a fluorescently-tagged ajoene analogue (**DP**) to the ER of cancer cells (Figure 1.15). Due to the prospective biochemical properties discussed below, we therefore intend to investigate Protein Disulfide Isomerase (PDI), an ER-resident protein, as a possible protein target of OSC.

PDI, which forms part of the thioredoxin protein family, is an ER resident protein whose active site cysteine residues are involved in disulfide bond formation, isomerisation and reduction within newly synthesised proteins (Freedman *et al*. 1994). PDI was first isolated from liver in 1963 (Goldberger *et al*. 1963). Structurally, PDI has five domains (Figure 1.16), of which four (**a**-**b**-**a'**-**b'**) have thioredoxin folds made up of α-helices and β-strands (β-α-β-α-β-α-β- α) (Kemmink *et al*. 1997; Ferrari *et al*. 1998), followed by a **c**-domain which does not have a secondary or tertiary structure (Kemmink *et al*. 1997). There are extensive internal sequence similarities between the **a** and **a'** domains which each have a common active site sequence (-Cys-Gly-His-Cys-) (indicated in Figure 1.16) involved in the redox and isomerisation activities of PDI. The N-terminus cysteine residue of the **a'**-domain was shown to have a greater reducing capacity, and is thought to be responsible for the redox/isomerase activity of PDI with a pK_a of 4.5, compared to the pK_a of cysteine which is 8.0 at pH 7.0, indicating that the active site thiol is predominantly in a thiolate form at physiological pH, thereby more readily able to reduce its target. The low pK_a of the cysteine thiol in the PDI active site is due to the partial stabilizing ability of the nearby histidine imidazole group within the active site, as well as the partial positive charge of the N-terminal of the α-helix after the N-terminal cysteine residue (Chivers *et al*. 1996; Vuori *et al*. 1992; Darby *et al*. 1994; Wunderlich *et al*. 1995; Kortemme *et al*. 1996). Although the **b**- and **b'**-domains have thioredoxin-like folds similar to the **a**- and **a'**-domains, they do not have active site residues, and also have low sequence similarities. It has previously been reported that the **b'**- and **c**-domains have low-affinity hydrophobic interactions with peptides or proteins as to assist with the correct positioning for catalysis by PDI (Noiva *et al*. 1993; Klappa *et al*. 1998). Furthermore, the c-terminus of PDI has an ER retention signal, which interacts with the ER membrane for localisation, with a Lys-Asp-Glu-Leu (KDEL) amino acid sequence, as indicated in Figure 1.16.

PDI makes up ~ 0.8 % of total cellular protein (Freedman *et al*. 1994), reaching near millimolar concentrations in the lumen of the ER in some cells (Zapun *et al*. 1992). The redox potential of PDI is dependent on its environment, which is controlled by the ratio of oxidised to reduced glutathione in the ER (GSH:GSSG ≈ 2:1) (Hwang *et al*. 1992). The standard redox potential of PDI is about -180 mV (Hawkins *et al*. 1991). Furthermore, the oxidative environment of the ER supports the stability of the anion leaving group which would be expelled in a protein-OSC reaction.

a.

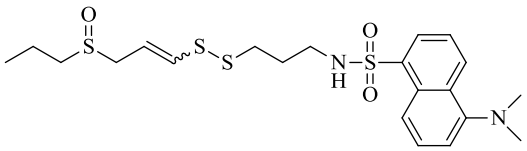

b. i

ii

iii

iv

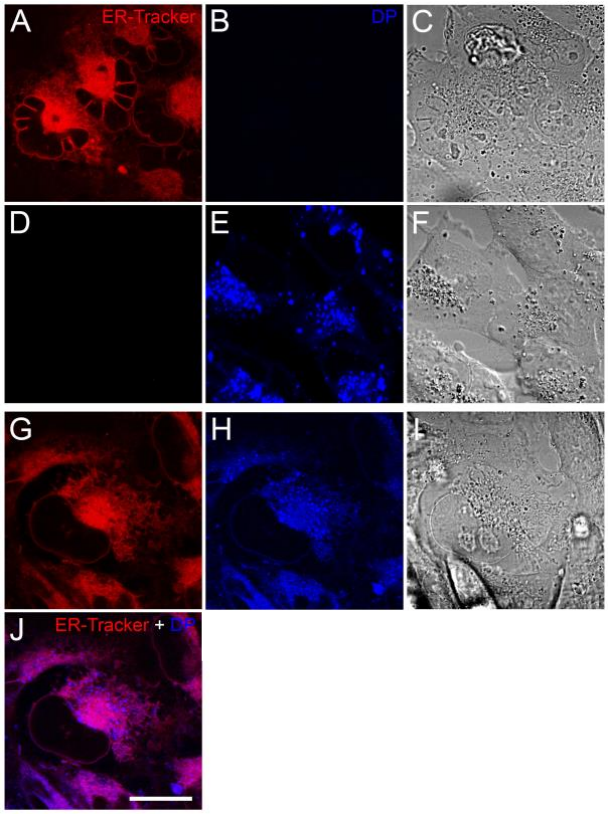

Figure 1.15.The chemical structure of (**a**) **DP**, a fluorescent ajoene analogue, with an IC_{50} of 25 μM against MDA-MB-231 breast cancer cells are represented. Co-localisation between **DP** (blue) and an ER-tracker (red) in MDA-MB-231 cancer cell-line is shown with confocal images (**b**); row **i** represent cells treated with ER-tracker alone (red) (**A**) with no signal from the blue filter (**B**) as well as the representative phase contrast image (**C**). Row **ii** represents cells treated with **DP** (blue) (**E**) with no signal from the red filter (**D**) as well as the representative phase contrast image (**F**). Row **iii** represents cells treated with an ER-tracker (red) (**G**) and **DP** (blue) (**H**) with the representative images for phase contrast (**I**) and co-localisation (pink) (**J**) between the ER-tracker and **DP**.

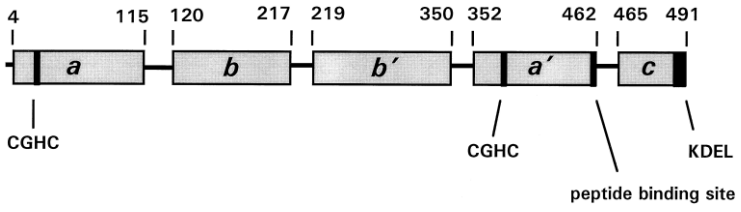

Figure 1.16. The structure of mammalian PDI. Domain boundaries as proposed by Darby *et al.* (1994) are noted. The location of the proposed peptide binding site and the C-terminal -KDEL ER-retention signal are also depicted (Noiva 1999).

Several compounds are known to inhibit PDI, to include bacitracin (Figure 1.17**A**), 5,5-dithio-bis(2-nitrobenzoic acid) (DTNB) (Figure 1.17 **B**) as well as phenyl arsine oxide (Figure 1.17**C**).

DTNB contains a disulfide functional group (encircled in Figure 1.17**B**) and is therefore structurally similar to the garlic-derived OSC, DADS. Although the mechanism of PDI inhibition has not yet been confirmed for DTNB, it is generally proposed that the disulfide functional group of DTNB may form a mixed disulfide with the active site cysteine residues of PDI, leading to the inhibition of PDI isomerase and its redox activities; the same hypothesis that we propose for PDI and garlic-related OSC. It has recently been confirmed that bacitracin inhibits PDI through mixed disulfide bond formation (Dickerhof *et al*. 2011). Using Matrix-Assisted Laser Desorbtion/Ionisation Time Of Flight Mass Spectromtery (MALDI-TOF MS), Dickerhof *et al*. (2011) showed that a direct interaction forms between an open thiol form of the bacitracin thiazoline ring (sulfur encircled in Figure 1.17**A**) and Cys314 and Cys345 residues in the substrate binding domain of PDI, leading to the inhibition of PDI isomerase and redox activities.

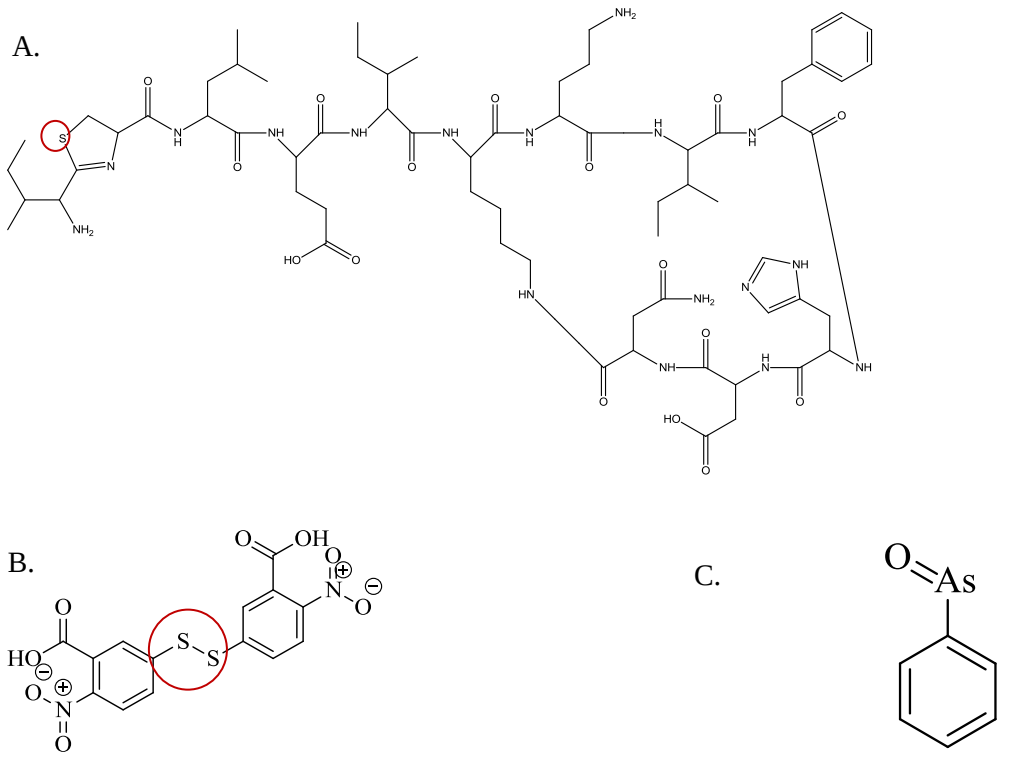

Figure 1.17. The chemical structures of PDI inhibitors; bacitracin from *bacillus licheniformis* (**A**), 5,5-dithio-bis(2-nitrobenzoic acid) (DTNB) (**B**) and phenylarsine oxide (**C**).

We propose that the garlic-derived OSC inhibit the redox and isomerase activities of PDI by forming mixed disulfides with the PDI active site residues, the result being that the protein substrates of PDI do not form their proper tertiary structure. We therefore propose that the anti-cancer mechanism of OSC may occur through PDI thiolation within the active site to possibly disrupt protein folding, with the concurrent generation of ROS, which may lead to apoptosis and cell death.

1.9. Analogues of garlic-derived OSC

For the Masters project, a small library of thiosulfonates and a thiosulfinate (Figure 1.18) as well as disulfides (Figure 1.19) were designed and synthesised in the Chemistry Department at UCT by Post-Doctoral student, Dr. Nashia Stellenboom. The compounds were used to probe the structure / anti-cancer activity relationships for this class of compounds. It was envisaged that increased electrophilicity of the sulfur atom in the OSC and/or increased stability of an expelled anion leaving group may favour both protein thiolation and ROS production to thereby generate a more reactive analogue with a lower IC_{50}-value. The thiosulfonates are completely synthetic analogues of garlic-derived OSC, although a natural product thiosulfonate, *S*-MMTS (Figure 1.4) is reported to be present in cauliflower and has also been found to display *in vivo* anti-cancer activity (Kawamori *et al*. 1995; Reddy *et al*. 1999). The thiosulfinate and disulfides are structural variants of the parent compounds, allicin and DADS respectively, which are found naturally in crushed or processed garlic.

Apart from the key disulfide or an "activated disulfide" group being present, we have additionally inserted various side groups with either electron withdrawing or/and electron donating character. Since it has previously been found that increased lipophilic character is related to enhanced activity (Kaschula *et al*. 2012), a lipophilic analogue (**NSZ**) and a water-soluble analogue (**92**), were also included in the series. Random numbers were previously assigned to each compound, and were thus used to name them.

Thiosulfonates	
t-benzyl 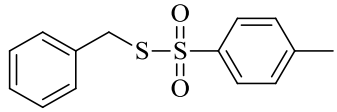	**t-fluoro** 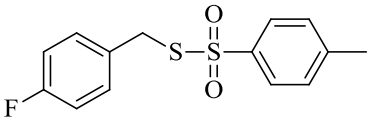
t-PMB 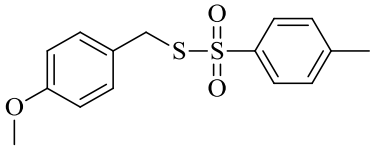	**t-propyl** 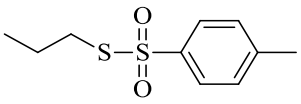
Allicin analogue	
Allicin -16 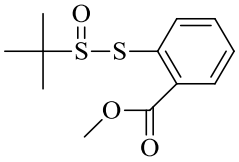	

Figure 1.18. List of thiosulfonate and thiosulfinate compounds used in the study. Compounds include **t-benzyl**, **t-fluoro**, **t-PMB**, **t-propyl** and **Allicin-16**.

Disulfides

Electropositive sulfur, electron withdrawing side-groups:

21

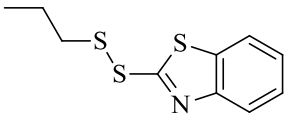

200

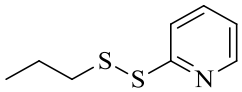

30

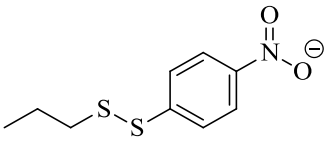

16

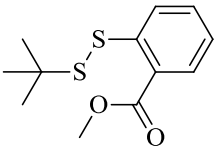

Neutral side-groups, lipophilic molecules:

8

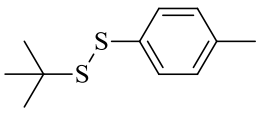

2

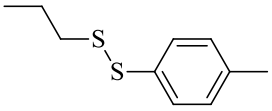

NSZ

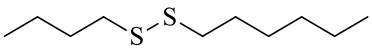

Water-soluble side-group:

92

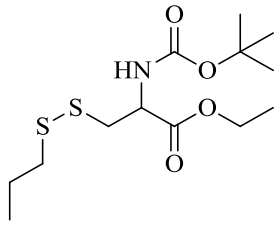

Mixed featured side-groups

46

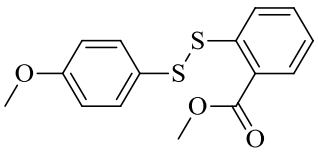

59

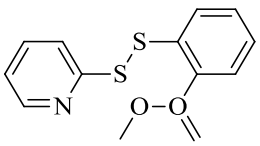

Figure 1.19. List of the disulfide analogues used in the study. These include those with electron withdrawing side-groups: **21**, **200**, **30**, **16**; compounds with neutral side-groups: **8**, **2**, **NSZ**, compound with a water-soluble side-group: **92**; and those with side-groups which have mixed functions: **46** and **59**.

1.10. Hypothesis

We hypothesise that the pharmacophore of garlic disulfide compounds, and related compounds, is the disulfide functional group, and that these compounds exert their anti-cancer effects through increased ROS production and protein thiolation, where PDI may be a potential protein target. We also hypothesise that the anti-cancer activity of the disulfide may be improved through increased electrophilicity of the sulfur atom and the presence of a good leaving group.

1.11. Objectives

The objectives are to carry out a structure-anti-activity assessment of a small library of disulfide, thiosulfinate and thiosulfonate compounds against WHCO1 oesophageal cancer cells. If the classes of compounds are found to be active, the mechanism of action of two compounds, one from the disulfide and one from the thiosulfonate compound class, will be selected for further evaluation to include cell-cycle analysis, ROS production, apoptosis induction and morphological changes.

If ROS production is found to be important, we will assess whether the anti-proliferative activity is dependent on ROS generation using ROS scavengers.

Lastly we intend to investigate whether garlic OSC inhibit PDI enzyme activity.

Chapter 2

Investigating structure-anti-proliferation relationships of DADS and thiosulfonate compounds in WHCO1 oesophageal cancer cells

2.1. Introduction

Organosulfur compounds (OSC) from garlic which are reported to have *in vitro* and *in vivo* anti-cancer activity share common structural features to include either a disulfide or polysulfide backbone. It is hypothesised that the disulfide or polysulfide functional group of OSC may react with the free cysteine nucleophile within a target protein, resulting in the formation of alkylated protein product and the expulsion of anion leaving group. The alkylated protein may therefore be unable to perform its proper cellular function, potentially leading to the deregulation of protein pathway signals and eventually cell death.

In the current chapter, we assessed the structure-anti-proliferation relationships in a small library of 10 diallyl disulfide (DADS) analogues, 4 thiosulfonate compounds, a compound class not reported to be found in garlic, and 1 allicin analogue against WHCO1 oesophageal cancer cell proliferation by using the thaizolyl blue tetrazolium bromide (MTT) viability colorimetric assay.

2.2. Results

2.2.1. Cell viability (MTT assay)

To assay for the ability of thiosulfonate compounds and DADS analogues to inhibit cancer cell viability, an MTT assay was performed. The MTT assay is a colorimetric assay which is based the conversion of MTT to formazan by metabolically active cells. WHCO1 cells were seeded in 96-well plates and treated with either a thiosulfonate or disulfide analogue at concentrations varying from 0 to 200 µM for 48 hours. The cells were then treated with the MTT reagent for 4 hours after which they were lysed to solubilise the crystalline MTT, and the relative absorbance was quantified at 595 nm using a multi-plate reader. Independent triplicate experiments were performed. The absorbance obtained was fitted against concentration to generate a dose-response curve, from which an inhibitory IC_{50} concentration was obtained, defined as the concentration of the compound required to inhibit the viability of 50% of the cells after 48 hours.

The IC_{50}'s obtained against WHCO1 cell proliferation are displayed in Table 2.1 and Table 2.2 alongside their respective chemical structures together with a representative IC_{50} curve. It is evident that the thiosulfonate compounds as well the DADS analogues; **2**, **21**, **200**, **30**, **54**, **46** and **59** all decreased WHCO1 cell viability after a 48 hour treatment. The four thiosulfonate compounds were all found to be equally active, with an IC_{50} around 15 µM. The disulfides exhibited a broader range of activities from 5 µM to inactive (IC_{50} > 200 µM). The most active disulfide was found to be **54** with an IC_{50}-value of 4.87 µM, which is ~ 10-fold more active than the parent, diallyl disulfide (DADS). On the other side, compounds **NSZ**, **92**, **8** and **16** were all found to be inactive. **Allcin-16**, an OSC analogue whose IC_{50} was previously determined in our lab (unpublished data), was found to be active with an IC_{50} of 71.1 µM and was included in the series for comparison as, it belongs to a different compound class being thiosulfinates.

Table 2.1. List of thiosulfonate compounds, with their respective chemical structures and a representative IC_{50} curve obtained by the MTT colorimetric assay against WHCO1 cell proliferation.

Compound Name	Chemical structure	Dose –Response Curve	WHCO1 IC_{50} ± SD (µM) (n=3)
Thiosulfonates			
t-benzyl	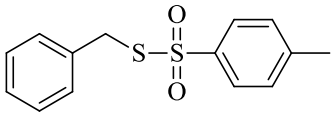	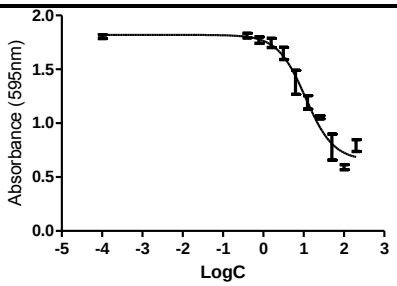	**12.8 ± 2.3**
t-fluoro	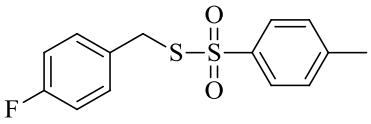	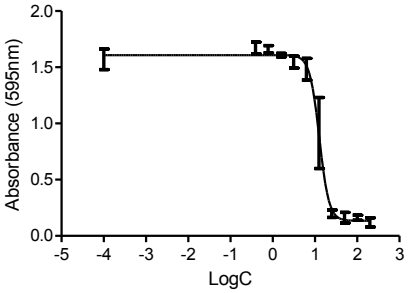	**15.9 ± 3.0**
t-PMB	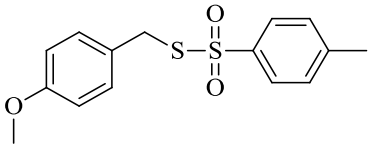	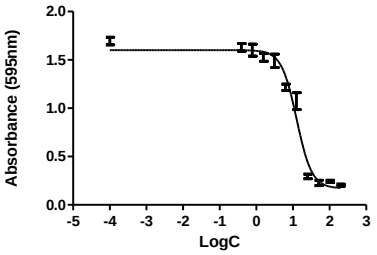	**14.8 ± 1.9**
t-propyl	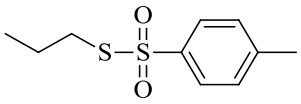	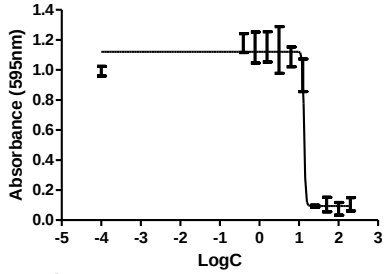	**13.1 ± 1.2**
Allicin-16	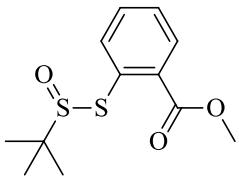	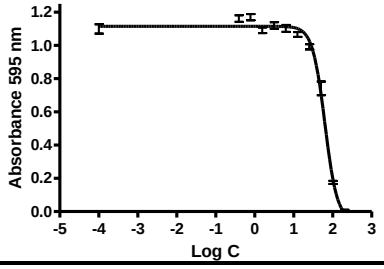	**71 ± 22[a]**

[a] Unpublished data from our laboratory.

Table 2.2. List of diallyl disulfide (DADS) analogues, with their respective chemical structures and representative IC_{50}-curves obtained through the MTT colorimetric assay on WHCO1 cells.

Compound Name	Chemical structure	Dose-response curve	WHCO1 IC_{50} ± SD (µM)
DADS analogues			
2	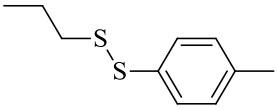	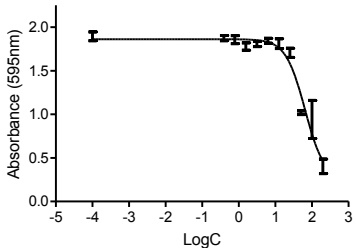	**61.1 ± 6.3**
200	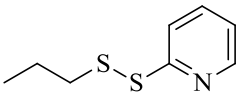	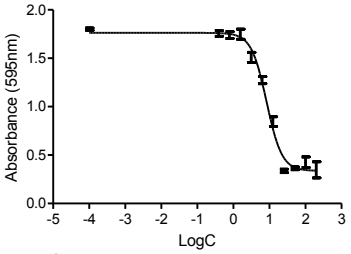	**9.9 ± 1.9**
30	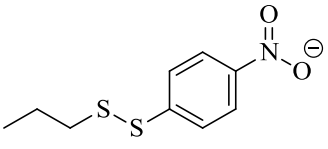	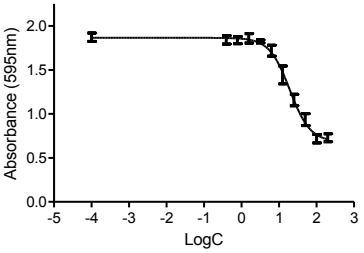	**22.3 ± 3.0**
21	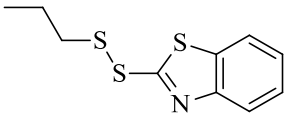	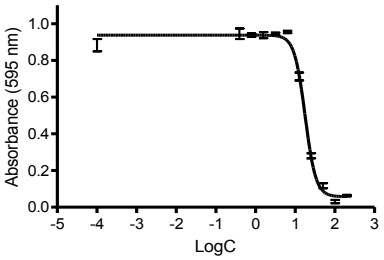	**23.0 ± 1.1**
54	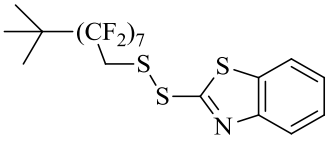	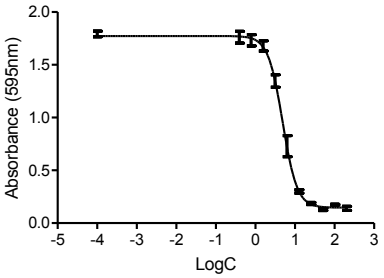	**4.87 ± 0.55**
NSZ	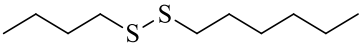	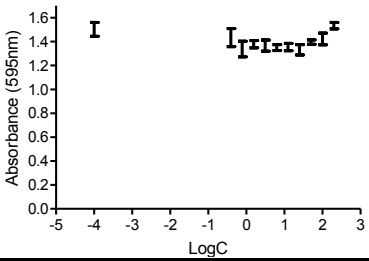	**>200**

Table 2.2. continued. List of diallyl disulfide (DADS) analogues, with their respective chemical structures and representative IC_{50}-curves obtained through the MTT colorimetric assay on WHCO1 cells.

Compound Number	Chemical structure	Dose-response curve	WHCO1 IC_{50} ± SD (µM)
92	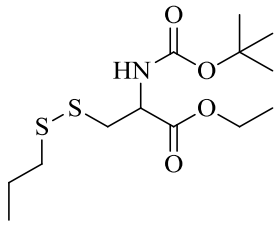	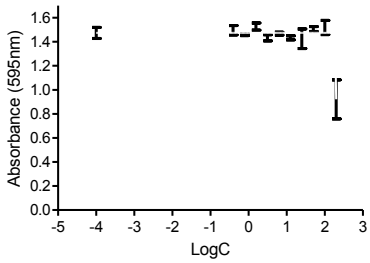	**>200**
8	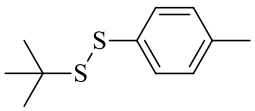	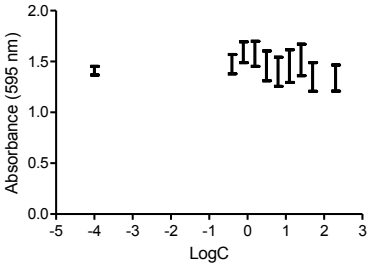	**>200**
16	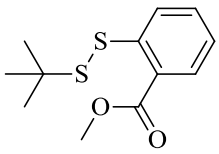	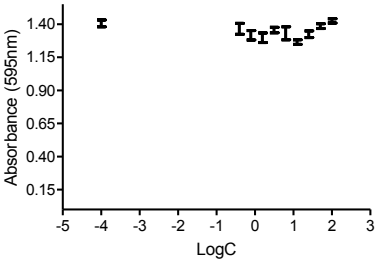	**>200**
46	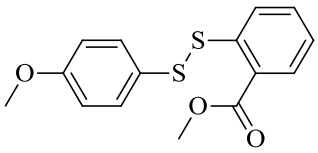	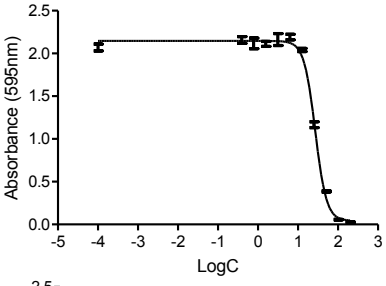	**27.5 ± 0.7**
59	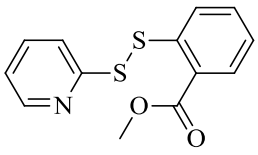	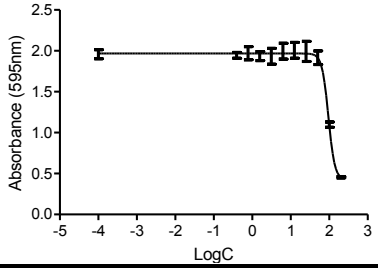	**95 ± 0.38**

2.2.2. Predictive pK_a-values of OSC leaving groups

We propose that in a reaction between a free cysteine thiol of a protein and an OSC containing a disulfide functional group, the cysteine thiol will act as the incoming nucleophile

to form a mixed disulfide with the OSC, with the expulsion of an anion leaving group. We hypothesise that an OSC having a more stable leaving group will result in a more thermodynamically favoured reaction. The leaving group stability can be assessed qualitatively through resonance predictions (see Discussion), and quantitatively by assessing its pK_a-value. Using the Pipeline® predictive programme, the predictive pK_a-values were computer generated for each leaving group as shown in Table 2.3. The thiosulfonate leaving group was the same for all compounds in its class and had a predicted pK_a-value of 6.82, whereas the predicted pK_a-values for the DADS analogues varied greatly from 2.71 for **200** to 10.53 for **NSZ**. To determine if a relationship exists between the measured IC_{50}-values and the predicted pK_a-values for the various DADS analogues, compounds **200**, **30**, **21** and **2** were selected for correlation studies as their left side-groups are all propyl. A scatter plot of the predicted pK_a-value and log IC_{50}-values is shown in Figure 2.1 with an R^2-value of 0.88.

Table 2.3. The chemical structures of selected DADS analogues and their respective leaving groups, alongside their respective IC_{50}-values and predicted pK_a-values which were determined using the Pipeline® predictive programme.

Compound name	Compound structure	Compound leaving group structure	IC_{50} (µM)	Predictive pK_a-value of leaving group
200	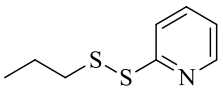	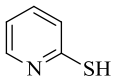	10	2.71
30	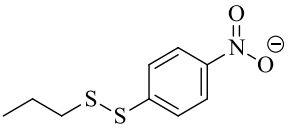	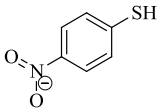	20	4.6
21	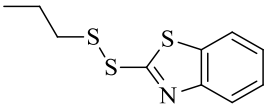	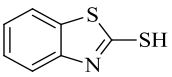	23	6.93
2	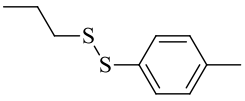	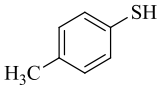	61	8.82
NSZ	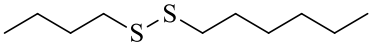	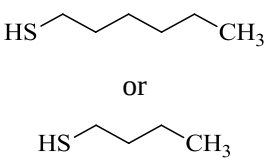	> 200	10.53
Thiosulfonates	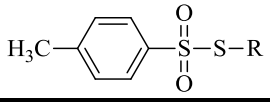	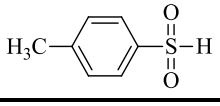	15	6.82

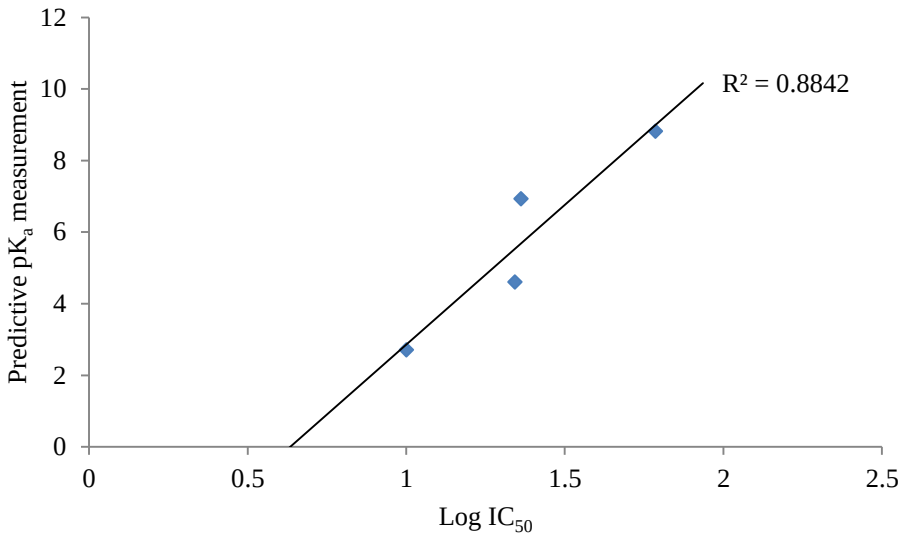

Figure 2.1. Scatter plot of log IC_{50} vs predicted pK_a for DADS analogue leaving groups. A positive correlation was found between the predicted pK_a-and log IC_{50}-values, with an R^2-value of 0.88.

2.3. Discussion

Thiosulfonate series: The MTT results for thiosulfonates show that they all had similar activities with IC_{50}'s ~ 15 μM (Table 2.1). This could be explained due to the probability that the electronic effects of benzyl-, fluoro-, *para*-methoxybenzyl- and propyl-side-groups on the benzyl group are not able to modulate the electronics of the thiosulfonate or the stability of the leaving group due to the presence of the sp^2 carbon which separates these side groups from the thiosulfonate functional group. The sp^2 carbon prevents the transfer of resonance from the ring to the thiosulfonate. The thiosulfonate itself is an activated disulfide due to the presence of the two oxygen atoms which present an electron-withdrawing effect on the adjacent sulfur, which may be activated to nucleophilic attack from a cysteine residue within a protein (Figure 2.2). The finding that the IC_{50} remained unchanged between the analogues with the same functional group implied that it was solely the presence of the reactive group that confers activity, and that the side-groups did not have any modulatory effect, resulting in a low IC_{50} of 15 μM.

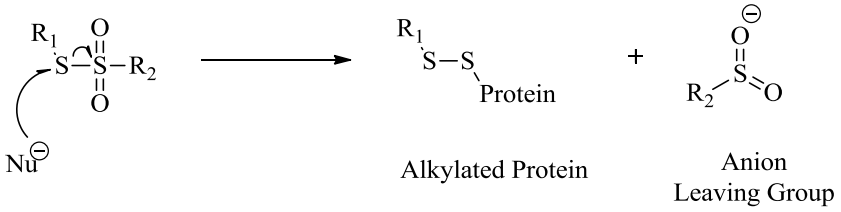

Figure 2.2. The proposed reaction between a cysteine nucleophile and the more electropositive sulfur of the thiosulfonate, resulting in the formation of a mixed disulfide between the sulfur of the thiosulfonate and the cysteine residue of the protein, with the expulsion of the anion leaving group.

Disulfide series: For this series of compound, a correlation was observed between the IC_{50} and the degree of resonance stabilization of the leaving group anion. The IC_{50} of **200** (9.9 μM) was found to be ~2.5-fold lower than **30** (22.3 μM). The leaving group, of both **30** and **200,** have 4 resonance forms (Figure 2.3 and Figure 2.4 respectively), however the negative charge acquired by the pyridine leaving group of **200** is more stable than the negative charge acquired by the *p*-nitrobenzene leaving group of **30** due to the presence of the electronegative nitrogen in the ring being endocyclic in the pyridine of **200** compared to the nitro group being exocyclic in *p*-nitrobenzene in **30**, conferring greater anion stability to **200**. This explanation in terms of resonance is also supported quantitatively by the predicted pK_a's which were found to be 2.71 for **200** and 4.60 for **30**.

The DADS analogue, **54** was found to be the most active disulfide in the series with an IC_{50} of 4.87 μM. Similar to **21**, it has a heteroaromatic benzothiazole side-group. It is hypothesised that in the reaction with cysteine, the heteroaromatic benzothiazole anion in both the cases of **54** and **21** is expelled as the leaving group. The heteroaromatic benzothiazole anion has six resonance forms (Figure 2.5), resulting in the highest number of resonance forms in the series. The difference in IC_{50} between **21** (23 μM) and **54** (4.87 μM) must therefore be due to the presence of the long hydrophobic chain containing lipophilic fluorines in **54** which are predicted to increase the lipophilicity leading to a more active compound. Contrary to resonance theory, **21,** with 6 resonance forms, has a higher IC_{50} (23.0 μM) when compared to **200** and **30** (10 and 20 μM respectively), which have 4 resonance forms. According to the predictive pK_a-value of the heteroaromatic benzothiazole side-group of **21**, which is 6.93, **21** should be less active than both **200** and **30**, whose leaving groups have pK_a-values of 2.71 and 4.60 respectively. The predictive pK_a results therefore suggest that the heteroaromatic benzothiazole side-group is actually less stable than resonance would suggest and are in-line with the IC_{50} data. Furthermore, **2** and **NSZ**, whose IC_{50}'s were 61.1 and > 200 μM respectively, had pK_a-values of 8.82 and 10.53, which predict a much less active compound based on leaving group stability and correlates well in a linear plot of predicted pK_a-values versus log (IC_{50})-values (Figure 2.1).

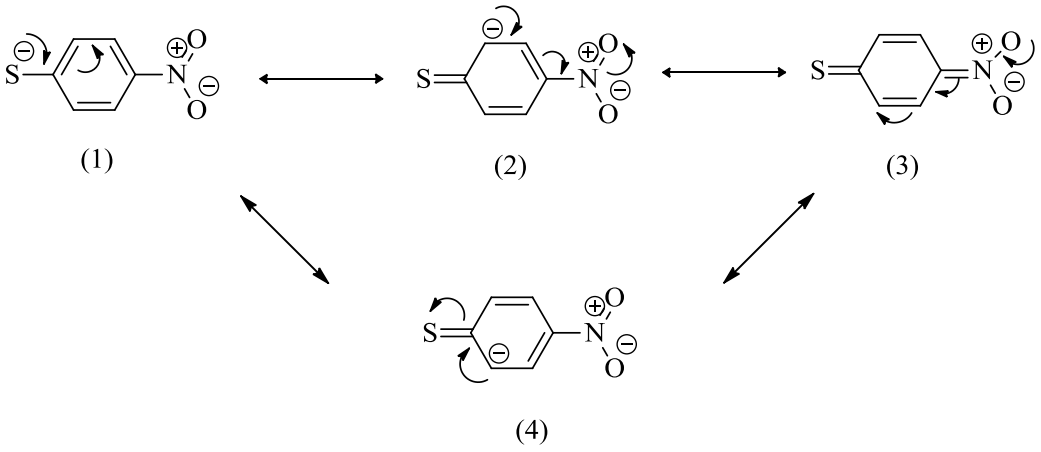

Figure 2.3. The four different resonance forms of the leaving group anion of **30**. The arrows in and around each resonance form indicates the movement of electrons and charge around the molecule.

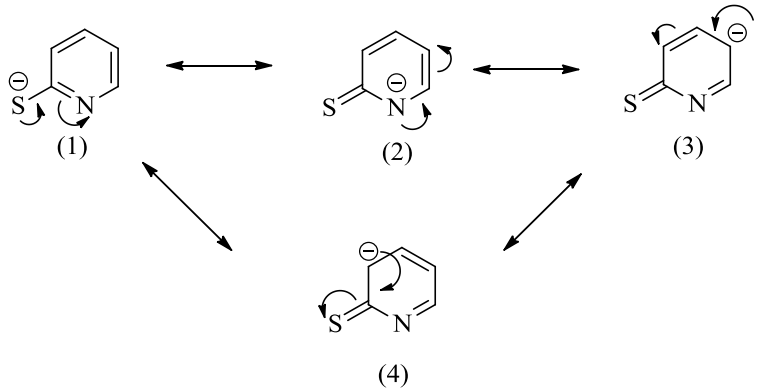

Figure 2.4. The four different resonance forms of the anion leaving group of **200**. The arrows in and around each resonance form indicates the movement of electrons and charge around the molecule.

The leaving group in compounds **2** and **8** is the same, with three possible resonance forms (Figure 2.6), indicating that the thermodynamic driving force should be equal for both compounds. However, **8** was found to be inactive, and **2** has an IC_{50} of 61.1 µM. This may be due to the presence of the bulky *t*-butyl group of **8**, which is substituted with a propyl group in **2**. The bulky *t*-butyl group of **8** likely introduces some steric hindrance to the incoming nucleophile, thereby affecting the reaction kinetics between **8** and the cysteine nucleophile.

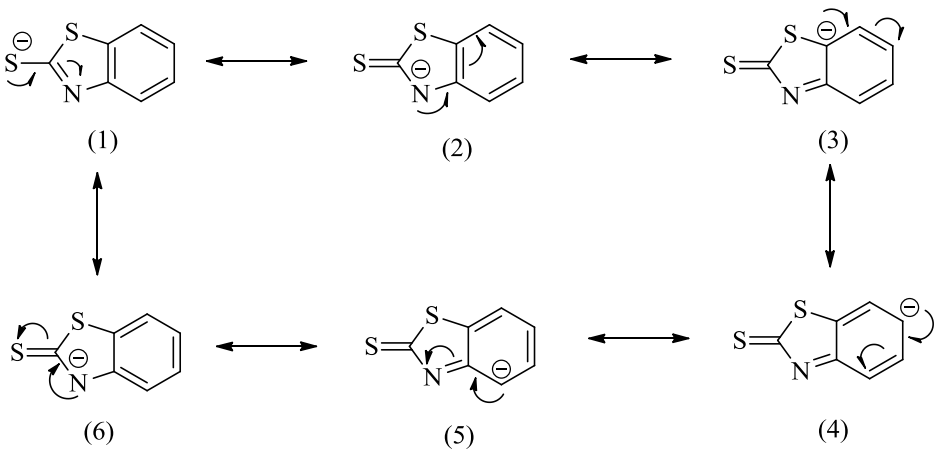

Figure 2.5. The six different resonance forms of the benzothiazole leaving group of **54** and **21**. The arrows in and around each resonance form indicates movement of electrons and charge around the molecule.

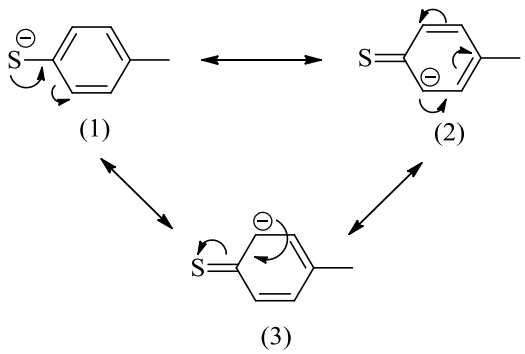

Figure 2.6. The three different resonance forms for the leaving group anion of both compound **2** and **8**. The arrows in and around each resonance form indicates movement of electrons and charge around the molecule.

In comparing the structures of **8** and **16**, the difference being that **16** has an exocyclic methyl benzoate group on its benzene ring and **8** does not. The exocyclic methyl benzoate group of **16** has an electron withdrawing effect on its disulfide group. The leaving group of **16** has four resonance forms (Figure 2.7), and **8** has three (Figure 2.6), indicating that the leaving group of **16** is more stable compared to **8**. Both compounds are however inactive, possibly due to the steric hindrance of t-butyl group, preventing nucleophilic attack from an incoming cysteine nucleophile. It is possible that these predicted selectivity's could possibly be observed if assaying was carried out at a higher concentration.

Allicin-16 has a similar structure to **16**, with the exception that **allicin-16** is a thiosulfinate, compared to **16** which is a disulfide. **Allicin-16**s stronger activity, with an IC_{50} of 71 μM, compared to **16** which was inactive (IC_{50} > 200 μM), supports the hypothesis that the presence of the oxygen on **allicin-16** enhances its anti-cancer activity by activating the disulfide towards thiolation.

Compound **46** has mixed characteristics in which one side-group is electron withdrawing and the other is electron donating. The methyl benzoate group is possibly the leaving group of **46** due to its electron withdrawing ability and the existence of four resonance forms (Figure 2.7).

Compound **59** is unique in the series as it is the only compound that has an electron-withdrawing group on either side of the disulfide. Both side groups of **59** are therefore able to stabilise an anion. The pyridine group is possibly the better leaving group due to the presence of an endocyclic nitrogen (Figure 2.8). It would be anticipated that the IC_{50} of **59** should have been ~ 10 μM, similar to **200**, due to the presence of the pyridine ring leaving group, however

the IC_{50} was found to be 95 μM, which could possibly be explained on kinetic grounds where the bulky methyl benzoate group may provide steric hindrance towards the incoming nucleophile. This reaction may be too slow in the timeframe of the experiment, resulting in decreased activity.

NSZ was found to have an IC_{50} greater than 200 μM, which is not unexpected based on the absence of stabilising side groups in this compound. A similar finding was observed when the allyl side-groups of DADS were substituted for propyl (Sundaram *et al*, 1996). A rationale for this observation was not described, but our results indicate that the loss of activity of DADS with propyl side-groups could be due to propyl being a poor leaving group, as it cannot stabilise an acquired negative charge. This may be because the attack of a cysteine nucleophile on the disulfide bond of DADS does not generate a leaving group that can stabilise the expelled negative charge, therefore the reaction is not favoured (Figure 2.9, ii). In comparison, dipropyl ajoene which contains a vinyl disulfide functional group may generate a leaving group (Figure 2.9, i) hence conferring activity to dipropyl ajoene but not dipropyl disulfide. So, instead of this reaction being exothermic as that which we could expect for **54**, the reaction for **NSZ** may be endothermic.

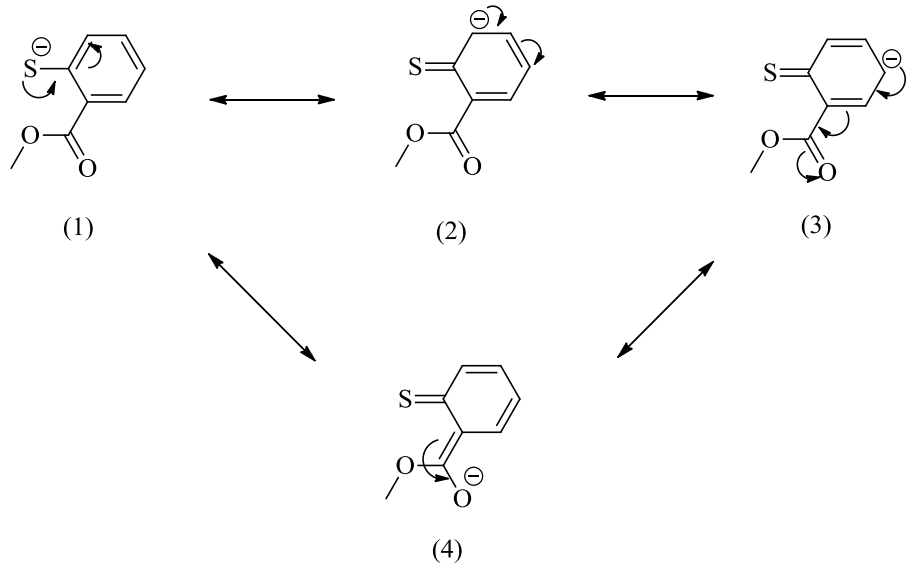

Figure 2.7. The four different resonance forms for the leaving group anions for compounds **46**, **16** and allicin-**16**, methyl benzoate. The arrows in and around each resonance form indicates the movement of electrons and charge around the molecule.

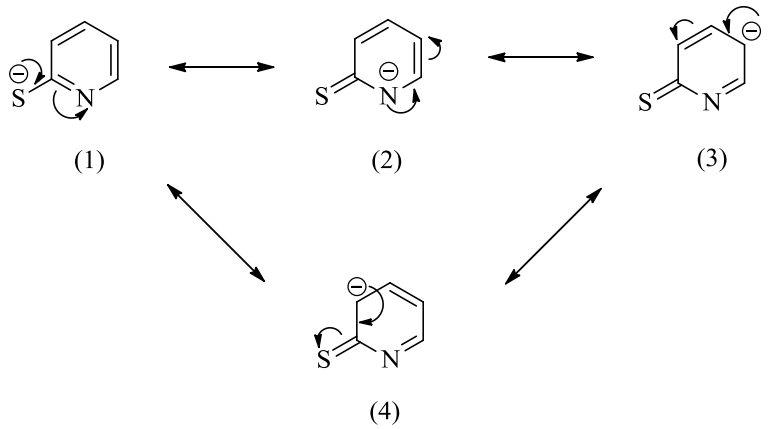

Figure 2.8. The four different resonance forms of the leaving group anion for **59**. The arrows in and around each resonance form indicate the movement of electrons and charge around the molecule.

Compound **92**, which is hydrophilic compared to the other compounds, was found to be inactive with an IC_{50} greater than 200 µM. The high IC_{50} obtained is not surprising as it has previously been reported that the water-soluble counterpart of DADS, *S*-allylmercaptocystine, is three-fold less active against human colon cancer and leukaemia cell-lines (IC_{50} = 150 µM) (Yang *et al*, 2009; Kwon *et al*, 2002; Xiao *et al* 2003). The hydrophilic character of compound **92** may prevent it from crossing the lipophilic membranes of cells, and is therefore unable to carry out its potential anti-cancer effects.

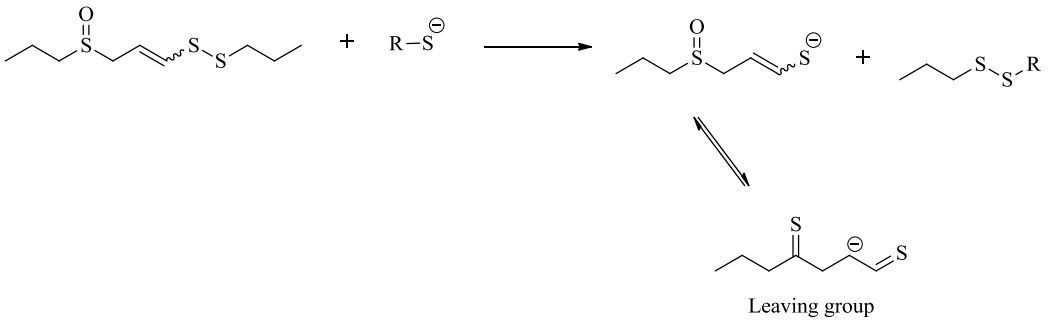

(**i**)

(**ii**)

Figure 2.9. A schematic of the chemical reaction of (**i**) dipropyl ajoene and (**ii**) dipropyl disulfide with the cysteine nucleophile of a protein, resulting in the expulsion of an anion leaving group.

In summary, there appears to be a correlation between thermostability of the leaving group anion of the disulfide and the potency of the compound at inhibiting proliferation of WHCO1 cells. It is also apparent that steric hindrance of side-groups about the disulfide pharmacophore appears to decrease the activity of the compound. It appears that a degree of lipophilicity is required for the compounds to be active. The strength of activity for this series of disulfide compounds appears to correlate to the stability of the leaving group anion which is shown in order of decreasing stability. Furthermore, the predicted pK_a-value for each leaving group, which served as a quantitative means to determine leaving group stability, showed a correlation between leaving group stability and the IC_{50} for the corresponding compound.

The data generated in this study strongly support the hypothesis that garlic OSC compounds act as thiolating agents to proteins in WHCO1 cancer cells and that the mechanism of thiolation is largely thermodynamically controlled.

Chapter 3:

Investigating the *in vitro* anti-cancer mechanism of t-PMB and 200 in WHCO1 oesophageal cancer cells

3.1. Introduction

Evidence from the literature into the *in vitro* anti-cancer mechanism of OSC-induced cancer cell death show that although ajoene, allicin, DATS, DADS and DAS fall into different compound classes, they appear to act via a similar mechanism in cancer cells; by inducing increased levels of ROS and cell-cycle arrest, with the end result being apoptosis. Thus, it is likely that these compounds may have similar targets in cancer cells, and we hypothesise that this reactivity is linked to the presence of the disulfide/polysulfide/thiosulfinate functional group.

For our study, one thiosulfonate and one DADS analogue was selected for further mechanistic analysis. The compound selected from the DADS group was **200,** with an IC_{50} of 9.9 μM, as we had a considerable amount of the compound and it had a lower IC_{50} compared to other DADS analogues. Since the IC_{50}'s for all analogues within the thiosulfonate group were similar in the range of 15 μM, any could be opted for, but we selected **t-PMB** based on the amount of material available. The anti-cancer mechanism of **t-PMB** and **200** were evaluated by assessing morphological changes in treated cells, and assaying whether the compounds induce apoptosis and cell-cycle arrest. Furthermore, a ROS assay was employed to determine whether treatment with **t-PMB** or **200** resulted in increased levels of ROS, which was further probed with the use of inhibitors.

3.2. Results

3.2.1. Proliferation assay (BrdU assay)

The MTT assay measures cell viability, and therefore indirectly measures cell proliferation. To confirm that compounds **t-PMB** and **200** are in fact inhibiting cell proliferation, the BrdU-cell-proliferation assay was used. This assay directly measures cell-proliferation by quantitating the incorporation of tagged uracil into newly synthesised DNA. For the assay, WHCO1 cells were treated with 2 × IC_{50} of **t-PMB** (30 μM) or **200** (20 μM) for 48 hours, with negative controls being cells in media alone or cells treated with the vehicle alone (0.1 % DMSO in media). All experiments were performed in quadruplicate, and significance differences were assessed using the student *t*-test. In agreement with the MTT assay, complete inhibition of cell proliferation was observed when treating with 2 × IC_{50} of both **t-PMB** (*p*-value = 0.001) and **200** (*p*-value = 0.0009) in WHCO1 cells (Figure 3.1).

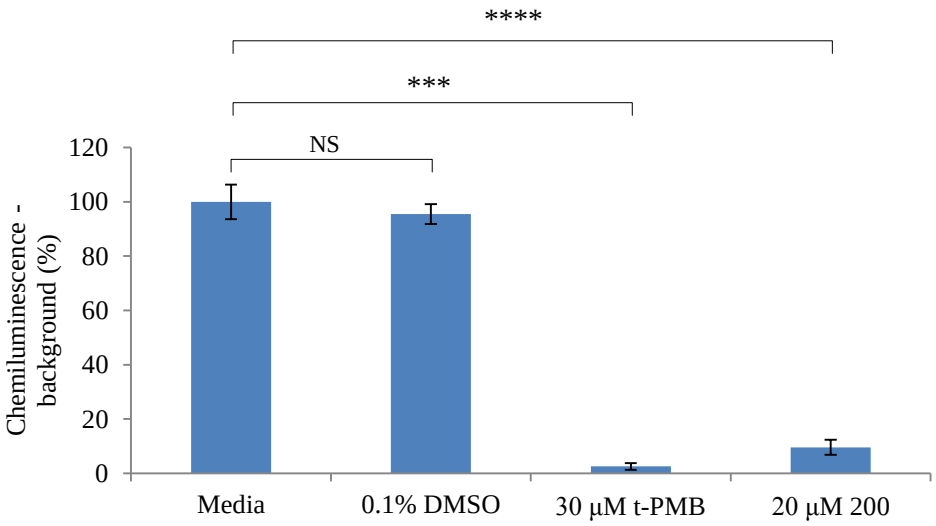

Figure 3.1. Cell proliferation determined through the BrdU assay performed on WHCO1 cells treated with t-PMB and 200. WHCO1 cells were treated with 2 × IC_{50} of **t-PMB** or **200** for 48 hours and cell proliferation was measured using the BrdU assay. Cells in media alone or cells treated with 0.1 % DMSO in media, were used as negative controls. The data was recorded in quadruplicate and are indicated with standard deviations, and significant changes are highlighted (*** indicates *p*-value < 0.005; **** indicates *p*-value < 0.001; NS indicates No Significance).

3.2.2. Cytotoxicity of t-PMB and 200 in tumour and non-tumour cell-lines

The cytotoxicity of **t-PMB** and **200** was assessed by comparing the IC_{50}'s obtained against WHCO1 proliferation at 24-hours to that obtained on the control oesophageal cell-line,

Het1A, which is a non-cancer cell-line of oesophageal epithelial origin, immortalised with the SV40 large T antigen (Het-1A [Het1A] ATCC® CRL-2692™). The 24-hour IC_{50} against WHCO1 cells, which was obtained in independent triplicate experiments, was found to be 25.6 μM for **t-PMB** and 21.6 μM for **200** (Table 3.1), with dose-response curves displayed in Table 3.2. The 24-hour-IC_{50}'s for **t-PMB** and **200** against WHCO1 cells were found to be about 2-fold higher than their 48-hour IC_{50}'s, indicating that both compounds exert a greater inhibitory effect at 48-hours compared to 24-hours. As shown in Table 3.1, the 24-hour IC_{50}'s of **t-PMB** and **200** against Het1A cells, obtained in independent triplicate experiments, were found to be 64.8 μM and 206 μM respectively, indicating that **t-PMB** was 2.5-fold more selective, and **200** was 10-fold more selective, to the WHCO1 oesophageal cancer cell-line over Het1A non-cancer control cell-line. The dose-response curves for **t-PMB** and **200** on Het1A cells are displayed in Table 3.2.

Table 3.1. The 24-hour IC_{50}-values (μM) for **200** and **t-PMB** against WHCO1 and Het1A oesophageal cells using the MTT colorimetric assay obtained in independent triplicate experiments.

Compound Name	Chemical structure	WHCO1 24-hour IC_{50} ± SD (μM)	Het1A 24-hour IC_{50} ± SD (μM)	Fold-selectivity
t-PMB	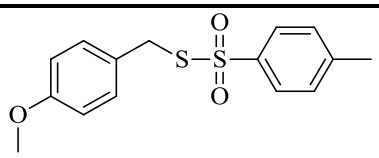	25.6 ± 1.5	64.8 ± 10.9	2.5
200	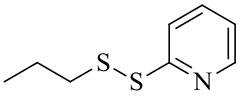	21.6 ± 1.5	206.1 ± 15.1	10

In order to ascertain whether **t-PMB** and **200** are also toxic to other cancers, the 48-hour IC_{50}'s of **t-PMB** and **200** were also determined against A375 human melanoma cells, and were found to be 2.27 μM for **t-PMB** and 3.17 μM for **200** (Table 3.3) for triplicate independent experiments. This data reveals that these compounds are ~ 4-fold more selective at inhibiting the growth of A375 human melanoma cells over WHCO1 oesophageal cancer cells.

Table 3.2. The 24-hour dose–response curves for **t-PMB** and **200** on the WHCO1 oesophageal cancer cells and Het1A cells are displayed.

Compound Name	WHCO1	Het1A
t-PMB	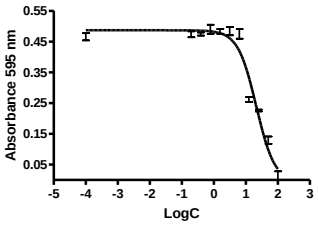	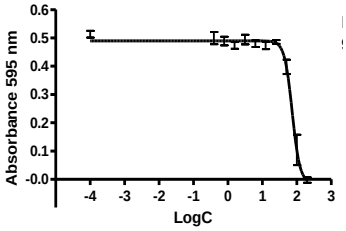
200	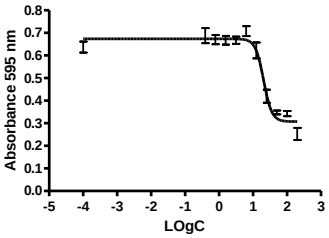	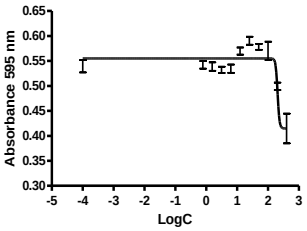

Table 3.3. The dose-response curves and 48-hour IC_{50}-values of **t-PMB** and **200** against A375 human melanoma cell proliferation obtained in independent triplicate experiments.

Compound Name	Chemical structure	Dose-response curve	A375 IC_{50} ± SD (µM)
t-PMB	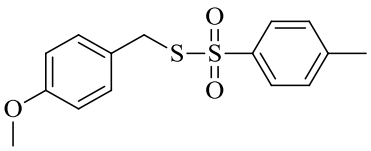	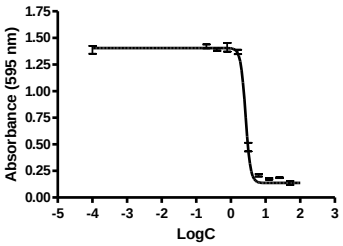	**2.27 ± 1.0**
200	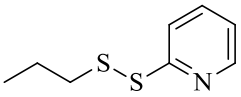	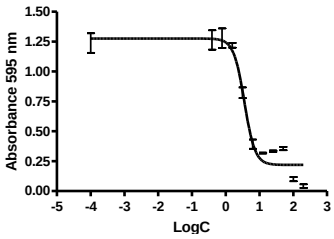	**3.17 ± 0.4**

3.2.3. Morphology

The morphology changes in WHCO1 cells treated with **t-PMB** or **200**, at 2 × their respective 48-hour IC_{50}-values, were assessed through phase contrast images at 1000 × magnification, which were captured at time intervals; 0, 24 and 48 hours post-treatment (Figure 3.2). The morphology images show that some of the cells treated with either **t-PMB** or **200** for 24

hours appear to have condensed and rounded-up, with no defined nucleus and a few cells appearing to have lysed (indicated by the arrow in Figure 3.2), features indicative of apoptosis. These features were found to be present in more cells 48-hours post-treatment with both compounds. All of the cells adopted this morphology in the 48-hour samples, which is to be expected as cells were treated with 2 × 48-hours IC_{50} concentrations.

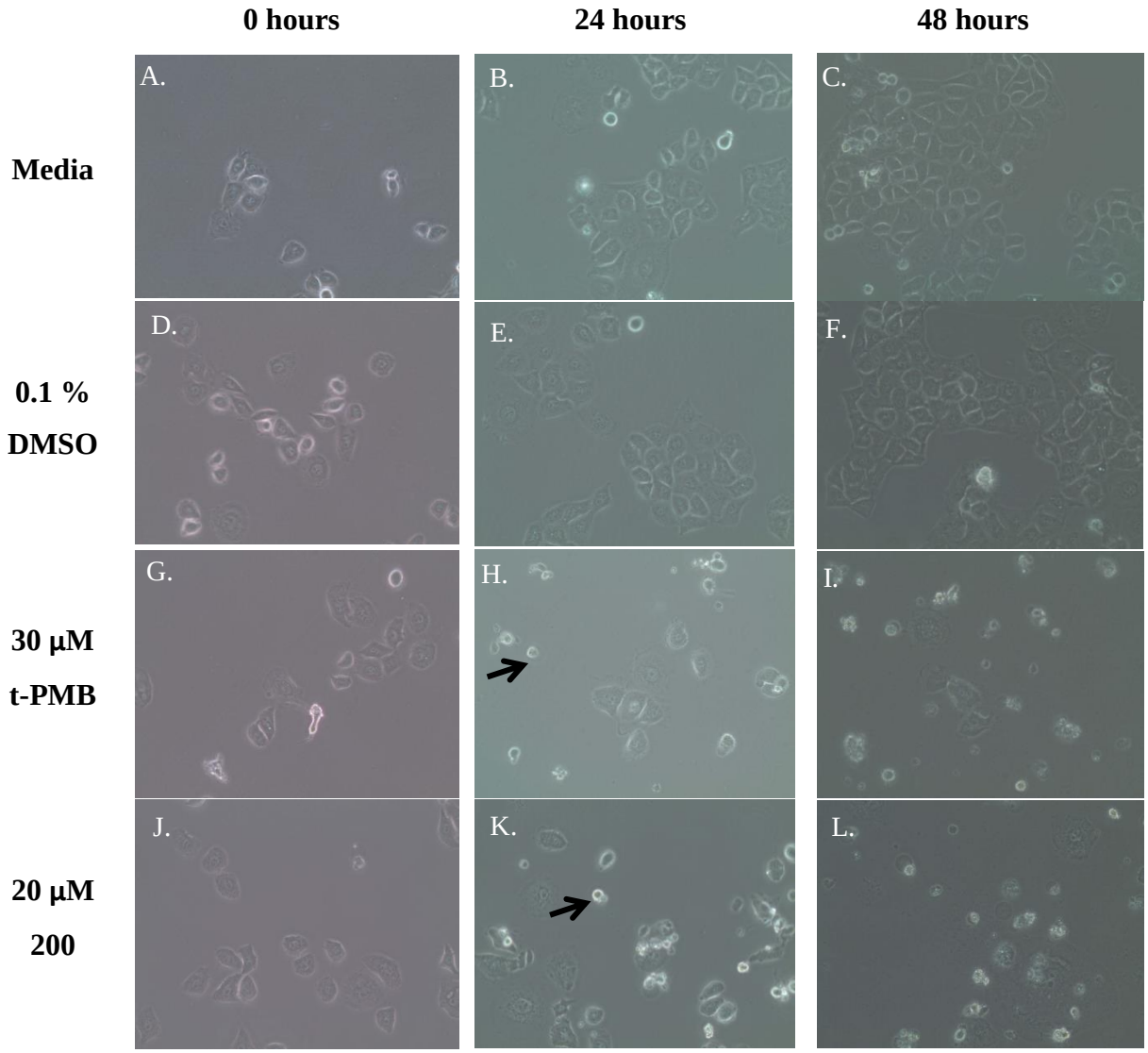

Figure 3.2. Phase contrast images of WHCO1 cells treated with 2 × 48-hour IC_{50} of either t-PMB or 200 for 0, 24 and 48 hours. To determine whether treatment with either **t-PMB** or **200** at 2 × their respective 48-hour IC_{50}'s caused changes in WHCO1 cellular morphology, phase contrast images of treated and untreated cells were taken at 0, 24 and 48 hours at 1000 × magnification. Images **A**, **B** and **C** represent the negative controls with WHCO1 cells in media alone for 0, 24 and 48 hours respectively. Images **D**, **E** and **F** represent the negative control where WHCO1 cells were treated with the vehicle, 0.1 % DMSO in media, at times 0, 24 and 48 hours respectively. Images **G**, **H** and **I** represent WHCO1 cells treated with **t-PMB** at twice the 48-hour IC_{50} (30 µM) for 0, 24 and 48 hours respectively. Images **J**, **K** and **L** represent WHCO1 cells treated with **200** at twice its 48-hour IC_{50} (20 µM) for 0, 24 and 48 hours respectively. The arrow highlights a cell that has condensed and rounded up indicative of apoptosis.

3.2.4. Cell-cycle analysis

Fluorescence activated cell sorting (FACS) analysis was performed to determine whether **t-PMB** or **200** elicit any changes to the cell-cycle in WHCO1 cells. Cell-cycle analysis was performed on WHCO1 cells at 0, 6, 12 and 24 hours post-treatment using 2 × 24-hour IC_{50} concentrations of **t-PMB** (52 μM) or **200** (40 μM). Data were compared to the negative controls of WHCO1 cells treated with 0.1 % DMSO in media or media alone. Propidium iodide (PI) was used to stain the DNA of cells fixed with 70% ethanol. Since PI stains ribonucleic acids (RNA) and DNA, the cell lysate was treated with RNase A to remove the RNA. Once the DNA was stained, fluorescence was measured at 480 nm, and the cells were grouped according to cell-cycle phase. Over 10000 cells were counted per analysis which is the minimum requirement for FACS analysis. The percentage of coefficient of variance (% CV) was set at 8 % for significance. For all samples tested, the % CV was found to be below 8 %. For WHCO1 cells treated with either **t-PMB** (Figure 3.3 and 3.4) or **200** (Figure 3.5 and 3.6), a time-dependent increase in the number of cells arrested in the G_2/M-phase of the cell cycle, with a concurrent decrease in the population of cells in the S- and G_1-phases, were observed. An increase in the amount of debris formed after the 24-hour treatment was also observed, indicative of cell lysis.

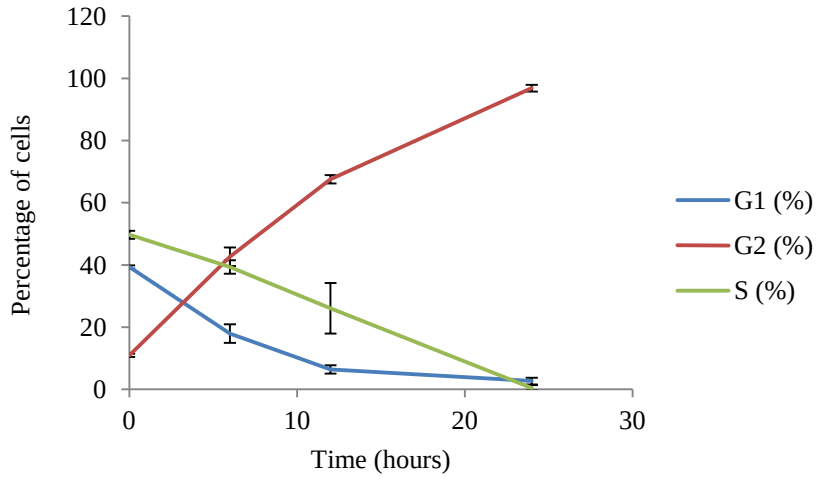

Figure 3.3. Populations of cells in the S, G_1 and G_2 phases of the cell-cycle in WHCO1 cells treated with t-PMB. To determine whether **t-PMB** induced cell-cycle arrest in WHCO1 cells, cells were treated with **t-PMB** at 2 × 24-hour IC_{50} concentration (52 μM), and FACS analysis was performed 0, 6, 12 and 24 time-intervals post-treatment.

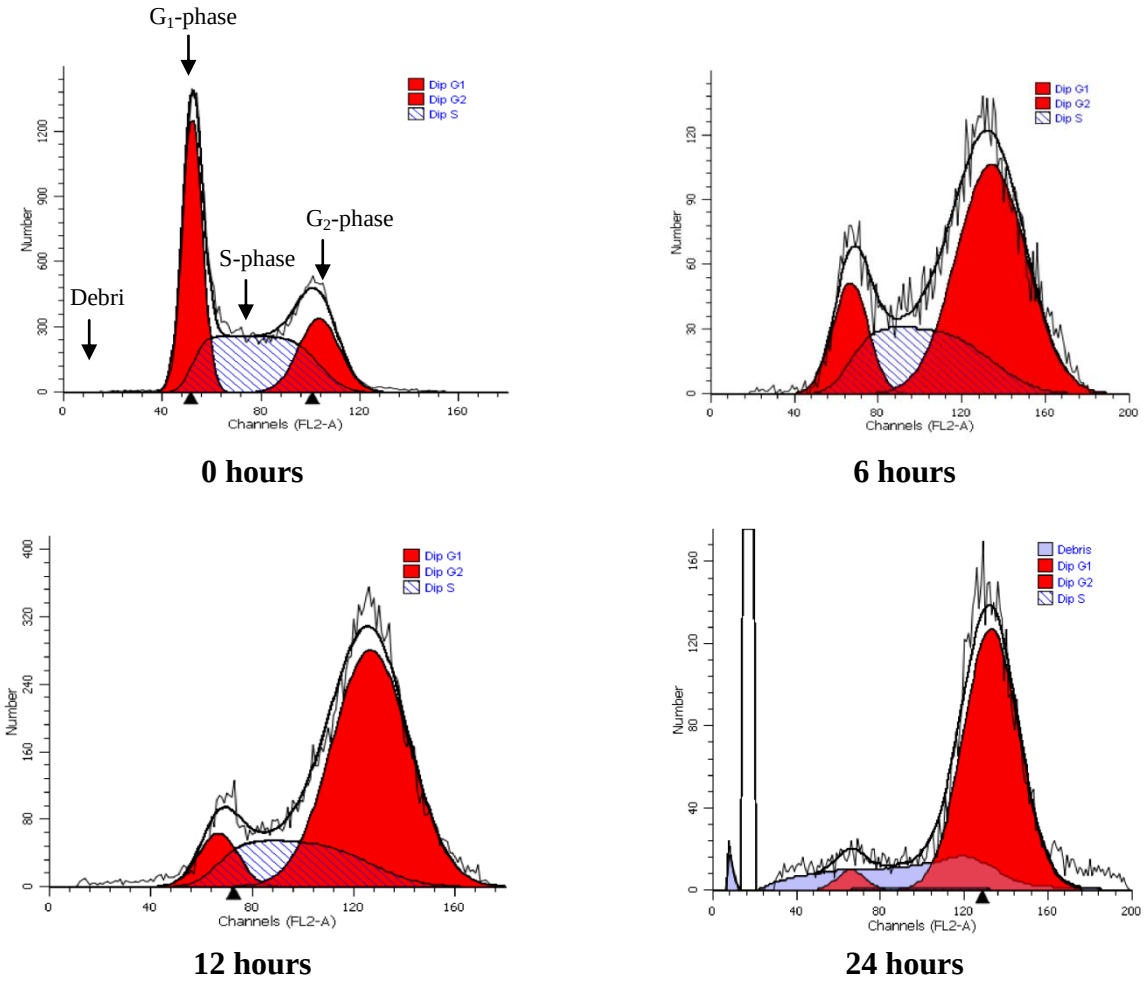

Figure 3.4. Cell-cycle profiles of WHCO1 cells treated with t-PMB in a time-dependent manner. WHCO1 cells were treated with 2 × 24-hour IC_{50} of **t-PMB** (52 µM) for 0, 6, 12 and 24 hours for FACS analysis. A time-dependent increase in G_2/M cell-cycle arrest was observed, with a concurrent decrease in the G_1- and S-populations.

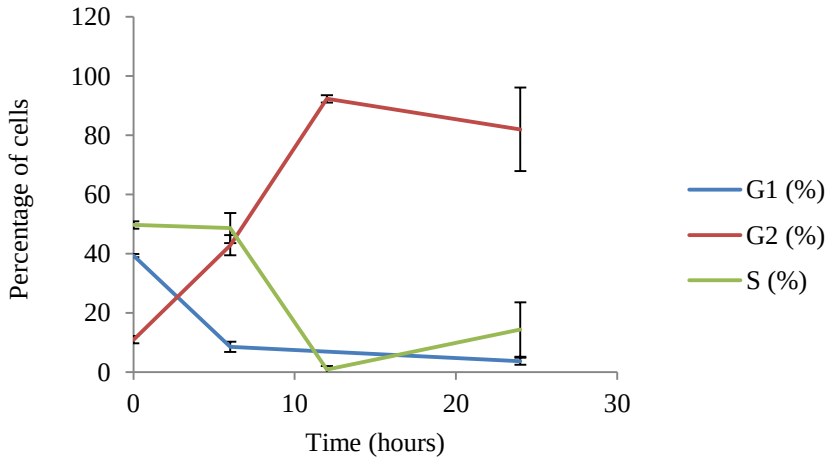

Figure 3.5. Populations of cells in the S, G_1 and G_2 phases of the cell-cycle in WHCO1 cells treated with 200. To determine whether **200** induced cell-cycle arrest in WHCO1 cells, cells were treated with **200** at 2 × 24-hour IC_{50} concentration (40 µM), and FACS analysis was performed 0, 6, 12 and 24 time-intervals post-treatment.

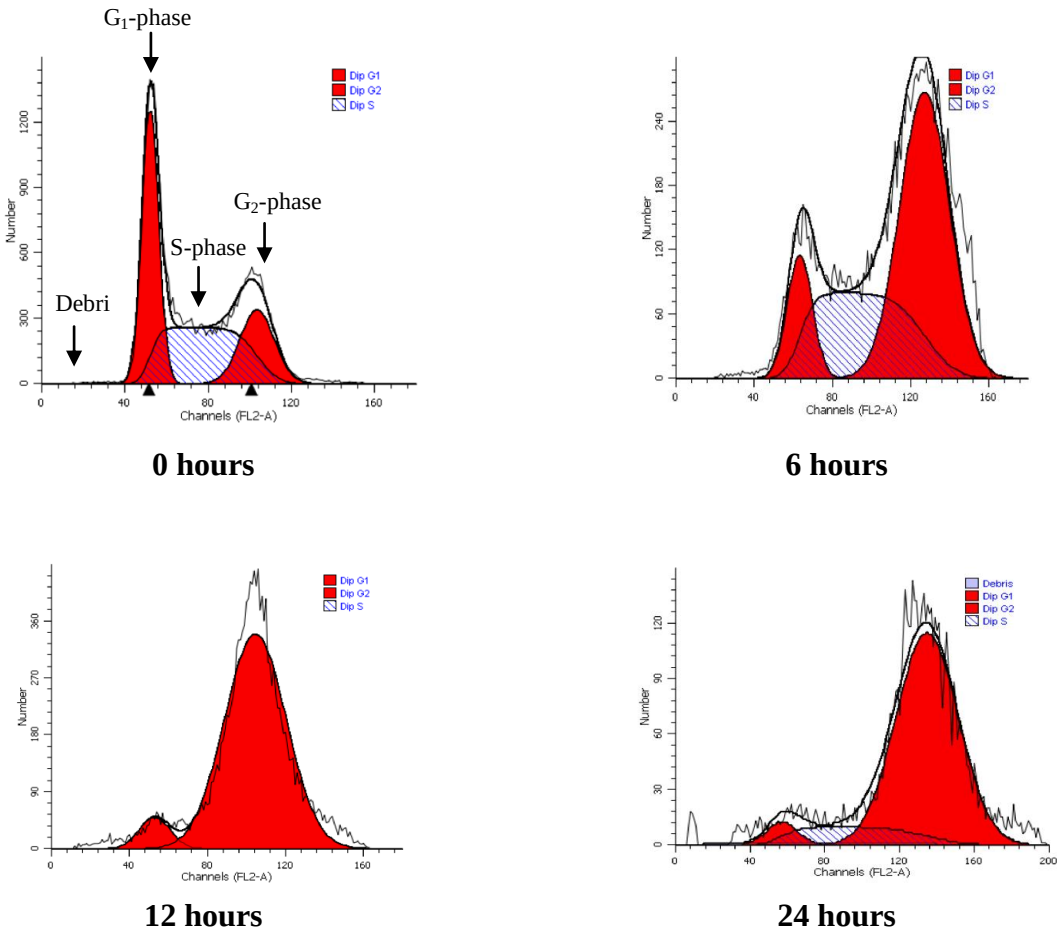

Figure 3.6. Cell-cycle profiles of WHCO1 cells treated with 200 in a time-dependent manner. WHCO1 cells were treated with 2 × 24-hour IC_{50} of **200** (40 µM) for 0, 6, 12 and 24 hours for FACS analysis. A time-dependent increase in G_2/M cell-cycle arrest was observed, with a concurrent decrease in the G_1- and S-populations.

3.2.5. Apoptosis (histone dissociation)

During apoptosis, the DNA within cells become fragmented to produce histone-associated DNA fragments of ~ 200 base pairs, which are released into the cytoplasm, providing a method for apoptosis detection and quantification. Roche has developed an ELISA-based assay that detects histone-associated DNA fragments in the cytoplasm after treatment, which can be used as a measure of apoptosis. WHCO1 cells were treated with **t-PMB** or **200** for 24 hours and then lysed, where after the lysate was transferred to a streptavidin-coated multi-plate. Thereafter, a mixture of anti-histone-biotin (which binds to the streptavidin multi-plate through biotinylation) and anti-DNA-POD was added to the multi-plate to detect cytoplasmic histone-associated DNA fragments. Unbound components were removed through a wash-step, and the amount of histone-associated DNA fragments were detected photometrically

using the ABTS substrate (see Materials and Methods section). Experiments were performed in triplicate and significance was determined using the student *t*-test.

The positive control used in the assay was a DNA-histone complex provided with the Roche® Cell Death Detection ELISA^{PLUS} kit, and the negative control was cells in 0.1 % DMSO in media. Apoptosis was observed in WHCO1 cells treated with IC_{50} (*p*-value = 0.02) and 2 × IC_{50} (*p*-value = 0.02) of **t-PMB** for 24 hours, although it was not observed in WHCO1 cells treated with **t-PMB** ½ IC_{50} or $^1/_8$ IC_{50} (Figure 3.7). This finding supports the morphology changes shown in Figure 3.9, where WHCO1 cells treated with **t-PMB** at 2 × IC_{50} and IC_{50} appeared shrivelled indicative of apoptosis, but WHCO1 cells treated with **t-PMB** at ½ IC_{50} and $^1/_8$ IC_{50} had similar morphologies to the untreated control cells.

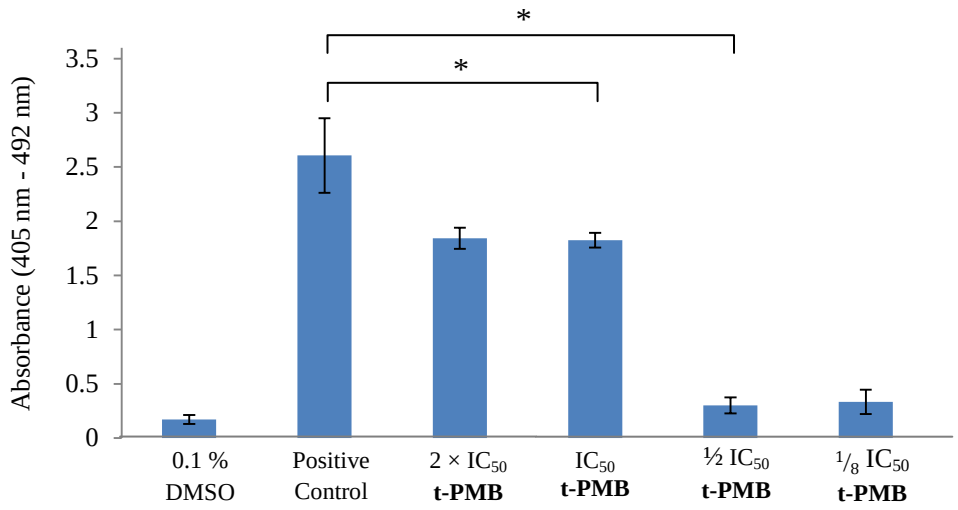

Figure 3.7. Apoptosis in WHCO1 cells treated with t-PMB in a dose-dependent manner. A histone-associated DNA fragmentation assay was performed to quantitate apoptosis in WHCO1 cells treated with **t-PMB** at 2 × IC_{50}, IC_{50}, ½ IC_{50} and $^1/_8$ IC_{50} for 24 hours. The negative control was cells treated with 0.1 % DMSO in media alone, and the positive control was a DNA-histone-complex, which was provided with the kit. The data are indicated with ± SD and significant changes are highlighted (* indicates *p*-value < 0.05).

WHCO1 cells treated with **200** were also found to display increased levels of apoptosis in cells treated with 2 × IC_{50} (*p*-value = 0.01), IC_{50} (*p*-value = 0.003) and ½ IC_{50} (*p*-value = 0.001), with no significant effect at $^1/_8$ IC_{50} (Figure 3.8). Furthermore, morphology images indicated in Figure 3.9 show that cells treated with at least 10 μM **200** have shrivelled and undertaken a morphology indicative of apoptosis.

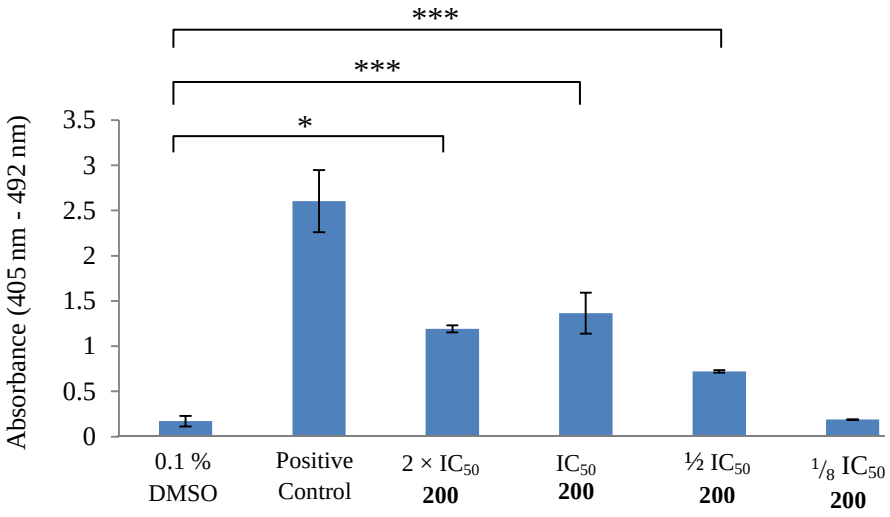

Figure 3.8. Apoptosis in WHCO1 cells treated with 200 in a dose-dependent manner. A histone-associated DNA fragmentation assay was performed to quantitate apoptosis in WHCO1 cells treated with **200** at 2 × IC_{50}, IC_{50}, ½ IC_{50} and $^{1}/_{8}$ IC_{50} for 24 hours. The negative control was cells treated with 0.1 % DMSO in media alone and the positive control was a DNA-histone-complex, which was provided with the kit. The data are indicated with ± SD, and significant changes are highlighted (* indicates *p*-value < 0.05, *** indicates a *p*-value < 0.005).

3.2.6. ROS production

To determine whether ROS production is related to the ability of disulfides and thiosulfonates to inhibit cancer cell proliferation, ROS production was investigated. To this end, the 2', 7' – dichlorodihydroflourescin diacetate (DCFH-DA) reagent, which fluoresces upon reaction with ROS, was used. For the assay, WHCO1 cells were treated with **t-PMB** or **200** at ½ IC_{50}, IC_{50} or 2 × IC_{50} concentrations, and subsequent fluorescence was recorded at 0, 1, 2, 3 and 6 hours post-treatment. The positive control used in the assay was doxorubicin (DOX), which is a clinical cancer drug with a mechanism that involves production of ROS.

As seen in Figure 3.10, treatment with the positive control, 5 μM DOX, resulted in a significant increase in ROS levels for up to 6-hours. The levels of ROS in the untreated sample also appear to increase with time, which may be a result of more cells being present due to cell-proliferation, hence more endogenous ROS being detected. Furthermore, a time- and dose-dependent increase in ROS was detected for WHCO1 cells treated with **t-PMB**.

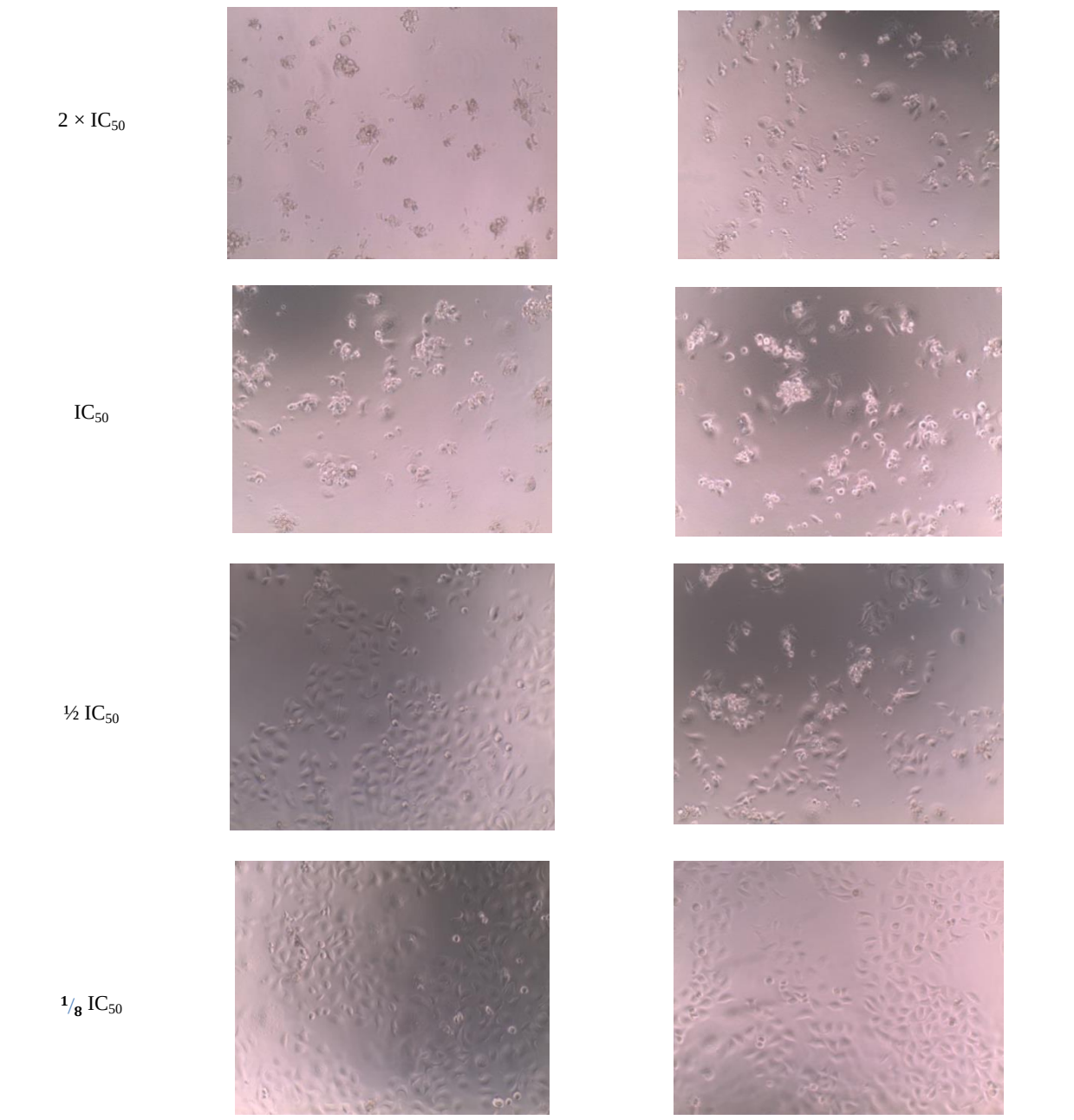

Figure 3.9. Phase contrast images of morphological changes in WHCO1 cells treated with either t-PMB or 200 for 24 hours. The phase contrast images represent WHCO1 cells treated with **t-PMB** or **200** at 2 × IC_{50}, IC_{50}, ½ IC_{50} and $^{1}/_{8}$ IC_{50} for 24 hours. Apoptosis induction was detected using the Roche® Cell Death Detection ELISA^{PLUS} kit.

Neither a dose- nor a time- dependent increase in ROS levels were detected for WHCO1 cells treated with **200** when compared to media alone, although treatment with **200** at 2 × IC_{50} (40 μM) at the 1-hour time-point was found to be significant (Figure 3.11). It should be noted that **t-PMB** is far more effective at inducing ROS compared to **200**, even though **200** had a lower

IC_{50}, which raises the question as to whether ROS production is important for the anti-proliferative activity of garlic OSC.

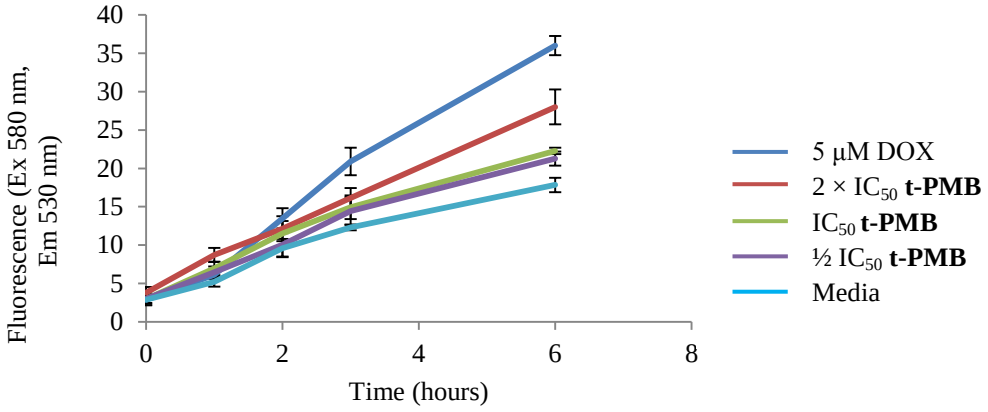

Figure 3.10. ROS production in WHCO1 cells treated with t-PMB in a dose- and time-dependent manner. WHCO1 cells were treated with **t-PMB** at 2 × IC_{50}, IC_{50} and ½ IC_{50} for 0, 1, 2, 3 and 6 hours. Control cells were treated with media alone or 0.1 % DMSO in media. As a positive control, WHCO1 cells were treated with 5 µM doxorubicin (DOX). The experiment was performed in triplicate and the data are indicated with ± SD.

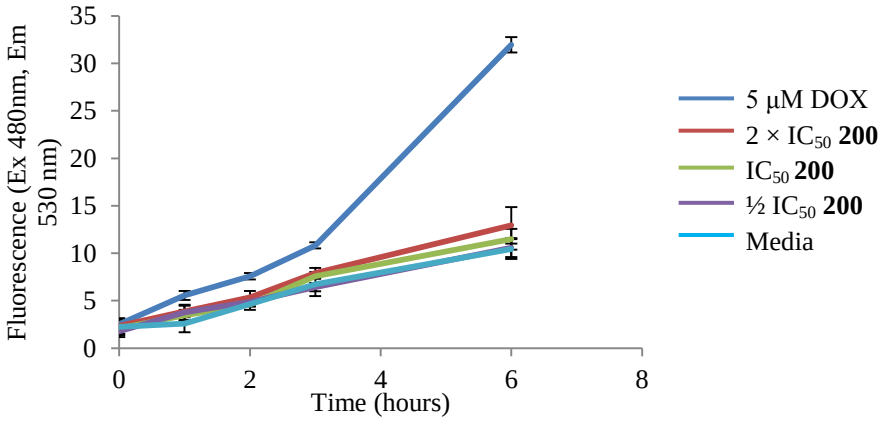

Figure 3.11. ROS production in WHCO1 cells treated with 200 in a dose- and time-dependent manner. WHCO1 were cells treated with **200** at 2 × IC_{50}, IC_{50} and ½ IC_{50} for 0, 1, 2, 3 and 6 hours. Control cells were treated with media alone or 0.1 % DMSO in media. As a positive control, WHCO1 cells were treated with 5 µM doxorubicin (DOX). The experiment was performed in triplicate and the data are indicated with ± SD.

3.2.7. ROS inhibition

To determine whether ROS production is important in the anti-proliferative activity of **t-PMB** and **200**, WHCO1 cells were pre-treated for 1 hour with known ROS inhibitors, and subsequent cell viability was assessed through the MTT assay.

Firstly, ROS scavengers were tested for their ability to scavenge OSC-induced ROS production in WHCO1 cells treated with **t-PMB** or **200**. The ROS scavengers, whose concentrations were based on literature, were chosen to be *N*-acetyl-L-cysteine (NAC) (Dirsch et al. 1998), L-ascorbic acid (ascorbate) (Das et al. 2007) and TROLOX (Kelkel et al. 2012).

*Compound **t-PMB**; ROS inhibitors and ROS production:* In agreement with previous findings, WHCO1 cells treated with **t-PMB** for 3 hours at the IC_{50} concentration generated a 1.5-fold increase in ROS relative to the untreated controls (Figure 3.12). The levels of ROS production by **t-PMB** (*p*-value = 0.003) were found to be similar to the levels produced by DOX (*p*-value = 0.008). Treatment with any of the 3 ROS inhibitors alone resulted in a significant decrease in ROS levels to below baseline levels, indicative of scavengers removing endogenous ROS from the WHCO1 cells. Treating WHCO1 cells with **t-PMB** in combination with ROS scavengers; NAC (*p*-value = 8×10^{-5}), ascorbate (*p*-value = 8×10^{-5}) and TROLOX (*p*-value = 4×10^{-5}) significantly decreased ROS levels compared to the **t-PMB**-treated sample, indicating that all ROS inhibitors effectively scavenged **t-PMB**-induced ROS production.

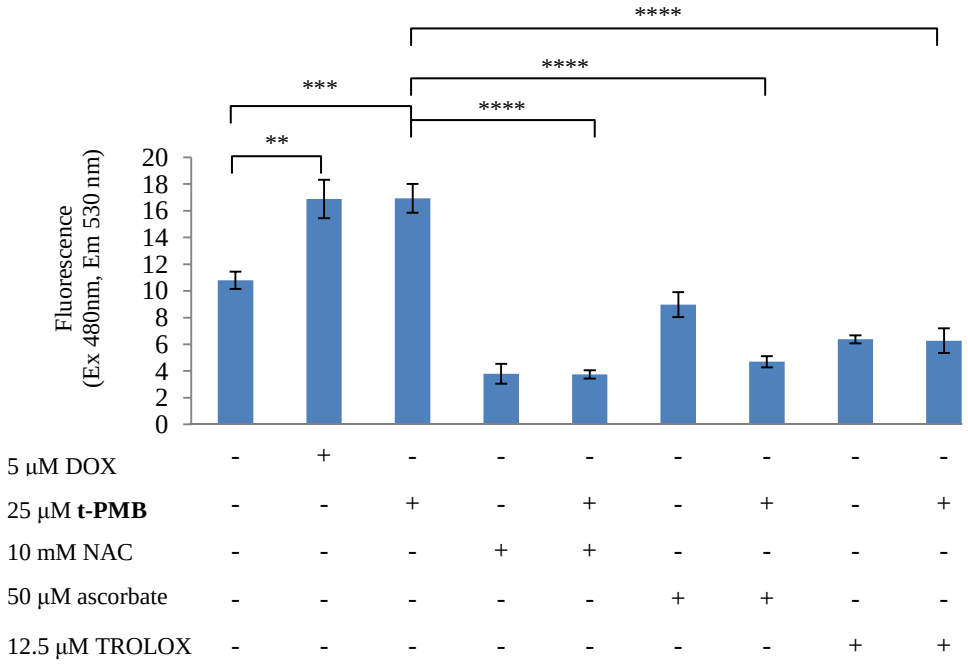

Figure 3.12. ROS inhibition assay in t-PMB-treated cells. To confirm whether ROS scavengers; NAC, ascorbate or TROLOX scavenge **t-PMB**-induced ROS production, WHCO1 cells were treated with either 25 µM **t-PMB** alone or 25 µM **t-PMB** in combination with ROS scavengers; NAC, ascorbate or TROLOX for 3 hours. The data was collected in triplicate and is displayed as a mean ± SD. Significant changes are highlighted (** indicates *p*-value < 0.01, *** indicates *p*-value < 0.005, **** indicates *p*-value < 0.001).

*Compound **t-PMB**; ROS inhibitors and cell proliferation:* To determine whether ROS production is important for the anti-proliferative activity of **t-PMB**, WHCO1 cells were treated with the IC_{50} concentration of **t-PMB** in the presence of ROS scavengers; 7.5 mM NAC, 50 µM ascorbate or 12.5 µM TROLOX, and the viability was assayed using the MTT assay. As expected (Figure 3.13), treating WHCO1 cells with **t-PMB** at its IC_{50} concentration resulted in a 50 % reduction in cell viability (*p*-value = 0.01). Treating WHCO1 cells with the inhibitors alone was found to have no effect on cell viability. When treating WHCO1 cells with **t-PMB** in the presence of the ROS scavengers, different effects on cell viability were observed. WHCO1 cells treated with **t-PMB** in the presence of NAC resulted in cell viability levels similar to that of the untreated control, indicating that pre-treatment with NAC prevented **t-PMB**-induced reduction in cell viability. On the other hand, treatment with **t-PMB** in the presence of ascorbate (*p*-value = 0.01) or TROLOX (*p*-value = 0.01) resulted in a significant reduction in cell viability, similar to the viability levels observed for WHCO1 cells treated with **t-PMB** alone, indicating that although ascorbate and TROLOX reduce ROS levels in **t-PMB**-treated cells, they are ineffective at inhibiting the **t-PMB**-induced reduction in cell viability.

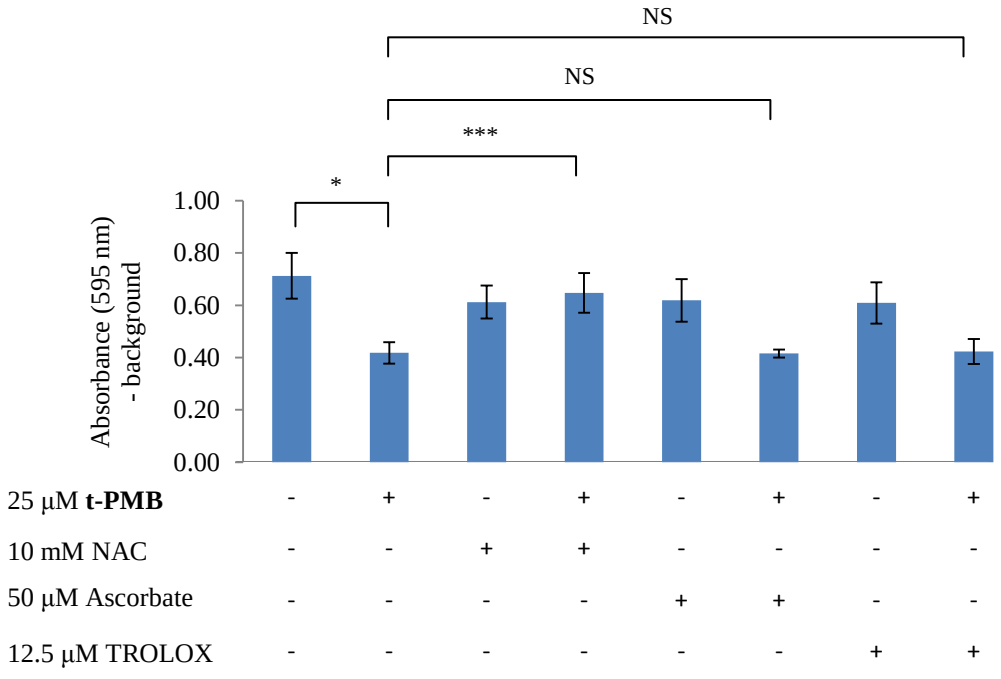

Figure 3.13. Cell viability (MTT) of WHCO1 cells treated with t-PMB in the presence of ROS scavengers. WHCO1 cells were treated with either 25 µM **t-PMB** alone or 25 µM **t-PMB** in combination with ROS inhibitors; NAC, ascorbate or TROLOX for 24 hours, and cell viability was quantified using the MTT assay. The data was collected in triplicate, and displayed as a mean ± SD with significant changes highlighted (* indicates *p*-value < 0.05, *** indicates *p*-value < 0.005; NS indicates No Significant difference).

These data seem to imply that NAC is capable of reversing the anti-proliferative effects of **t-PMB**, however, the ROS scavengers, ascorbate and TROLOX are ineffective. The implication of these results will be discussed in greater detail in the Discussion section.

*Compound **200**; ROS inhibitors and ROS production:* As observed before, DOX treatment for 3 hours caused a significant (*p*-value = 0.003) increase in the levels of ROS in WHCO1 cells, and treatment with any of the three ROS inhibitors alone resulted in a significant decrease in ROS levels of untreated WHCO1 cells to below baseline levels, indicative of scavengers removing endogenous ROS from the WHCO1 cells. Treatment with **200** at IC_{50} concentration for 3 hours resulted in no significant increase in ROS (Figure 3.14). It was therefore expected that co-treatment of **200** with the ROS inhibitors should have no effect on cell viability, as ROS was not generated by **200**.

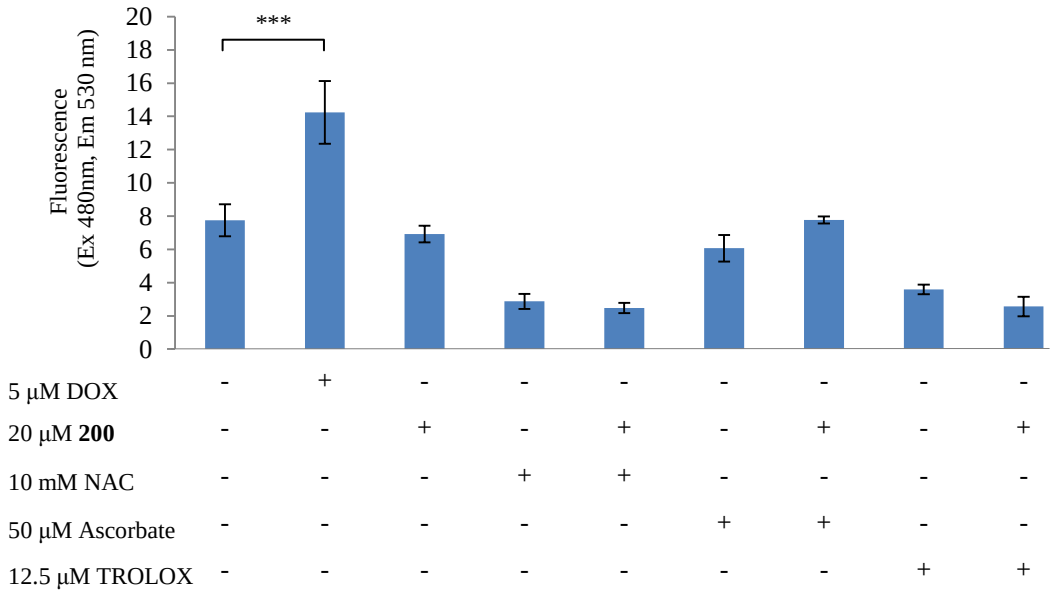

Figure 3.14. ROS inhibition assay in 200-treated cells. To confirm whether ROS scavengers; NAC, ascorbate or TROLOX scavenge **200**-induced ROS production, WHCO1 cells were treated with either 20 µM **200** alone or 20 µM **200** in combination with ROS scavengers; 7.5 mM NAC, 50 µM ascorbate or 12.5 µM TROLOX for 3 hours. The data was collected in triplicate and is displayed as a mean ± SD. Significant changes are highlighted (*** indicates *p*-value < 0.005).

*Compound **200**; ROS inhibitors and cell proliferation:* In the MTT assay (Figure 3.15), we observed that treating WHCO1 cells with **200** at its IC_{50} concentration resulted in the expected 50 % decrease in cell viability. Furthermore, pre-treating the cells with NAC, ascorbate or TROLOX alone resulted in cell-viability levels similar to that of untreated cells,

indicating that treatment with the ROS scavengers does not change cell viability. However, treating WHCO1 cells with **200** and NAC (*p*-value = 0.02) resulted in cell-viability similar to that of the untreated control, even though ROS production was clearly not observed (Figure 3.14). This result suggests that NAC may not be restoring cell-viability through its ROS scavenging properties, but may be interacting directly with the compound. We hypothesised that NAC, a cysteine-derivative with a thiol group, may be restoring WHCO1 cell viability by directly reacting with the disulfide and thiosulfonate functional groups of **200** and **t-PMB**, thereby lowering the concentrations of the OSC within the cell, and preventing the OSC from inhibiting WHCO1 cell viability through a mechanism independent of ROS. This is supported as treatment of WHCO1 cells with **200** in the presence of ascorbate and TROLOX did not restore cell viability, even though both scavengers reduce ROS levels in WHCO1 (Figure 3.14).

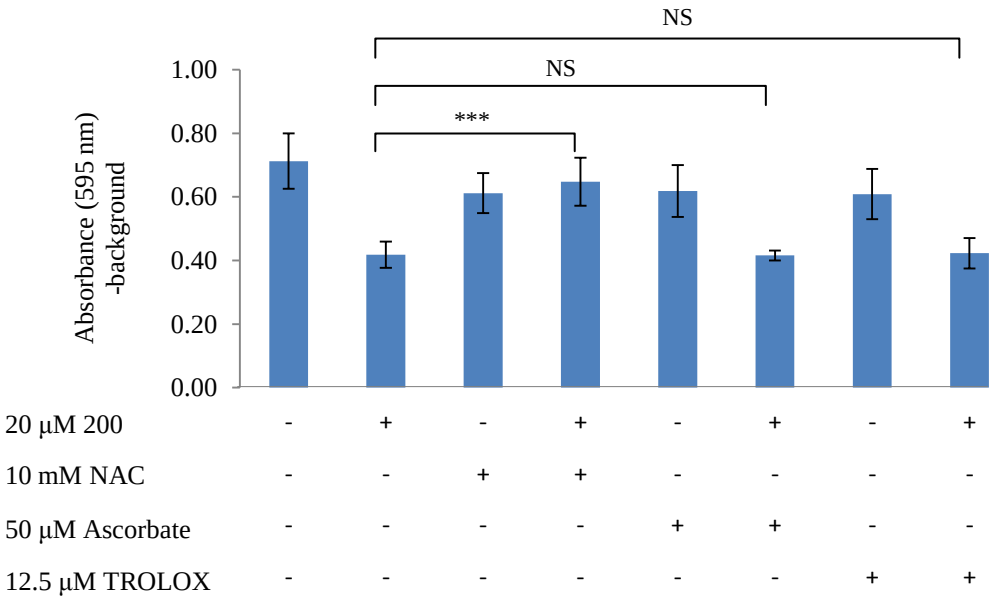

Figure 3.15. Cell viability (MTT) of WHCO1 cells treated with 200 in the presence of ROS scavengers. WHCO1 cells were treated with either 20 µM **200** alone or 20 µM **200** in combination with ROS scavengers; NAC, ascorbate or TROLOX for 24 hours and cell viability was quantified using the MTT assay. The data was collected in triplicate and displayed as a mean ± SD with significant changes highlighted (*** indicates *p*-value < 0.005; NS indicates No Significant difference).

3.2.8. Reaction between NAC and t-PMB

Although NAC, TROLOX and ascorbate scavenged **t-PMB**-induced ROS production, only pre-treatment with NAC restored the cell viability of WHCO1 cells treated with **t-PMB**. Furthermore, although ROS production was not detected in WHCO1 cells treated with IC_{50} concentrations of **200** for 3 hours, pre-treatment with NAC also restored cell viability within these **200**-treated cells. We therefore hypothesised that pre-treatment with NAC may have restored WHCO1 viability through a mechanism other than ROS scavenging. We proposed that NAC, a cysteine-derivative with an acetyl group attached at the nitrogen, may be reacting with **t-PMB** and **200** through mixed disulfide bond formation between the disulfide functional group in the OSC and the thiol group in NAC, thereby lowering the concentration of the OSC within the cell. To determine whether **t-PMB** and NAC are able react, an *in vitro* reaction between **t-PMB** and NAC was performed by Mr. Daniel Kusza at the Chemistry Department of UCT, in tetrahydrafuran (THF) at room temperature overnight. The reaction product was isolated and characterised by NMR (Figure 3.17), and was shown to be *N*-acetyl cysteine methoxybenzyl disulfide (Figure 3.16), a mixed disulfide product of **t-PMB** and NAC. This result supports the hypothesis that NAC may reacting directly with **t-PMB** or **200** in the WHCO1 cells to form a mixed disulfide product, thereby preventing **t-PMB**- or **200**-from inhibiting WHCO1 cell growth.

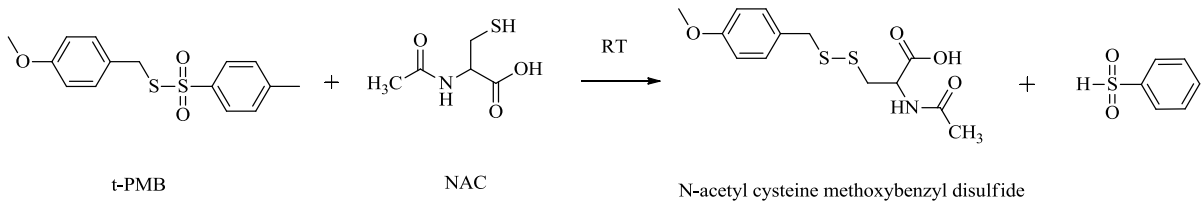

Figure 3.16. Chemical reaction between NAC and t-PMB. The schematic represents the reaction between **t-PMB** and NAC, resulting in the product, *N*-acetyl cysteine methoxybenzyl disulfide, which may result in lower **t-PMB** concentrations within cells, preventing **t-PMB** from inducing its anti-cancer effects.

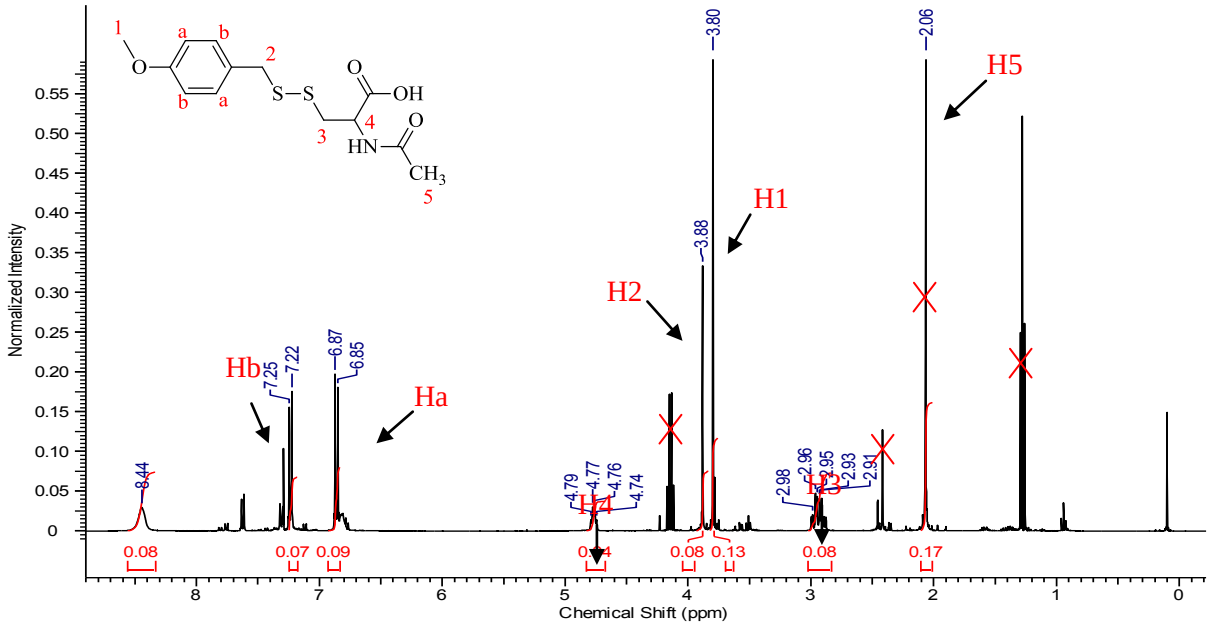

Figure 3.17. NMR profile for *N*-acetyl cysteine methoxybenzyl disulfide. To determine whether NAC and **t-PMB** react, an *in vitro* chemical reaction between NAC and **t-PMB** was carried out in THF at room temperature. The product of the reaction was purified by silica gel chromatography and characterised through nuclear magnetic resonance (NMR), and found to be *N*-acetyl cysteine methoxybenzyl disulfide, a mixed-disulfide product of **t-PMB** and NAC. Characterisation of each hydrogen atom is colour-coded and numbered, with the representative hydrogen atom numbered in the *N*-acetyl cysteine methoxybenzyl disulfide chemical structure. Each peak representing the solvent, ethyl acetate, is crossed out in red.

3.3. Discussion

One compound from each of the disulfide and thiosulfonate compound classes were chosen for further mechanistic evaluation against WHCO1 cell death. Compounds **t-PMB** and **200** were selected based on their low IC_{50}-values, and because large amounts of the synthesised material was available.

It was evident that a degree of selectivity was observed for cancer cells over non-cancer cells when treating with **t-PMB** and **200**. Compound **t-PMB** was found to be 2.5-fold selective, and **200** was 10-fold selective, to the WHCO1 cancer cell-line over the Het1A non-cancer cell-line. The lower IC_{50}, and greater selectivity to cancer cells over non-cancer cells, suggests that **200** may be a better candidate as a chemotherapeutic in terms of reduced cytotoxicity. The 48-hour IC_{50} of **t-PMB** and **200** against the A375 human melanoma was found to be 2.27 μM and 3.17 μM respectively, indicating that both compounds are more active against the A375 cell growth than WHCO1 cell growth, suggesting that the compounds may be selective in their anti-cancer activity.

The MTT assay, which is a measure of cell viability, is commonly used as an indirect measure for cell-proliferation. To confirm the anti-proliferative effects of **t-PMB** and **200**, the BrdU assay was performed on WHCO1 treated with either compound at 2 × IC_{50}, which reduced cell proliferation levels similar to that of background levels. This result is in strong agreement with the MTT assay, and furthermore suggests that the MTT results for the remaining data series are reliable. Phase contrast images of morphological changes in WHCO1 cells treated with 2 × 48 hour IC_{50} of **t-PMB** (30 μM) or **200 (**20 μM) showed that most cells had lost their regular morphology and shrivelled, indicative of apoptosis.

Garlic OSC's, to include; ajoene (Li *et al*. 2002; Dirsch *et al*. 2002), DATS (Kim *et al*. 2007; Xiao *et al*. 2004), DADS (Filomeni *et al*. 2003; Das *et al*. 2007; Yang *et al*. 2009), and allicin (Kim *et al*. 2008), have been reported to induce apoptosis in a number of cancer cell-lines. Both **t-PMB** and **200**, like garlic-derived organosulfur compounds, appeared to induce a dose-dependent increase in the levels apoptosis, although the measured levels of apoptosis for each compound was found to be the same when treating with IC_{50} and 2 × IC_{50} concentrations. An explanation for this may be that treating cells with the compounds at twice their respective 24-hour IC_{50}'s for 24 hours may result in most of the cells dying, resulting in broken extracellular membranes. The histones therefore escape the intracellular

environment, and enter the media environment, where it may become unstable and degrade, becoming undetectable to the histone anti-body. We observed that the apoptosis levels in WHCO1 cells treated with **t-PMB** at ½ IC_{50} were similar to background levels, however the levels of apoptosis were elevated in cells treated with **200** at ½ IC_{50}, which seems to imply that **200** is more effective at inducing apoptosis than **t-PMB**.

FACS analysis in WHCO1 cells treated with 2 × 24-hour IC_{50} of **t-PMB** or **200** showed a time-dependent increase in G_2/M cell-cycle arrest, with a concurrent decrease in the number of cells in the G_1- and S-phase of the cell-cycle, although the G_2/M arrest for **200** peaked earlier than for **t-PMB**, which implies that the kinetics of cell-cycle arrest by **200** may be more rapid compared to **t-PMB**. Although G_2/M cell-cycle arrest has been reported for garlic-derived OSCs; ajoene (Li *et al*. 2002; Dirsch *et al*. 2002), DATS (Kim *et al*. 2007; Xiao *et al*. 2004), DADS (Filomeni *et al*. 2003; Das *et al*. 2007; Yang *et al*. 2009), and allicin (Kim *et al*. 2008), this is the first time it is reported for a thiosulfonate compound.

The ROS assay showed a significant dose- and time- dependent increase in the levels of ROS produced in WHCO1 cells treated with **t-PMB,** but not for **200**, which only showed a significant increase in ROS levels when treating with 2 × IC_{50} (40 μM) for 1 hour. It has previously been reported that treating cancer cells with garlic OSCs, to include; ajoene (Dirsch *et al*. 1998), DATS (Kim *et al*. 2007), DADS (Das *et al*. 2007; Kwon *et al*. 2002; Wu *et al*. 2005; Filomeni *et al*. 2003) and DAS (Das *et al*. 2007), result in increased ROS productions, and although thiosulfonates are not reported to be found in garlic, **t-PMB** appears to also induce increased levels of ROS in cancer cells, similar to that of garlic-derived OSC.

To determine whether ROS production is important for the anti-cancer mechanism of OSC, WHCO1 cells were treated with **t-PMB** or **200** in combination with ROS scavengers; NAC, ascorbate and TROLOX. It was observed that WHCO1 cells treated with **t-PMB** in combination with either ROS scavenger showed a significant reduction in ROS levels. Although, pre-treatment with NAC, but not ascorbate or TROLOX, resulted in restored WHCO1 cell viability, and so we hypothesised that NAC, a cysteine derivative with a thiol group, may have reacted with **t-PMB** and **200** to form a mixed-disulfide product, thereby lowering the concentration of **t-PMB** and **200** in the cell. To determine whether **t-PMB** and NAC are able to react *in vitro*, the two compounds were combined in THF at room temperature overnight. A product was found to be produced, which was isolated and

characterised to be *N*-acetyl cysteine methoxybenzyl disulfide, a mixed disulfide product of **t-PMB** and NAC. It is possible that the reaction between **t-PMB** and NAC may have taken place within the WHCO1 cells, thereby lowering the concentration of **t-PMB** in the cell and preventing **t-PMB** from inhibiting WHCO1 cell viability. This result may provide a rationale as to why pre-treatment with NAC, but not ascorbate and TROLOX, resulted in viability levels similar to that of untreated cells. Furthermore, although ROS production was not observed in WHCO1 cells treated with the IC_{50} concentration of **200**, pre-treatment with NAC still restored cell viability. This result supports our proposal that NAC may not be restoring cell viability in **t-PMB**-treated through its ROS scavenging property. A study by Kelkel *et al*. (2012) showed that when DAS4, a garlic-derived OSC, was co-incubated with NAC, DAS4 was no longer able to induce β-tubulin polymerisation. It may be that DAS4, like **t-PMB**, formed a mixed disulfide with NAC, preventing the interaction between DAS4 and β-tubulin. In a study by Dirsch *et al*. (1998), it was shown that ajoene-induced apoptosis in HL-60 leukemia cells was blocked by NAC, but not by catalase. It may be that ajoene, like **t-PMB**, formed a mixed disulfide product with NAC, thereby lowering the concentrations of ajoene within the cell.

These results indicate that although treatment of WHCO1 cells with **t-PMB** resulted in increased levels of ROS production, ROS production did not appear to form part of the anti-cancer mechanism in WHCO1 leading to cancer cell-death; a finding which contradicts the results by Das *et al*. (2007), who observed that when DADS-treated T98G and U87MG glioblastoma cells are pre-treated with ascorbate, a decrease in apoptosis levels was observed. The reason as to why Das *et al*. (2007) observed the importance of ROS production, and we did not, may be because the anti-cancer mechanism through ROS production may be cancer cell-line specific or analogue specific or possibly by some other explanation.

Although **t-PMB** contains a thiosulfonate functional group, a compound class not reported to be found in garlic, it appeares to bring about its anti-cancer effects through mechanisms that have been described for garlic-derived OSCs, by inducing cell-cycle arrest and apoptosis. Furthermore, even though the DADS analogue, **200**, has varied side groups, it still displayed anti-proliferative activity, inducing its anti-cancer mechanism through G_2/M cell cycle arrest and apoptosis, supporting the hypothesis that the disulfide functional group may be important for the anti-cancer activity of OSC. There is much evidence in the literature to support a ROS generating mechanism for garlic OSC, and much of this evidence is supported by using the ROS scavenger, NAC. Our studies however have found that **t-PMB** and **200** appeared to not

induce its anti-cancer mechanism through ROS production, and that **NAC** is a poor choice of ROS scavenger in garlic OSC assays due to the direct interaction between the **t-PMB** and NAC.

Chapter 4:

In vivo anti-cancer activity of t-PMB and 200 (UCT AEC protocol number 012/003)

4.1. Introduction

Previous *in vivo* studies on garlic-derived OSC have shown that they are able to reduce tumour sizes in mouse and rat models. It has been observed that mice with human colon cancer xenografts showed a significant reduction in tumour size when treated with 0.5 mg DADS (Sundaram & Milner 1996b), 6 mg/kg DATS (Hosono *et al*. 2005) or 80 ppm *S*-methylmethane thiosulfonate (*S*-MMTS) via IP injection (Kawamori *et al*. 1995; Reddy *et al*. 1999). It has also been reported that 25 mg/kg ajoene reduced melanoma size by 3-fold in mice, when compared to the untreated control (Tilli *et al*. 2003), and furthermore, topical application of 250 μg ajoene reduced the size of chemically-induced skin tumours in rodents and humans (Nishikawa *et al*. 2002). Application of ajoene to human patients with basal cell skin carcinoma also reduced tumour sizes in 81 % of patients (Taylor *et al*. 2006).

Based on the literature evidence for *in vivo* anti-cancer activity of garlic-derived OSC, and after observing the promising *in vitro* anti-cancer activity of **t-PMB** and **200**, together with the low cytotoxicity profiles, we decided to investigate whether the compounds showed any *in vivo* anti-cancer activity against both WHCO1 oesophageal cancer and A375 human melanoma xenografts in nude mice.

4.2. Results

4.2.1. Nude mice with A375 xenografts treated intraperitonealy with 200

Since both **t-PMB** and **200** were found to have superior activity against the A375 human melanoma cells over the WHCO1 oesophageal cancer cells in culture, we decided to test whether **t-PMB** and **200** were active at inhibiting the growth of an A375 xenograft in nude mice. For the experiment, tumour sizes were measured with callipers, and the tumour volume was determined using the formula: $Tumour\ volume = \ tumour\ length^2 \times \frac{Tumour\ height}{2}$.

Eighteen nude mice were randomised into two groups (N = 9) and inoculated with 5×10^6 A375 cells in the right flank, and then immediately given the first intraperitoneal (IP) injection with 50 mg/kg **200** (solubilised in 50 % polyethylene glycol (PEG), 10 % DMSO and 2.5 % chondroitin, a solubilisation formulation that was developed by our collaborator, Dr. Andriy Garfov, in Finland). The untreated control group was IP injected with the vehicle alone (50 % PEG, 10 % DMSO and 2.5 % chondroitin). For the first 4 days, mice were treated with 50 mg/kg **200** daily. Following the death of 4 mice in the treated group, treatment was stopped for 3 days, where after the dose was decreased to 25 mg/kg **200** to the remaining 5 mice, administered only every second day via IP injection. The remaining 5 mice treated with **200** every second day appeared normal and gained weight (Figure 4.3). Furthermore, histopathalogical analysis of organs in the **200**-treated mice killed on day 24 showed no toxicity to the liver, adrenal glands, kidneys, lymphocytes and heart (Figure 4.4). It can therefore be concluded that a dose of 25 mg/kg **200** every second day is acceptable, and not toxic.

As seen in Figure 4.1, the remaining 5 nude mice treated with **200** every second day showed a significant decrease in tumour size at 15 days (*p*-value = 0.01) and 18 days (*p*-value = 0.01) post-treatment; however after 18 days, when the tumours began to grow rapidly, this significance was lost. On day 24, the mice were euthanized and the tumours were harvested, with the exception of one tumour which turned necrotic in an untreated mouse. The tumours were weighed to reveal no significant decrease in tumour weight between the untreated and **200**-treated groups (Figure 4.2), which is in agreement with calliper measurements on day 24 (Figure 4.1) at the end of the experiment.

Whole blood analysis was performed at IDEXX laboratories on blood isolated from a **200**-treated mouse (Figure 4.5). The result showed a decrease in red blood cell count,

haemoglobin levels, white cell count, as well as lymphocyte and eosinophil levels; with an increase in the percentage of segmented neutrophils and monocytes compared to healthy mice.

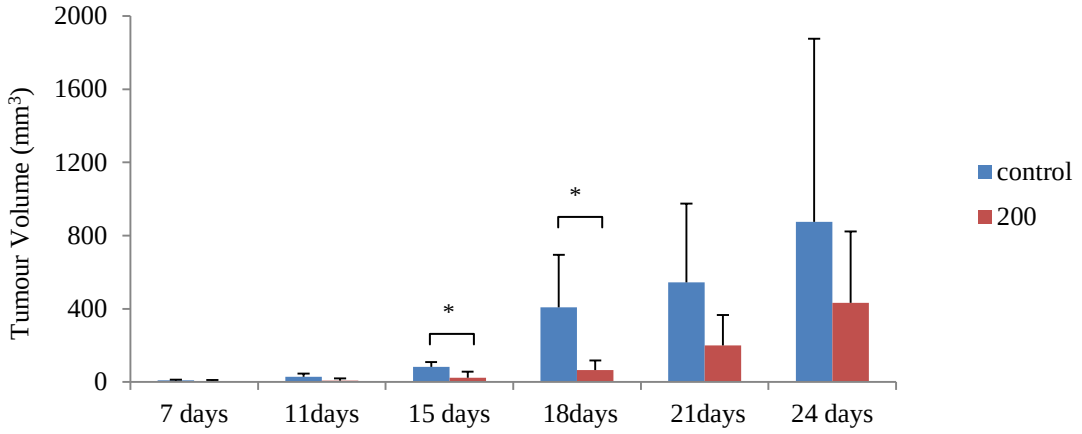

Figure 4.1. A375 tumour volumes (mm^3) from nude mice treated by daily IP injection of 200. To determine the *in vivo* anti-cancer activity of **200**, nude mice were inoculated with 5×10^6 A375 cells in the right flank, and initially treated with 50 mg/kg **200** daily via IP injection, but after observing toxicity, the dose was decreased to 25 mg/kg **200** every second day for up to 24 days. The tumour volumes were measured twice a week with callipers. The data are indicated with ± SD and significant changes are highlighted (* indicates *p*-value < 0.05).

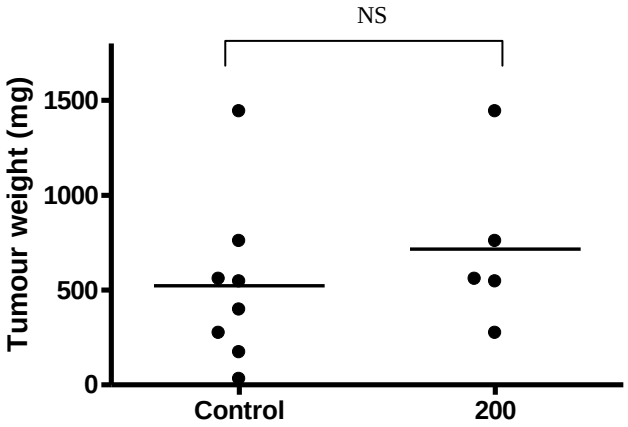

Figure 4.2. A375 tumour weights (mg) from 200-treated and –untreated nude mice removed after 24 days. On completion of the *in vivo* study, the A375 tumours were isolated and weighed, with 8 mice in the control group and 5 mice in the treated group. No significant (NS) difference in tumour weight was observed between treated and untreated mice groups.

.

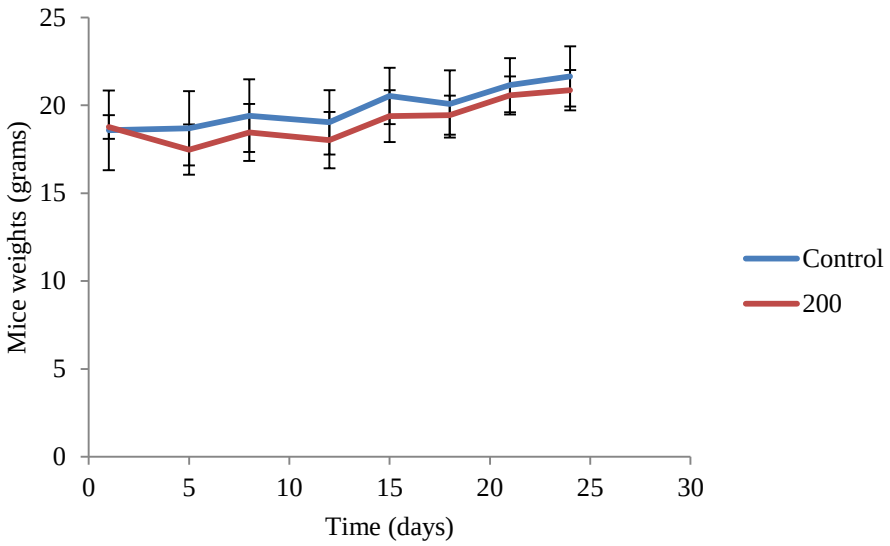

Figure 4.3. Body weight of 200-treated and -untreated nude mice with A375 xenografts. The body weights of **200**-treated and -untreated nude mice with A375 xenografts were measured twice a week and recorded. We observed no significant difference in the weights recorded for the treated and untreated groups for the entire duration of the experiment (24 days).

Histopathalogical findings	
Liver :	No specific histopathalogical lesions visible
Kidney:	Mild interstitial congestion. The peri-renal fat tissue at the hilus reveals a blood vessel that contains anaplastic appearing round cells and some are attached to the vascular wall. Nuclei are large and active and appear hyperchromatic with large nucleoli, and scattered mitoses are visible.
Adrenal gland:	No specific histopathological lesions evident
Lymph node:	Diffuse lymphocytic presence without distinction between cortex and medulla in this section.
Heart:	The pericardial mesenteric fat tissue shows multifocal mild lymphocytic presence compatible with thymic tissue. Few perivascular lymphocytic aggregates are also visible.
Lung:	Mild alveolar atelectasis multifocally and capillaries show moderate leukostasis and in certain areas the alveolar walls also reveal mild thickening due to leukocyte presence.

Figure 4.4. Histopathalogical analysis of nude mice treated with 25 mg/kg 200 via IP injection as tested by IDEXX laboratories. To determine whether treatment with 25 mg/kg **200** via IP injection every second day had potential side effects to non-cancer tissue in mice; the liver, kidneys, adrenal glands, lymph nodes, heart and lungs were sent for histopathalogical analysis at IDEXX laboratories.

Full blood count				
Test name	**Test value**	**Units**	**Flag**	**Range**
Blood count				
Red blood cell count	7.57	$\times 10^{12}$/ litre	Low	7.90 – 10.0
Haemoglobin	12.9	g/dl	Low	13.9 – 16.7
Haematocrit	37.0	%	-	37.0 – 42.0
Mean cell volume	48.0	fl	-	45.0 – 50.0
Mean cell haem. cons.	35.0	g/dl	-	35.0 – 38.0
White cell count	2.17	$\times 10^9$/litre	Low	2.90 – 11.9
Platelet count	900	$\times 10^9$/litre	-	860.0 – 1400
Differential count				
Segmented neutrophils %	68.0	%	High	8.00 – 33.0
Band neutrophils %	0.00	%		0.00 – 1.00
Lymphocytes %	23.0	%	Low	63.0 – 90.0
Monocytes %	9.00	%	High	0.00 – 5.00
Eosinophils %	0.00	%		0.00 – 2.00
Basophils %	0.00	%		0.00 – 0.00
Segmented neutrophils (Abs)	1.48	$\times 10^9$/litre		0.17 – 2.47
Band neutrophils (Abs)	0.00	$\times 10^9$/litre		0.00 – 0.00
Lymphocytes (Abs)	0.50	$\times 10^9$/litre	Low	3.36 – 12.7
Monocytes (Abs)	0.20	$\times 10^9$/litre		0.08 – 4.52
Eosinophils (Abs)	0.00	$\times 10^9$/litre	Low	0.11 – 0.39
Basophils (Abs)	0.00	$\times 10^9$/litre		0.00 – 0.00

Figure 4.5. Whole blood cell count on 200-treated nude mice with an A375 xenograft. In order to determine whether treatment with **200** in nude mice affects blood constituent concentrations, a whole blood count was performed at the IDEXX laboratories.

4.2.2. Nude mice with WHCO1 xenografts treated intraperitonealy with 200

Based on the apparent activity of **200** at early time-points in A375 tumour growth, we decided to test whether **200** was active against WHCO1 tumour growth. For the experiment, 16 nude mice were randomised into two groups (N = 8), and implanted in the right flank with 5×10^6 WHCO1 oesophageal cancer cells, where the tumour was allowed to establish for the first 3 days. Two aggressive mice, one from the treated group and one from the untreated group were removed from the study when their tumours were damaged after fighting, leaving only 7 mice in each group. Treatment began on day 3, where mice were initially treated with 20 mg/kg **200** (solubilised in 50 % PEG, 10 % DMSO and 2.5 % chondroitin) via IP injection daily, although after observing abdominal swelling in the treated mice with this daily dose, the dose was decreased to 10 mg/kg daily (from day 6). Mice in the control group received the vehicle alone (solubilised in 50 % PEG, 10 % DMSO and 2.5 % chondroitin). As shown in Figure 4.6, the control and treated nude mice displayed similar tumour sizes on day 3 (first day of treatment). From day 7 (fourth day of treatment), we observed a decrease in the

tumour size in the **200**-treated group, although a significant difference in tumour size was only seen at 10 days (seventh day of treatment) (*p*-value = 0.04). Thereafter, the significance was lost, as the tumour grew rapidly. At the end of the experiment, the mice were euthanized and the tumours harvested, and weighed. In Figure 4.7 we see no significant difference in tumour weight between the treated and control groups. Although abdominal swelling appeared when administered 20 mg/kg daily, the weight of all of the mice appeared increased with time (Figure 4.8), suggesting that the compound was not causing the mice to lose weight.

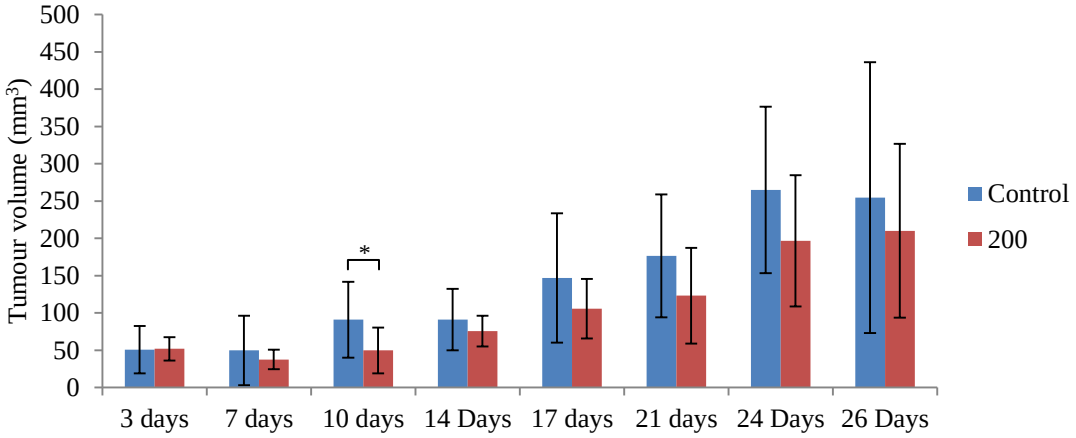

Figure 4.6. WHCO1 tumour volumes (mm^3) from nude mice treated by daily IP injection of 200. To determine the *in vivo* anti-cancer activity of **200**, 16 nude mice were randomised into a treated and untreated group (N = 8). The mice were inoculated with 5×10^6 WHCO1 cells in the right flank on day 1 and treated via IP injection with 20 mg/kg **200** for the first 6 days (from day 3), thereafter the dose was decreased to 10 mg/kg **200** up to 23 days. The tumour volumes were measured twice a week with callipers. The data is indicated as a mean ± SD and significant changes are highlighted (* indicates *p*-value < 0.05).

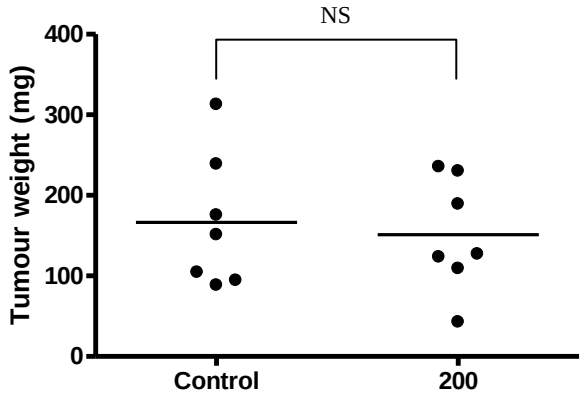

Figure 4.7. WHCO1 tumour weights (mg) of 200-treated and untreated nude mice removed after 26 days. On completion of the *in vivo* study, the WHCO1 tumours were isolated and weighed, with 7 mice in the treated and 7 mice in the untreated groups. No significant (NS) difference in tumour weight was observed between treated and untreated mice groups.

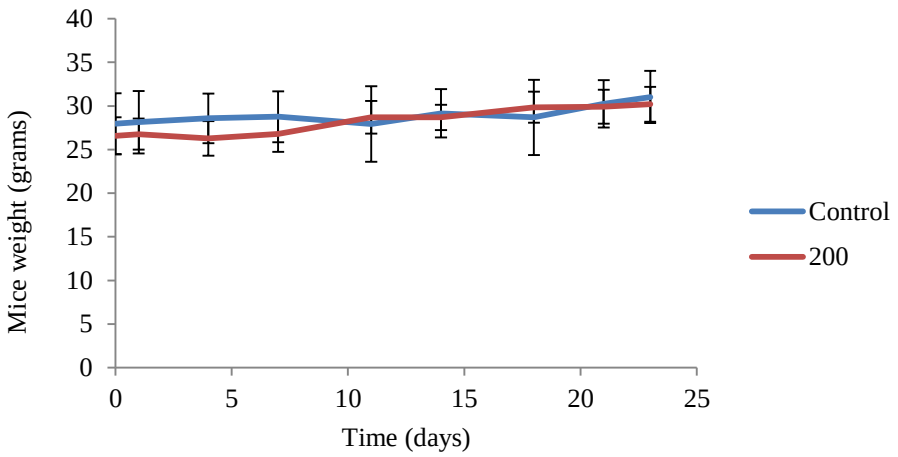

Figure 4.8. Body weight of 200-treated and -untreated nude mice with WHCO1 xenografts. The body weights of **200**-treated and -untreated nude mice with WHCO1 xenografts were measured twice a week and recorded. We observe no significant difference in the weights recorded for treated and untreated groups for the entire duration of the experiment (26 days).

The blood volume of 4 nude mice treated with 10 mg/kg **200** and 4 control mice treated with vehicle alone (50 % PEG, 10 % DMSO and 2.5 % chondroitin) were isolated on the final day of the experiment (day 26) 1 hour after the final dose of **200** was administered intraperitonealy. The blood plasma samples were analysed for **200** by Ms. Carmen de Kock at the Pharmacology department of UCT. A calibration curve was first established for **200** (Figure 4.9), which ranged from 15.6 to 1000 ng/ml of **200** in mouse plasma. On the day of the experiment, quality controls of **200** were prepared in duplicate at two concentrations; 400 ng/ml (QC1) and 800 ng/ml (QC2). QC1 and QC2 were detected, and found to be 447 ± 21.3 ng/ml and 859 ± 24.8 ng/ml respectively in mouse plasma. Compound **200**, however, was not detected in the blood samples from the nude mice treated intraperitonealy with **200**. The fact that no **200** was observed in the blood 1 hour after IP injection implies that the compound is metabolically instable, and may explain the apparent low activity against *in vivo* tumour growth when it is so strongly active *in vitro*. This result may imply that (1) **200** gets to the tumour site and acts very quickly *i.e.* under an hour, or (2) a secondary metabolite of **200** is reducing tumour size in the treated group, or (3) that **200** may be altering tumour growth through a secondary effect and is never reaching the tumour to act according to the mechanism we have observed *in vitro*. The combination effects of low metabolic stability and poor *in vivo* activity does not support **200** as a viable candidate for future drug development.

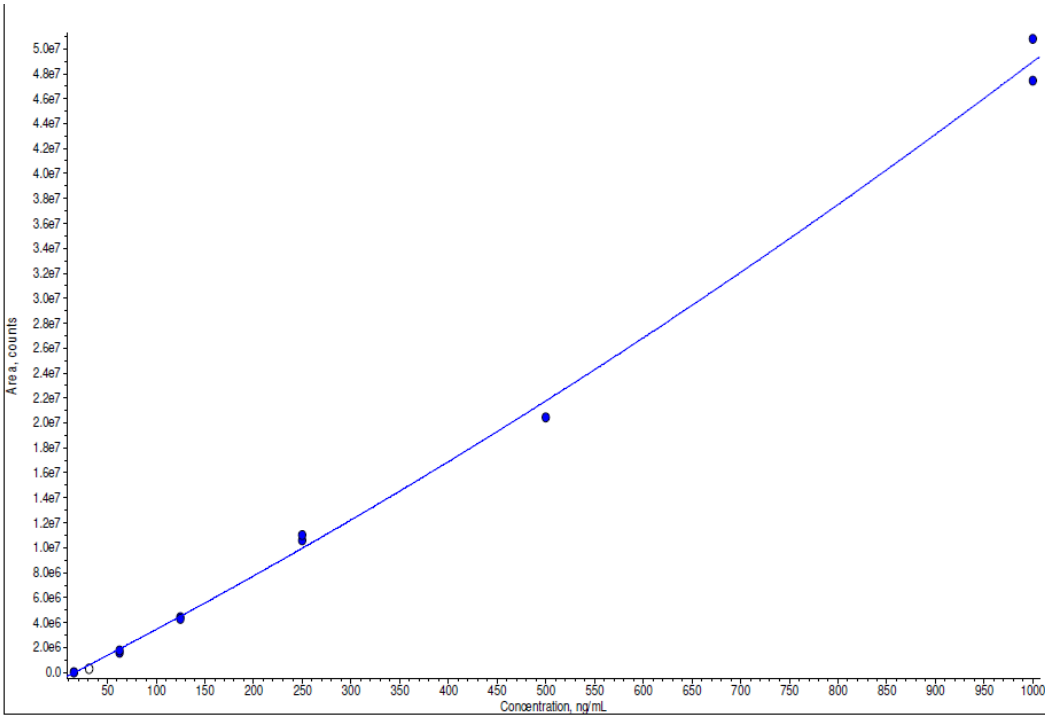

Figure 4.9. Calibration curve for 200. The graph represents a calibration curve used to determine the concentration of **200** in blood isolated from nude mice 1-hour after IP injection of 10 mg/kg **200**.

4.2.3. Nude mice with A375 xenografts treated intraperitonealy with t-PMB

For the *in vivo* study of **t-PMB**, 20 nude mice were randomised into two groups (N = 10), and inoculated with 5×10^6 A375 cells in the right flank, and then immediately given the first IP injection of 30 mg/kg **t-PMB** (solubilised in 50 % PEG, 10 % DMSO and 2.5 % chondroitin). Thereafter, the nude mice were treated with 30 mg/kg **t-PMB** once a day for up to 21 days and untreated control mice received the vehicle alone (50 % PEG, 10 % DMSO and 2.5 % chondroitin) (Figure 4.10). Six days after treatment, the smallest mouse in the **t-PMB**-treated group died, however we cannot be sure whether the death was caused by the compound. A significant decrease in tumour volume was observed at 9 days (*p*-value = 0.04), 13 days (*p*-value = 0.02) and 16 days (*p*-value = 0.02) post-treatment, as determined by the student *t*-test. On completion of the study, the mice were euthanized and the tumours were isolated and weighed. In Figure 4.11 we see no significant decrease in tumour weight between the untreated and **t-PMB**-treated groups on day 21. Furthermore, when the mice were dissected at the end of the experiment, the intestines appeared to have swollen and hardened, a sign of inflammation, although mice in both groups appeared to have gained weight (Figure 4.12) and appeared normal throughout the experiment.

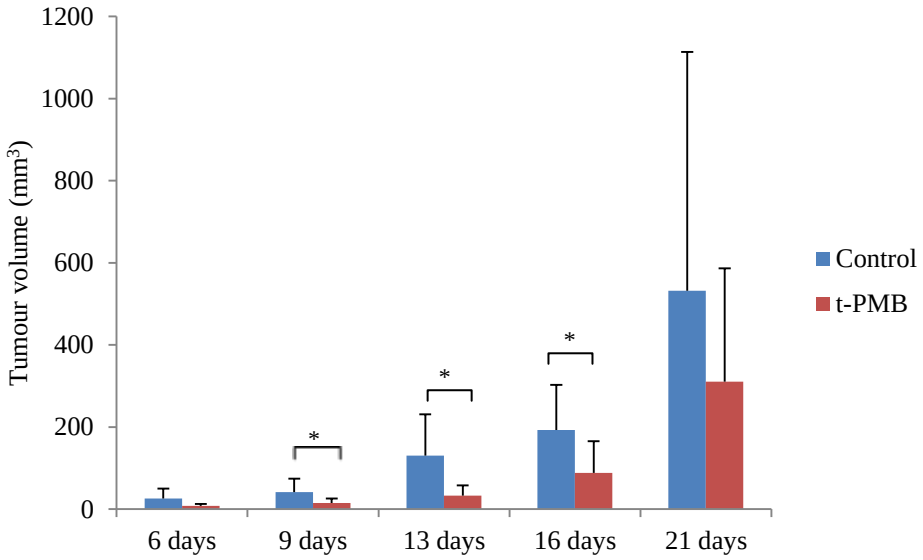

Figure 4.10. A375 tumour volumes (mm^3) from nude mice treated by daily IP injection of t-PMB. Nude mice were inoculated with 5×10^6 A375 cells on the right flank, and treated with 30 mg/kg **t-PMB** once a day for up to 21 days. The tumour volumes were measured twice a week with callipers. The data is indicated as an average ± SD and significant changes are highlighted (* indicates *p*-value < 0.05).

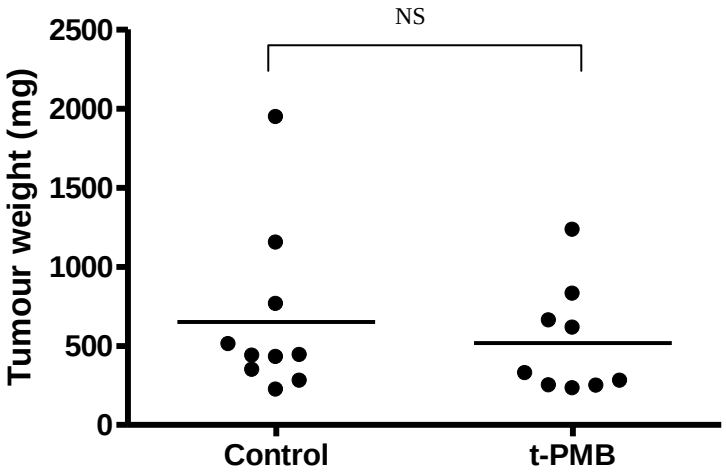

Figure 4.11. A375 tumour weights (mg) of t-PMB-treated and untreated nude mice removed after 21 days. On completion of the *in vivo* study, the A375 tumours were isolated and weighed, with 9 mice in the treated and 10 mice in the untreated group. No significant (NS) difference in tumour weight was observed between treated and untreated mice groups.

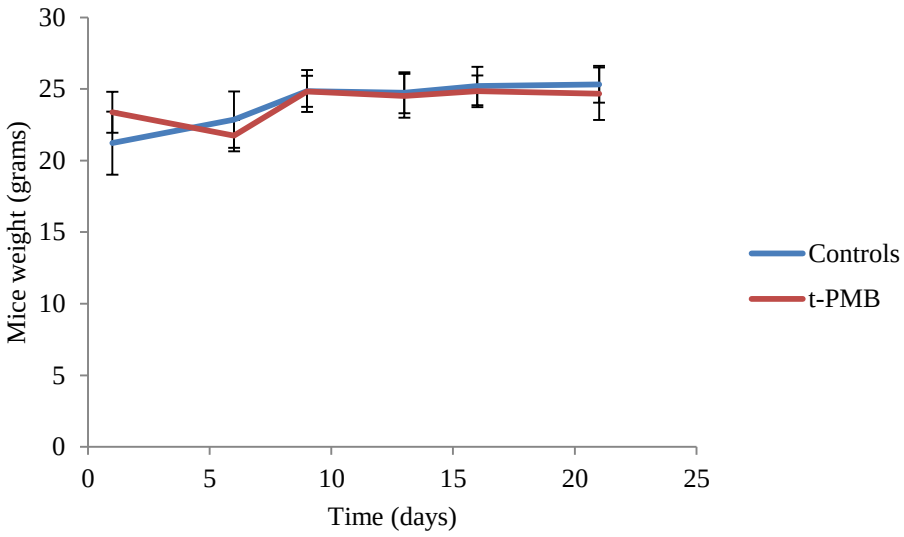

Figure 4.12. Body weight of t-PMB-treated and -untreated nude mice with A375 xenografts. The body weight of **t-PMB**-treated and -untreated nude mice with A375 xenografts were measured twice a week and recorded. Here we observe that there was no significant difference in the weight of the treated and untreated groups throughout the experiment (21 days).

4.3. Discussion

To investigate whether **200** is active at inhibiting A375 human melanoma xenograft growth in nude mice, mice were treated with 50 mg/kg **200** via IP injection daily, which was found to be toxic, resulting in 4/9 mice dying in the treatment group. The dose was then decreased to 25 mg/kg **200** every second day which appeared to have no toxic effects. In support of this, histopathalogical analysis of treated mice at the end of the experiment showed no toxicity to the liver, kidney, adrenal gland, lymph node, heart or lung in the **200**-treated mice, and furthermore, the body weights of mice in the treated group increased with time, and were similar to that of the controls. Nude mice treated with **200** showed a significant decrease in tumour volume up to 18 days, however, when the tumours started to grow more rapidly, the significance was lost. Upon isolation of the A375 tumours at the end of the experiment, we observed no significant difference in tumour volume or tumour weight between the treated and untreated groups, suggeting that **200** may only have been effective within the early stages of A375 tumourigenesis.

The *in vivo* anti-cancer activity of **200** on WHCO1 oesophageal cancer cells was also investigated, where nude mice with WHCO1 xenograft were initially treated with 20 mg/kg **200** daily. Although, after observing abdominal swelling in some mice treated with 20 mg/kg **200** daily for the first 6 days, the dose was decreased to a daily treatment of 10 mg/kg **200**, which appeared to be fine, as we no longer observed abdominal swelling, and the mice appeared to be healthy and gained weight. It was evident that although **200** displayed promising *in vitro* anti-cancer activity against WHCO1 cell growth, it did not display significant *in vivo* anti-cancer activity. Throughout the experiment, the average tumour volume of treated mice was found to be lower than that of the untreated mice; however a significant decrease was only observed day 10, which may have been due to the daily high dose of 20 mg/kg **200** for the first 6 days. When the tumours were removed and weighed at the end of the experiment, the average tumour weight was lower in the treated than the untreated mice; however this difference was not statistically significant. The apparent increased activity of **200** in nude mice with the A375 xenograft versus nude mice with the WHCO1 xenograft is not too surprising as the IC_{50} of **200** on the A375 cells was 3.17 μM, showing a 3-fold greater selectivity compared to the IC_{50} of **200** on WHCO1 cells, which was 9.9 μM. The result therefore suggests that treatment with **200** may be cancer cell-line selective. An alternative proposal for increased anti-cancer activity in nude mice with the A375 xenograft is that treating with 25 mg/kg **200** every second day, as was done on nude

mice with the A375 xenograft, may have resulted in a higher concentration of **200** at the tumour site, whereas treating nude mice with a lower concentration of 10 mg/kg **200** every day, as was done on nude mice with the WHCO1 xenograft, may have resulted in lower concentrations of compound reaching the tumour site. This result is supported by pharmacological analysis on blood isolated 1 hour after the nude mice were treated with 10 mg/kg **200**, which showed that **200** was not detected in the blood of the treated mice. In support of this, Sundaram & Milner (1996) has shown that nude mice with the human colon cancer xenograft, HCT-15, treated with 25 mg/kg DADS via IP injection thrice a week, reduced tumour size by 70 % without adverse side-effects (Sundaram Sg & Milner Ja 1996). Furthermore, mice with the colon cancer xenograft, COLO205, showed a significant reduction in tumour volume when treated with 42 mg/kg DADS via IP injection thrice a week (Liao *et al*, 2007), supporting the proposal that IP injection with a high dose of DADS given every second day may be more effective at inhibiting tumour growth, without adverse side-effects.

Lawson & Wang (1993) observed that when the garlic OSC, DADS, was incubated in whole blood, it had a half-life of 60 minutes, unlike ajoene and allicin which rapidly rearranged to form allyl-SH. We therefore suspected that **200**, a DADS analogue, would also have had a relatively long half-life in whole blood, although, the pharmacokinetic data showed that **200** was not detected in whole blood from mice 1 hour after IP administration. A possible explanation as to why **200** was not detected may be that like ajoene, **200** is an "activated" DADS analogue, as the disulfide functional group is flanked by an electron withdrawing pyridine group. Ajoene and **200**, which theoretically would form mixed disulfide products more readily than DADS, may be metabolised more rapidly, resulting lower concentrations of compound reaching the tumour site. This result may therefore provide a rationale as to why **200** was not detected in the blood after treatment. The observed decrease in tumour size by **200** may therefore be due to the anti-cancer activity of a metabolite of **200**, or that **200** may be altering tumour growth slightly through a secondary effect, and is never actually reaching the tumour to act according to the mechanism we have observed *in vitro*.

When nude mice with the A375 xenograft were treated with 30 mg/kg **t-PMB** via IP injection once a day for up to 21 days, we observed a significant decrease in tumour volume for up to 16 days of treatment, demonstrating moderate *in vivo* anti-cancer activity, as was observed with **200**. Importantly, although a modest decrease in tumour volume and a gain in mouse weight was observed, the mice in the treated group experienced abdominal swelling which

was only evident upon dissection at the end of the experiment, indicating that treating the nude mice with 30 mg/kg **t-PMB** via IP once a day was too high a concentration, and maybe treating mice with lower concentrations would decrease this observed effect, although it may also remove the anti-cancer effect. In contrast, Kawamori *et al*. (1995) observed that F344 rats fed with 80 ppm *S*-methylmethane thiosulfonate (*S*-MMTS), a cauliflower-derived thiosulfonate compound, significant reduced azoxymethane-induced colon carcinogenesis, without adverse side-effects.

In conclusion, although **200** appeared to be a good candidate as a cancer chemotherapeutic based on its *in vitro* data, with a low IC_{50} and 10-fold selectivity to WHCO1 cancer cells over Het1A non-cancer cells, it did not appear to significantly reduce WHCO1 tumour size *in vivo*. It does although appear to be more effective at inhibiting the growth of the A375 tumour size *in vivo*, which may indicate a certain selectivity to certain cancer types. Furthermore, a high dose (25 mg/kg) of **200** given every second say, which appears to have an effect only early in tumorigenesis (up to day 18), appeared to more effective than a lower dose (10 mg/kg) given daily. In support of this, pharmacokinetic data showed that **200** was not detected in the blood of mice 1 hour post-treatment with 10 mg/kg **200**. Due to the observed pharmacokinetic data, and the observed tumour reduction only within the early stages of tumour development, it is not recommended to pursue this line of compounds to drug development. Compound **t-PMB** was found to be effective at decreasing A375 xenograft volume within the early stages of tumourigenesisis (up to day 16), however due to the abdominal swelling observed, it is likely not a good candidate for further development.

Chapter 5

Investigating protein disulfide isomerase as a potential drug target for OSC

5.1. Introduction

Protein disulfide isomerise (PDI) is an endoplasmic reticulum (ER)-resident protein whose active site cysteine residues are involved in disulfide bond formation and isomerisation within newly synthesised proteins (Freedman *et al*. 1994). We hypothesise that the garlic-derived organosulfur compounds (OSC) may inhibit the redox and isomerase activities of PDI by forming a mixed disulfide with at least one of the PDI active site cysteines, which may then result in the inactivation of the enzyme. We decided to test this hypothesis by setting up a PDI enzyme assay.

A known PDI inhibitor, 5'5'-dithio-bis(2-nitrobenzoic acid) (DTNB), is structurally related to diallyl disulfide (DADS) in that it contains a disulfide functional group. Although the inhibitory mechanism of DTNB on PDI has not been confirmed, it is hypothesised that the disulfide functional group of DTNB may form a mixed disulfide with an active site cysteine residue of PDI, thereby leading to the inhibition of PDI isomerase and redox activities; a hypothesis that we propose for PDI and garlic-related OSC.

To determine whether PDI is a potential protein target of OSC within cells, we performed immunohistochemistry (IHC) with **DP**, a fluorescent ajoene analogue. We also performed a PDI enzyme assay to determine whether OSC are able to inhibit PDI enzymatic activity.

5.2. Results

5.2.1. Immunofluorescence

To ensure a strong signal for PDI, we wanted to perform IHC on a cancer cell-line which expressed high levels of PDI. Figure 5.1 is a western blot showing the protein levels of PDI in 7 different cancer cell-lines when probed with an anti-PDI antibody and detected using a secondary antibody linked to horse radish peroxidase (HRP). The extent of chemiluminescence of the PDI protein band is normalised for the loading control, glyceraldehyde 3-phosphate dehydrogenase (GAPDH), and is plotted on a histogram (Figure 5.2). The PDI protein expression levels were found to be highest in the KYSE-180 cell-line, an oesophageal cancer cell-line of Japanese origin. This cell-line was thus selected for IHC analysis. **DP** was found to be active at inhibiting the growth of KYSE-180 cells with an IC_{50} of 9.1 μM (Table 5.1).

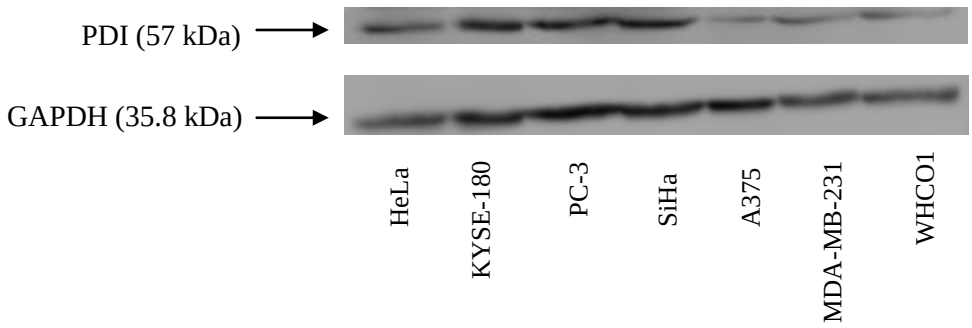

Figure 5.1. Relative quantities of protein disulfide isomerase (PDI) levels in different cancer cell-lines. The western blot represents PDI levels in various cancer cell-lines to include HeLa, KYSE-180, PC-3, SiHa, A375, MDA-MB-231 and WHCO1 cancer cell-lines.

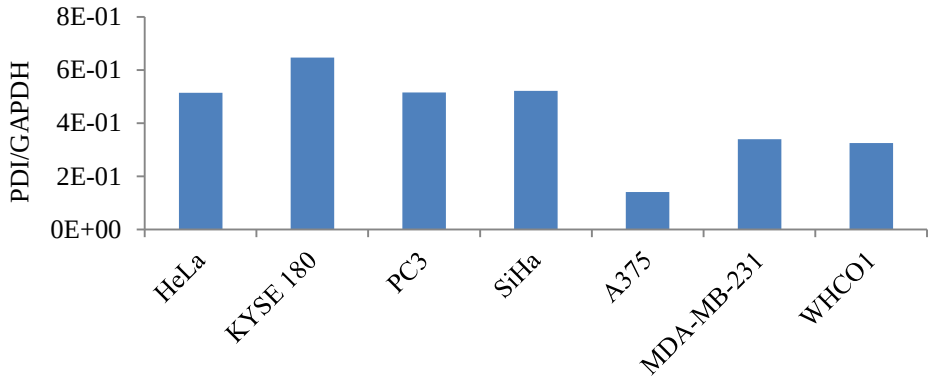

Figure 5.2. The bar graph represents the relative levels of PDI normalised for GAPDH in various cancer cell-lines including HeLa, KYSE-180, PC-3, SiHa, A375, MDA-MB-231 and WHCO1 cancer cell-lines.

For IHC, KYSE-180 cells were seeded on a glass cover-slip and treated with **DP** at its IC_{50} concentration (9.1 μM) for 6 hours. Thereafter, the cells were treated with the PDI polyclonal primary antibody and the cy-3 fluorescently-tagged secondary anti-body, and mounted on a glass slide for viewing under a fluorescence microscope. The KYSE-180 cells were treated with **DP** (9.1 μM), which fluoresces blue, and fluorescent images were taken 6 hours post-treatment. In Figure 5.3 we see that the PDI signal, which is stained red (**A**), and **DP**, which fluoresces blue (**B**), co-localise (**C**) with each other in the perinuclear region of the KYSE-180 cells. The phase contrast images of the cells are also shown (**D**) as well as the co-localisation signal, which is displayed graphically (**E**), where pink shows co-localisation between **DP** and PDI. Figure 5.3 **E** shows a strong pink signal, suggesting that most of the **DP** and PDI co-localised within the KYSE-180 cells, although, a blue signal is also detected, suggesting that **DP** localised to regions of the cells were PDI was not present. This result implies that **DP** may have other protein targets within the KYSE-180 cells. Interestingly, no red signal was detected, suggesting that all of the PDI detected co-localised with **DP**. Although IHC may provide evidence that **DP** and PDI co-localise within the KYSE-180 cells, it does not confirm whether the OSC and PDI directly interact, or whether this interaction affects PDIs enzymatic activity. We therefore went on to perform a PDI enzyme assay to test OSC-induced PDI inhibition.

Table 5.1. Dose-response-curve and IC_{50} of **DP** against the KYSE-180 oesophageal cancer cell-line.

Compound Name	**Chemical structure**	**IC_{50} curve**	**KYSE-180 IC_{50} (μM)**
DP	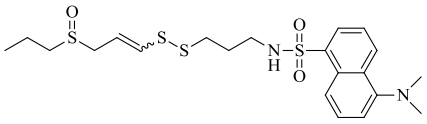	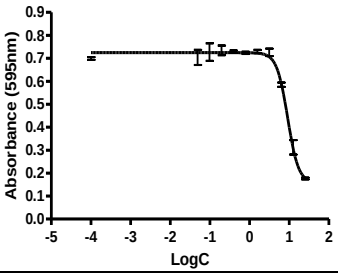	**9.1**

5.2.2. PDI enzyme assay

To determine whether analogues of the garlic-derived OSC are able to inhibit PDI enzyme activity, a PDI enzyme assay was performed. The assay chosen is based on the oxidative renaturation of reduced RNase A by active PDI (Lyles & Gilbert 1991). The renaturation and regain of RNase A protein activity was assessed by the ability of this active form to hydrolyse

cytidine 2',3'-cyclic monophosphate (cCMP). The hydrolysed cCMP product is UV active and can be detected spectrophotometrically at 296 nm. All reaction mixtures contained glutathione (GSH) and glutathione disulfide (GSSG), as PDI is strongly dependent on the presence of these molecules for proper function.

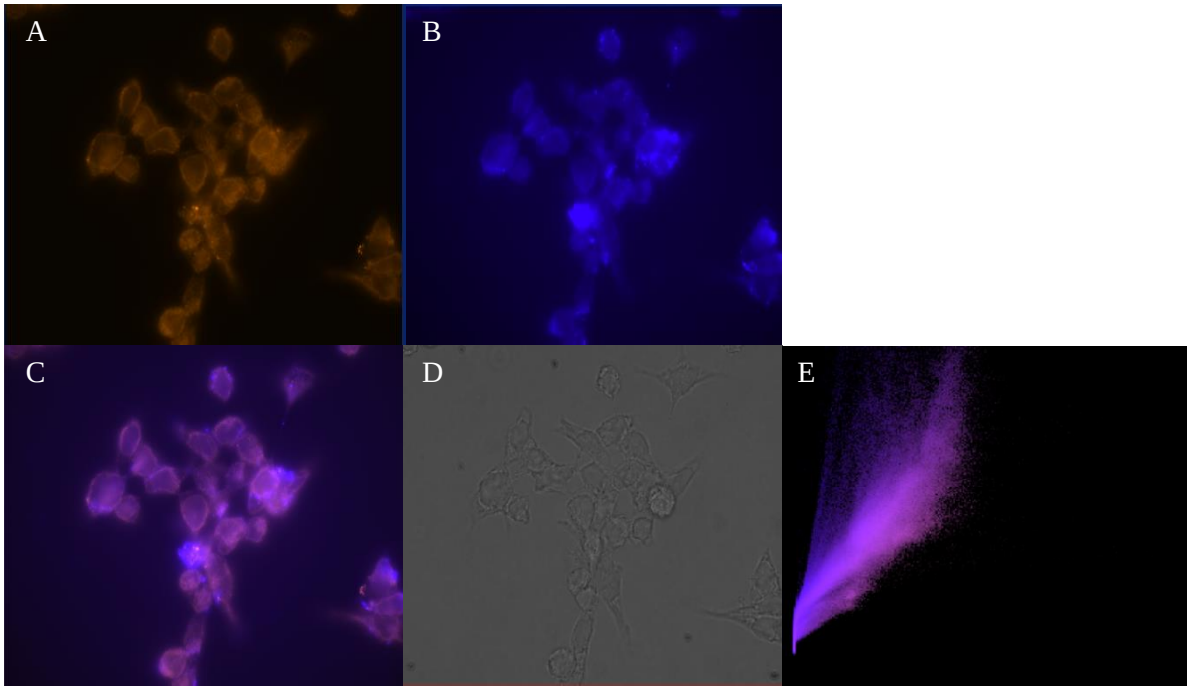

Figure 5.3. Co-localisation between PDI and DP in KYSE-180 oesophageal cancer cells. To determine whether PDI and ajoene co-localise in cancer cells, KYSE-180 cells were treated with the fluorescent ajoene analogue **DP**, and fluorescence was detected through immunohistochemistry (IHC). The image shows that PDI (**A**) and **DP** (**B**) co-localise (**C**) to the perinuclear region of the KYSE-180 cells. The phase contrast image is shown (**D**) and the co-localisation signal is displayed graphically (**E**).

Each reaction took place in a cuvette at 25 °C, and the reaction was allowed to proceed for 35 minutes before the absorbance at 296 nm was recorded. For the PDI enzyme assay, three control experiments were first performed. These included spectroscopic recordings of (1) Native RNase A (NR); (2) Reduced RNase A (RR); and (3) Reduced RNase A in the presence of PDI (R-PDI). Thereafter, an inhibitory experiment was performed to test whether OSC inhibited PDI enzymatic activity. Here, the inhibitory actions of **t-PMB**, **200**, and **DP** were tested at 20 μM, which is approximately the IC_{50} concentration for each compound. The inhibitory action of DTNB, a known PDI inhibitor with a functional disulfide group, was tested at 100 μM, according to concentrations used literature.

The NR and R-PDI controls were found to have similar absorbance values (Figure 5.4), whilst a 4-fold significant (*p*-value = 0.007) decrease in signal was observed for the RR sample, which is expected as the RNase A should re-nature slower in the absence of PDI, resulting in a slower rate of cCMP hydrolysis. Furthermore, when compared to the PDI control, DTNB, **t-PMB**, **200**, and **DP** samples displayed significantly decreased absorbance values, with *p*-values being 0.007, 0.03, 0.01 and 7.9×10^{-6} respectively, indicating a decrease rate of RNase A renaturation, and subsequent cCMP hydrolysis (Figure 5.4).

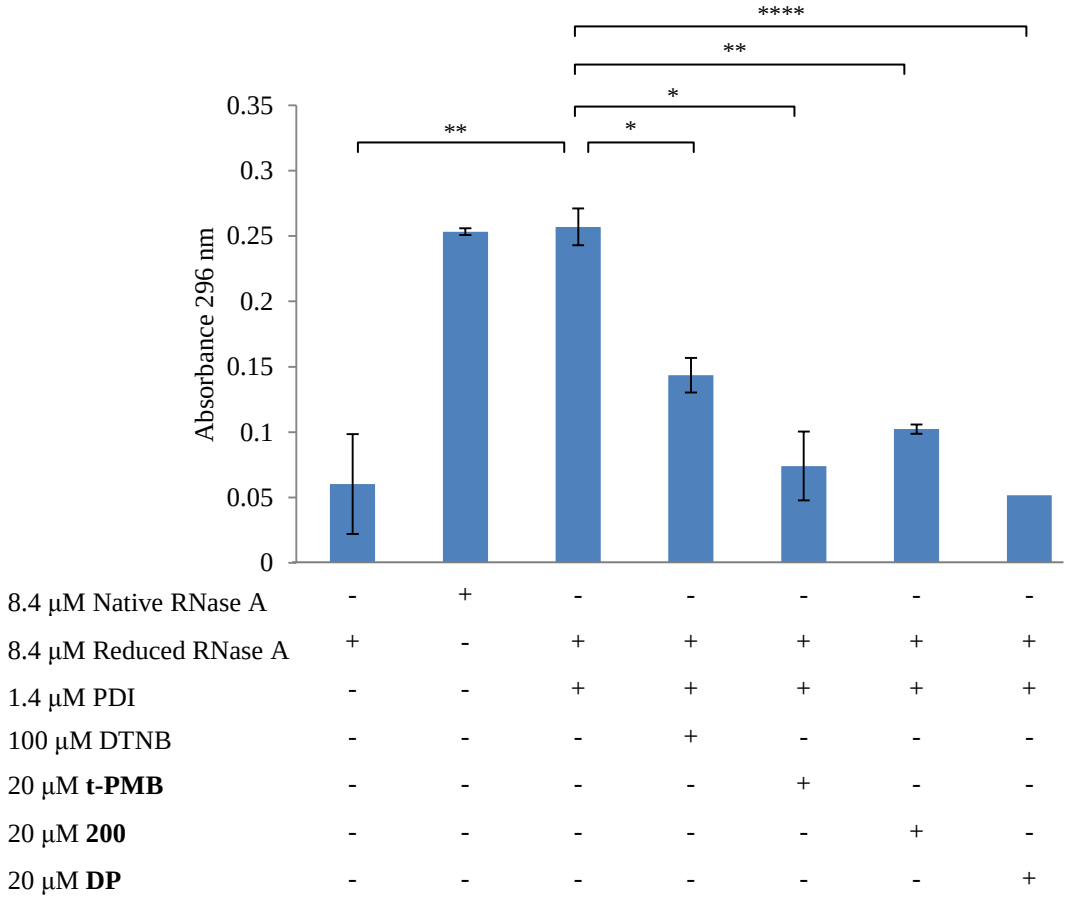

Figure 5.4. Protein disulfide isomerase (PDI) inhibition enzyme assay. The inhibitory activity of DTNB, **t-PMB**, **200** and **DP** against bovine PDI was determined using a PDI enzyme assay. The assay is based on the oxidative renaturation of RNase A by active PDI. The renaturation and regain of RNase A activity by PDI was assessed by its ability to hydrolyse cCMP, whose product can be detected spectrophotometrically at 296 nm. Independent triplicate experiments were performed at 25 °C for 35 minutes. The data are indicated with as a mean ± SD, and significant changes are highlighted (* indicates *p*-value < 0.05; ** indicates a *p*-value < 0.01, **** indicates a p-value < 0.001).

These results therefore show that DTNB**, t-PMB**, **200**, and **DP** are able to inhibit PDIs enzymatic activity, which could possibly occur through mixed disulfide bond formation between the OSC and active site cysteine residues in PDI. Furthermore, even though 100 μM DTNB is able to inhibit PDIs enzymatic activity, **t-PMB**, **200** and **DP** appear to inhibit PDIs enzymatic activity more effectively, and at a much lower concentration (20 μM). This result therefore supports our hypothesis that PDI may be a potential target for the OSC-induced anti-cancer mechanism.

5.3. Discussion

We propose that OSC may induce their anti-cancer mechanism by forming mixed disulfides with cysteine nucleophiles within target proteins, thereby inhibiting protein function, with the concurrent expulsion of an anion leaving group. Our previous results have shown a correlation between the leaving group stability and the IC_{50} of various DADS analogues, supporting the hypothesis that protein thiolation may be important for OSC-induced cell death. Furthermore, we have shown that **t-PMB** and NAC react to form a mixed disulfide product, further supporting the feasibility of protein thiolation as a potential anti-cancer mechanism.

Previous work in our laboratory has shown co-localisation of **DP**, a fluorescent ajoene analogue, to the ER (Kaschula *et al*, unpublished data). We therefore hypothesised that at least one of the OSC protein targets may reside within the ER. PDI, an ER-resident protein whose active-site contains cysteine residues (Lyles & Gilbert 1991), was investigated as a potential target of OSC in cancer cells.

To ensure a strong fluorescence signal for the IHC assay, we performed a western blot on various cancer cell-lines to determine relative PDI levels. After having observed that the KYSE-180 oesophageal cancer cell-line had the highest levels of PDI in the series, the cell-line was used for IHC. Although we observed that most of the **DP** co-localised with PDI, **DP** also appeared to have localised to other regions of the cell where PDI was not present. This implies that **DP** may have other cellular protein targets, like glutathione reductase (Krauth-Siegel *et al*. 1996) or β-tubulin (Hosono *et al*. 2005), which are proposed targets of garlic OSC. Interestingly, we observed no red signal apart from the blue signal, which indicates that all PDI detected had co-localised with **DP**. Although this result provides evidence that **DP** and PDI co-localise within the KYSE-180 cells, it does not confirm whether the OSC and PDI directly interact, or whether this interaction affects PDIs enzymatic activity. It was therefore important to test whether OSC were actually able to inhibit PDIs enzymatic activity.

To determine whether OSC inhibit the enzymatic activity of PDI, a PDI enzyme assay was performed. For the enzyme assay, we tested the inhibitory effects of **t-PMB**, **200**, **DP** at 20 μM (approximately IC_{50}), as well as **DTNB** at 100 μM. We observed that NR and R-PDI had similar absorbance values, whilst there was a 4-fold significant decrease in signal for the RR sample, which is expected as the RNase A would re-nature slower in the absence of the PDI enzyme, resulting in a slower rate of cCMP hydrolysis. When compared to the R-PDI control,

DTNB, **t-PMB**, **200**, and **DP** samples displayed significantly decreased absorbance values, suggesting a decrease rate of RNase A re-naturation, and subsequent cCMP hydrolysis. These results therefore provide strong evidence that garlic-related disulfides may inhibit PDIs enzyme activity *in vitro*, although whether this observed PDI inhibition occurs in the cancer cell will warrant further investigation.

For the first time, we observed that OSC are able to co-localise with, and inhibit PDI enzyme activity. Previous work in our laboratory has shown that when WHCO1 cells were treated with *E/Z*-**4l**, an ajoene analogue 12 times more active than the parent compound, an increase in the mRNA levels of CHOP, a protein marker of ER stress, were observed (Kaschula *et al*, unpublished data). With these results we hypothesise that should treatment with OSC result in PDI enzyme inhibition within cancer cells, the accumulation of unfolded proteins may lead to ER stress, which may be a trigger for apoptosis, a hypothesis which could be tested in future studies.

Chapter 6

General discussion

Garlic-derived organosulfur compounds (OSCs), to include *E/Z* ajoene, diallyl trisulfide (DATS), diallyl disulfide (DADS), diallyl sulfide (DAS) and allicin have all been shown to be active at inhibiting tumour cell proliferation both *in vitro* and *in vivo*. In our study, we propose that the disulfide or polysulfide functional group of the OSC may react with a cysteine nucleophile from a protein, to result in the formation of an alkylated protein product with altered function, and the concurrent expulsion of an anion leaving group. The chemical reactions between OSC and cysteine nucleophiles of proteins are governed by both thermodynamic and kinetic parameters, where the thermodynamics are largely driven by the stability of the products, which in our case is the expelled anion leaving group. Factors which increase the stability of an anion include degree of conjugation, resonance and number of electronegative atoms. Incoming nucleophilic attack by a cysteine thiol is kinetically controlled, and dependent on the accessibility of the cysteine nucleophile to the disulfide of the OSC. In our study, we determined the 48-hour anti-proliferation-IC_{50} of 15 organosulfur analogues, which included 10 DADS analogues, 1 allicin analogue and 4 thiosulfonate compounds, a compound class not reported to be found in garlic. Our results show that the DADS analogues displayed varying degrees of anti-cancer activity against WHCO1 oesophageal cancer cell proliferation, ranging from 5 μM to inactive (> 200 μM). We observed that a compound with a more stable leaving group produced a more active compound, and furthermore that steric hindrance over the disulfide functional group removed anti-cancer activity, regardless of leaving group stability.

The stability of the leaving group anion was also assessed by determining its pK_a-value, where a leaving group with a lower pK_a-value is considered to be more stable. Compounds **2**, **21**, **200** and **30** were all used to determine the relationship between leaving group stability and IC_{50} in the DADS series, where the common R_1-group was a fixed propyl, and therefore the reactivity was dependent solely on the nature of the R_2-leaving group. Our results showed a positive correlation between compound IC_{50} and the leaving group pK_a, with an R^2-value of 0.88. Although compounds **2** and **8** are structurally similar, the IC_{50} of **8** was significantly higher than **2**, which may be due to the presence of the *t*-butyl group on **8**, introducing steric

hindrance over the disulfide pharmacophore. **Allicin-16**, a thiosulfinate, is structurally similar to **16**, a DADS analogue. Although, the IC_{50} of **Allicin-16** (71 μM) is lower than **16** (> 200 μM). The higher activity of **allicin-16** may be due to the presence of the oxygen on its sulfur, which may enhance its anti-cancer activity by making the thiosulfonate more labile to thiolation. This is likely because the oxygen atom on the sulfur has electron-withdrawing properties, resulting in a better leaving group. The water-soluble compound, **92**, was found to be inactive, which was not too surprising as the water-soluble DADS analogue, *S*-allylmercaptocysteine (SAMC), is reported to be 3-fold less active than DADS (Kwon *et al*. 2002; Danhua Xiao *et al*. 2005; Yang *et al*. 2009)**.** This result implies that a degree of lipophilicity is required for anti-cancer activity. Since the leaving group in the thiosulfonate compound class was the same in all cases, it may offer an explanation as to why these compounds had similar IC_{50}'s in the range of 15 μM. These results suggest that the reaction between a disulfide and a cysteine nucleophile of a potential protein target may be thermodynamically and kinetically controlled. It furthermore supports the hypothesis that the disulfide functional group is important for the anti-cancer activity of OSC, and that the side-groups appear to play an important modulatory role.

To investigate the mechanism of action of disulfides and thiosulfonate compounds in WHCO1 oesophageal cancer cells, **200**, a DADS analogue, and **t-PMB**, a thiosulfonate compound, were selected for further evaluation. The anti-cancer mechanism was assessed by observing morphological changes in treated cells, assaying whether the compounds generate reactive oxygen species (ROS) and testing whether they induce cell-cycle arrest and apoptosis.

Although the MTT assay measures cell viability, it is also a good indirect measure of cell-proliferation. The BrdU assay, which directly measures cell proliferation, confirmed that 2 × IC_{50} concentration of **t-PMB** and **200** were able to reduce cell proliferation down to background levels. Furthermore, morphology images of WHCO1 cells treated with 2 × IC_{50} concentrations of **t-PMB** and **200** showed that cells appeared rounded, indicative of apoptosis. In literature, it is reported that ajoene (Li *et al*. 2002; Dirsch *et al*. 2002), DATS (Kim *et al*. 2007; Xiao *et al*. 2004), DADS (Filomeni *et al*. 2003; Das *et al*. 2007; Yang *et al*. 2009) and allicin (Kim *et al*. 2008) induce apoptosis in cancer cells, so we went on to investigate whether the OSC in our study also induce apoptosis in WHCO1 cells. Apoptosis, determined through the detection of histone-associated DNA fragments, was detected in WHCO1 cells treated with **t-PMB** or **200**. It was observed that **200** was more effective at

inducing apoptosis than **t-PMB**, implying that **200** may be a better drug candidate than **t-PMB** due to lower IC_{50} and increased levels of apoptosis in WHCO1 cells.

In the literature, there is evidence to suggest that ajoene (Dirsch *et al*. 1998), DATS (Kim *et al*. 2007), DADS (Das *et al*. 2007; Kwon *et al*. 2002; Wu *et al*. 2005; Filomeni *et al*. 2003) and DAS (Das *et al*. 2007) may mediate their anti-cancer effects through increased ROS production, although Kelkel *et al*. (2012) did not find increased levels of ROS in the U937 human histiocytic lymphoma cells treated with diallyl tetrasulfide (DAS4), another garlic-derived OSC. We have already identified the importance of thiolation based on anion leaving group stability (Figure 6.1, Scenario 2), so we decided to further investigate whether ROS production is also important. It is possible that ROS may be generated as a result of the expelled leaving group thiol which may undergo homolytic cleavage to produce a thiyl radical. The thiyl radical, which is very unstable, may react with free oxygen in the cell to produce superoxide, which in turn is a precursor to ROS (Figure 6.1, Scenario 1). It is predicted that a leaving group with a high pK_a may form a less stable thiyl radical, which would more readily react with free oxygen, and produce higher levels of ROS. In support of this hypothesis, we observed that **t-PMB** (pK_a = 6.82), produced a significant amount of ROS in a time- and dose-dependent manner, whereas **200** (pK_a = 2.71) produced very little ROS.

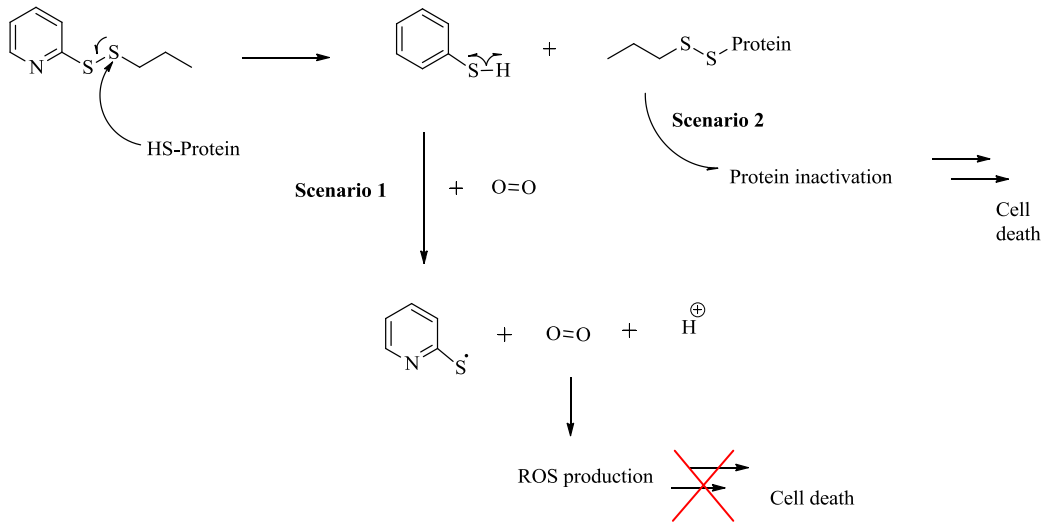

Figure 6.1 Possible model for OSC-induced cancer cell-death in WHCO1 cells, which was found not to occur through increased levels of ROS (**Scenario 1**), although protein thiolation by OSC was found to be important (**Scenario 2**).

To determine whether ROS production is important in the anti-cancer mechanism of OSC, WHCO1 cells were treated with the IC_{50} concentrations of **t-PMB** or **200** following pre-treatment with the ROS scavengers; NAC, ascorbate or TROLOX, which resulted in decreased levels of ROS to below that of the untreated control. WHCO1 cells treated with **t-PMB** or **200** in the presence of NAC resulted in cell-viability levels similar to that of the untreated control, indicating that pre-treatment with NAC prevented **t-PMB**-induced inhibition of cell viability. On the other hand, treatment with **t-PMB** in the presence of ascorbate and TROLOX resulted in viability levels similar to that of WHCO1 cells treated with **t-PMB** alone, indicating that although these scavengers decrease ROS levels in **t-PMB**-treated cells, they do not affect cell-viability. Since NAC, a cysteine-derivative with a free thiol group, restored cell-viability, but not ascorbate or TROLOX, we anticipated that NAC may be acting through a mechanism other than ROS scavenging. We proposed that NAC may in fact react with **t-PMB** to form a mixed disulfide product, thereby decreasing the concentrations of **t-PMB** within the WHCO1 cells. To test this hypothesis, a reaction between **t-PMB** and NAC was set up in THF at room temperature. The two compounds were in fact found to react to form a product, which was characterised by ^{1}H Nuclear Magnetic Resonance spectroscopy (^{1}H NMR) and found to be *N*-acetyl methoxybenzyl disulfide, a mixed disulfide product of **t-PMB** and NAC. It is therefore likely that this reaction may take place in the WHCO1 cells, thereby lowering the concentration of **t-PMB**, and preventing **t-PMB** from inhibiting WHCO1 cell viability. Treating WHCO1 cells with the IC_{50} concentration of **200** did not result in increased levels of ROS production, although pre-treatment with NAC still restored cell viability. This result further supports the argument that NAC may not be restoring cell-viability in **t-PMB-** and **200**-treated cells through its ROS scavenging property. A study by Kelkel *et al*. (2012) showed that when DAS4, a garlic-derived OSC, was co-incubated with NAC, DAS4 was no longer able to induce β-tubulin polymerisation. It is highly likely that DAS4, like **t-PMB**, may form a mixed disulfide with NAC, thereby preventing the interaction between DAS4 and β-tubulin. In a study by Dirsch *et al*. (1998), it was shown that ajoene-induced apoptosis in HL-60 leukemia cells was blocked by NAC, but not by catalase. It may be that ajoene, like **t-PMB**, also forms a mixed disulfide product with NAC, thereby lowering the concentrations of ajoene within the cell. The results from our study indicate that although treating WHCO1 cells with **t-PMB** results in increased levels of ROS, ROS production does not appear to be important in the anti-proliferative activity of **t-PMB**. Our findings therefore contradict the results of Das *et al*.

(2007) who observed that when DADS-treated T98G and U87MG glioblastoma cells were pre-treated with ascorbate, a decrease in apoptosis was observed. Our findings also contradict the findings by Kwon *et al*. (2002) who showed that pre-treatment with catalase prevented DADS-induced PARP cleavage in HL-60 leukaemia cells. It may therefore be that the OSC-induced anti-cancer mechanism through ROS production may be cancer cell-line specific or analogue specific.

Previous work in our laboratory has shown that **DP**, a fluorescent ajoene analogue, co-localises to the endoplasmic reticulum (ER) in MDA-MB-321 breast cancer cells (Kaschula *et al*, unpublished data). Since thiolation appears to be important in the anti-cancer mechanism of OSC analogues, we propose that the OSC drug target may reside in the ER. An attractive target that we decided to investigate in this regard is Protein Disulfide Isomerase (PDI) whose active-site cysteine residues are involved in the formation of correctly paired disulfide bonds involved in protein folding (Lyles & Gilbert 1991). Because the active site cysteine residues of PDI are able to react with, and rearrange disulfide bonds within proteins, we hypothesised that the disulfide within OSC may also react with the active site cysteine residues of PDI, thereby preventing the interaction between PDI and its substrate proteins. For IHC, we selected the KYSE-180 oesophageal cancer cell-line as it expresses the highest levels of the PDI protein within a series of cancer cell-lines tested. All of the PDI in the KYSE-180 cells appeared to co-localise with **DP**, although **DP** also appeared localised to regions of the cell where PDI was not detected, suggesting that **DP** may have additional targets within the cell, like glutathione reductase (Krauth-Siegel *et al*. 1996) or β-tubulin (Hosono *et al*. 2005), which are proposed targets of garlic OSC.

To determine whether OSC are able to inhibit PDI enzyme activity, a PDI enzyme assay was performed. **DTNB**, a known inhibitor of PDI (Jain *et al*. 2007; Mandel *et al*. 1993; Lara *et al*. 2011; Santos *et al*. 2009), as well as synthetic garlic analogues; **t-PMB**, **200** and **DP**, inhibited PDI enzyme activity compared to the untreated control. Furthermore, **200**, whose leaving group has a pK_a-value of 2.71, was shown to be more effective at inhibiting PDI's enzymatic activity than **t-PMB**, whose leaving group has a pK_a of 6.82, suggesting that the correlation we observed between pK_a and IC_{50} may also be translated into the inhibition of PDI enzymatic activity.

FACS analysis showed that WHCO1 cells treated with **200** or **t-PMB** showed a time-dependent increase in G_2/M cell-cycle arrest, with a concurrent decrease in the G_1- and S-

phases of the cell-cycle. The G_2/M cell-cycle arrest appeared earlier for **200**-treated cells than **t-PMB**-treated cells. Although OSCs form garlic have been shown to induce a G_2/M cell-cycle arrest, this is the first time it has been observed for the thiosulfonate class of compound. Previous work in our laboratory has shown that when WHCO1 cells are treated with *E/Z***4l**, ER stress is activated (Kaschula *et al*., unpublished). We hypothesise that should OSC inhibit PDI within cancer cells, it may lead to an accumulation of unfolded proteins and subsequently ER stress, and cell death. A study by Bourougaa *et al*. (2010) showed that ER stress promotes PERK-dependent induction of p53/47 homo-oligomerization, which subsequently induces G_2/M cell-cycle arrest, but not G_1 cell-cycle arrest (Bourougaa *et al*. 2010), a cascade of events which may take place in WHCO1 cells treated with OSC. It would therefore be important for us to test this pathway in WHCO1 cells treated with OSC, to determine whether the ER stress leads to the observed G_2/M cell-cycle arrest.

To determine whether a degree of selectivity exists for cancer cells over non-cancer cells, Het1A, a non-cancer cell-line of oesophageal epithelia origin, was treated with **t-PMB** and **200** and analysed using the MTT cell viability assay. The results showed that **t-PMB** displayed a 2.5-fold selectivity to WHCO1 cells over the Het1A cells, with **200** displaying a respective 10-fold selectivity. To investigate whether **t-PMB** and **200** are able to decrease cell viability in another cancer cell-line, the 48-hour IC_{50} of each compound was determined against the A375 human melanoma cell-line, and was found to be 2.27 μM for **t-PMB** and 3.17 μM for **200**, indicating that both compounds are more active against A375 cell proliferation than against WHCO1 cells. This result suggests that **t-PMB** and **200** display some selectivity for certain cancer types, similar to what has been observed for DADS, where the IC_{50} ranges from 22 μM for the human colon cancer cell-line, COLO205 (Yang *et al*. 2009), to 35 μM for the human prostate cancer cell-line, PC-3 (Dong Xiao *et al*. 2005). Importantly, the 48-hour IC_{50}'s of **t-PMB** and **200** against WHCO1 cells were found to be 14.8 μM and 9.9 μM respectively, both falling into the *in vitro* clinical range of known oesophageal cancer chemotherapeutics; cisplatin (48-hour IC_{50} = 9.2 μM) and 5-fluorouracil (48-hour IC_{50} = 7.9 μM), on the same cell-line (Kaschula *et al*, 2012). Together, these results suggest that both compounds may have potential as cancer chemotherapeutics.

To investigate the *in vivo* anti-cancer activity of **200**, nude mice with an A375 xenograft were treated with 50 mg/kg **200** through intraperitoneal injection (IP) daily, which was found to be toxic as 4/ 9 mice in the group died. The dose was therefore decreased to 25 mg/kg **200** via IP injection every second day, which appeared to have no toxic effects as the mice appeared

healthy and gained weight. In addition, histopathalogic analysis showed no toxicity to the liver, kidney, adrenal gland, lymph node, heart or lung when analysed at the end of the experiment. Tumour size in the treatment group was significantly reduced for up to 18 days, although, when the tumour started growing more rapidly, the significance was lost. An *in vivo* study with **200** in nude mice with the WHCO1 xenograft was also performed. Here, the nude mice were initially treated with 20 mg/kg **200** via IP injection daily for the first 6 days, although after observing abdominal swelling in some mice, the dose was then decreased to 10 mg/kg **200** via IP injection daily. Although an overall reduction in tumour size was observed in the treated mice, a significant reduction in tumour size was only observed at 7 days post-treatment, likely due to the high concentration of 20 mg/kg **200** given within the first 6 days. It is evident that **200**-treated nude mice with the A375 xenograft displayed a more significant reduction in tumour size compared to nude mice with the WHCO1 xenograft. The observed increase in *in vivo* anti-cancer activity of **200** in mice with the A375 xenograft over mice with the WHCO1 xenograft is not too surprising as the IC_{50} of **200** was 3-fold lower against the A375 cell-line (3.17 μM) compared to the WHCO1 cell-line (9.9 μM). Furthermore, nude mice with the A375 xenograft received 25 mg/kg **200** every second day, whereas mice with the WHCO1 xenograft received 10 mg/kg **200** daily. It is therefore possible that treating with a higher concentration of **200** every second day may be more effective than treating with a lower dose daily. This result is supported by previous findings where it was observed that mice with a human colon cancer xenograft (HCT-15) treated with 25 mg/kg DADS via IP injection three times a week, significantly reduced tumour size by 70 %, without adverse side-effects (Sundaram & Milner 1996b). Furthermore, mice with a human leukaemia (HL-60) xenograft also showed a significant decrease in tumour size when treated with 42 mg/kg DADS via IP 3 times a week (Liao *et al*, 2007).

Pharmacokinetic analysis on blood isolated from nude mice 1 hour post-treatment with 10 mg/kg **200** showed that **200** was not detected, implying metabolic instability. The observed over-all decrease in WHCO1 tumour size in **200**-treated mice may therefore have been because (1) **200** enters the blood stream and reaches the tumour site in under 1 hour following IP injection, or (2) that the tumour reduction was due to the effect of a metabolite of **200**, or (3) that **200** may be altering tumour growth through another effect and is never reaching the tumour to act according to the mechanism we observe *in vitro*. Furthermore, although **200** had higher *in vitro* anti-cancer activity compared to DADS ($IC_{50} \approx 50$ μM), DADS appears to have greater *in vivo* anti-cancer activity as observed by Sundaram & Milner (1996b) who

showed that nude mice with the HCT-15 human colon cancer xengraft treated with 1 mg DADS via IP injection thrice a week for 3 weeks, resulted in a 69 % reduction in tumour size, with no adverse side effects. The reduction in tumour size only within the early stages of tumorigenesis, and the fact that no compound was detected in the blood 1 hour after IP injection, suggests that **200** is not active enough *in vivo* or metabolically stable enough to be a suitable candidate for drug development in the future.

The *in vivo* anti-cancer activity of **t-PMB** was also investigated in nude mice with the A375 xenograft. Here, the nude mice were treated with 30 mg/kg **t-PMB** via daily IP injection. Although a significant reduction in tumour volume was observed up to 18 days of treatment, significance was lost when the tumour started to grow more rapidly, which was confirmed when no significant difference was observed between tumour weights in the **t-PMB**-treated and untreated groups at the end of the experiment. Furthermore, although the mice appeared healthy and gained weight over time, the mice experienced abdominal swelling, indicating that treating mice with 30 mg/kg **t-PMB** was too high. This result contradicts literature findings where it was observed that 80 ppm of the cauliflower-derived thiosulfonate, *S*-methylmethane thiosulfonate (*S*-MMTS), significantly reduced colon cancers in mice and rat models without adverse side-effects (Reddy *et al*. 1999; Kawamori *et al*. 1995). Our findings indicate that **t-PMB**, although displaying excellent *in vitro* activity, may not be suitable as a candidate for drug development.

Chapter 7

Conclusion

A small library of 15 garlic-related compounds were synthesised and assessed for *in vitro* anti-cancer activity. It was found that the stability of the leaving group plays a significant role in the WHCO1 anti-proliferative activity of disulfides, where compounds that don't have leaving groups that can stabilise a negative charge have IC_{50}'s greater than 200 µM. The strong anti-proliferative effects observed for the thiosulfonates is likely due to the electronegative effects of the oxygen atoms on the thiosulfonate, resulting in an electropositive sulfur which is more reactive towards an incoming cysteine nucleophile. The results in the structure-function study of disulfides and thiosulfonates supports the hypothesis that protein thiolation may be important in the anti-cancer mechanism of organosulfur compounds (OSC).

The mechanistic study revealed that thiosulfonate and disulfide analogues, similar to garlic-derived OSC, induce G_2/M cell-cycle arrest and apoptosis. Although ROS is produced in the thiosulfonate series, but not the disulfide series, it does not appear to be implicated in the anti-proliferation cancer mechanism of the thiosulfonates. Furthermore, we found that NAC and **t-PMB** chemically react, rendering NAC an inappropriate ROS scavenger for OSC studies.

For the first time, we have shown that OSC co-localise with, and inhibit the enzymatic activity of PDI, a protein involved in the correct pairing of disulfide bonds within proteins during tertiary folding. We hypothesise that OSC may inhibit PDI enzyme activity within cancer cells, leading to an accumulation of unfolded proteins and subsequent ER stress leading to cell death.

In vivo anti-cancer studies showed that **200** is more effective at reducing tumour growth in mice with an A375 xenograft than in the WHCO1 xenograft, and furthermore that a higher dose (25 mg/kg) given every second day appears to be more effective that a lower dose given (10 mg/kg) daily. Pharmacokinetic data showed **200** to be metabolically unstable, suggesting that **200** may not be a good candidate for drug development. *In vivo* studies in nude mice with an A375 xenograft showed that although 30 mg/kg **t-PMB** reduced the tumour size

significantly within the first 18 days of treatment, the mice experienced abdominal swelling, suggesting that **t-PMB** too may not be a good candidate for further drug development.

In summary, DADS analogues and thiosulfonate compounds, which each contain an activated disulfide functional group, appear to inhibit cancer cell viability, where the representative compounds, **t-PMB** and **200**, appear to be selective towards cancer cells over their non-cancer counterparts, inducing a G_2/M cell-cycle arrest as well as apoptosis in WHCO1 cells; anti-cancer properties observed for garlic-derived OSC. Although ROS production did not appear to be important in the anti-cancer mechanism of **t-PMB** and **200**, both compounds inhibited PDIs enzymatic activity, suggesting that PDI may be a prospective OSC target, and would be interesting to investigate in future studies. These findings, together with the *in vivo* results, support the idea that the regular consumption of garlic may inhibit tumour cell growth, but most like only within the early stages of tumorigenesis. Our results therefore refute the hypothesis that ROS production is important in the anti-cancer mechanism of OSC, but support the hypotheses that PDI may be a potential target for OSC within cancer cells, and that the disulfide functional group in garlic-derived OSC is important for their anti-cancer mechanism.

Chapter 8

Materials and methods

8.1. Determining compound purity and stability

8.1.1. Thin layer chromatography (TLC)

All garlic-related organosulfur compounds used were synthesised at the Chemistry department of UCT in Prof. Roger Hunter's Laboratory. An aliquot of each compound diluted in dimethyl sulfoxide (DMSO) (Sigma) was drawn up with a Hirschmann micropipette (Sigma) and then absorbed onto a TLC Silica gel 60 F_{254} aluminium plate (Merck). The plate was then placed into a developing tank with hexane and ethyl acetate (EtOAc), which was mixed in a ratio of either 10 % ethyl acetate (EtOAc):hexane for the DADS analogues or 50 % EtOAc:hexane for the thiosulfonates. After the hexane-EtOAc moved up by at least 3 cm of the plate, the solvent front was marked, and the distance the compound had migrated was viewed under ultra-violet light at 254 nm. The compound's relative purity was then gauged by viewing the number of "spots" on the sheet.

8.1.2. Nuclear Magnetic Resonance (NMR)

The purity of selected compounds giving only one spot on TLC was confirmed using Nuclear Magnetic Resonance Spectroscopy. ^{1}H NMR spectra were recorded at 300 MHz in deuteriochloroform. Chemical shifts were recorded using residual chloroform (δ 7.26 in ^{1}H NMR) as an internal standard. All chemical shifts are reported in parts per million (ppm) and all coupling constants quoted in hertz (Hz). The ^{1}H chemical shifts of the compounds were compared to those previously reported and were found to be identical. (Stellenboom *et al*, 2010).

8.2. Toxicity studies

8.2.1. Cell line used in assays

The toxicity and IC_{50} studies were conducted using an epithelial oesophageal cancer cell-line, WHCO1 (Veale & Thornly, 1989). For the animal studies, both the WHCO1 oesophageal cancer and A375 human melanoma cell-lines were used (A-375 [A375] ATCC® CRL-1619™). The PDI levels were determined in a number of different cancer cell-lines including

WHCO1, A375, HeLa, KYSE-180, PC-3, SiHa and MDA-MB-231 cancer cell-lines. The HeLa cell-line was derived from cervical cancer cell-lines from Henrietta Lacks in 1951 (Scherer & Syverton 1952). The KYSE-180 cancer cell-line was derived from a Japanese male with oesophageal squamous cell carcinoma. The PC-3 cancer cell-line was derived from a 62 year old Caucasian male with human metastatic prostate cancer of epithelial morphology (PC-3 [PC3] ATCC® CRL-1435™). The SiHa cancer cell-line is a grade 2 cervical squamous cell carcinoma derived from a 55 year old Asian female (SiHa [SiHa] ATCC®HTB-35™). Lastly, the MDA-MB-231 cancer cell-line is an epithelial breast cancer adenocarcinoma derived from a 51 year old Caucasian female (MDA-MB-231 [MDAMB231] ATCC® HTB-26™). As a non-cancer control cell-line, Het-1A cells were used, which is an oesophageal epithelial cell-line derived from a 25 year old black male, immortalised with the SV40 large T antigen (Het-1A [Het1A] ATCC® CRL-2692™).

8.2.2. Cell culture media

WHCO1 cells were cultured in Dulbecco's modified Eagles medium (DMEM) (Gibco) (See appendix for preparation), supplemented with 10 % foetal calf serum (FCS) (HyClone) and 1 % penicillin G/ streptomycinsulfate (PenStrep) (Biochrom) (See Appendix for preparation).

8.2.3. Cell maintenance

8.2.3.1. Storage of cells

Adherent cells were grown to an 80 % confluence in complete DMEM on a 100 mm dish. To collect cells, the media was removed and cells were washed with 5 ml phosphate buffer saline (PBS) (pH 7.5), where after the cells were incubated with 3 ml trypsin (37 °C, 5 % CO_2, 91 % humidity) (See appendix for preparation) for 2 minutes to detach cells from the dish. After transfer of the cells to a 12 ml tube, the trypsin was neutralised by the addiction of 4 ml complete DMEM and centrifuged at 4000 rpm for 3 minutes (Hettich Zentrifuge). The supernatant was removed and cells were re-suspended in 5 ml DMEM containing 10 % FCS. Once the cells were re-suspended, 10 µl was removed to count the cells (see Section 8.2.4). The cells were pelleted by centrifugation at 4000 rpm (1541 ×g) and re-suspended in DMEM containing 20 % FCS and 10 % DMSO at a concentration of ~ 1×10^6 cells/ml. Cells were stored in 1 ml aliquots in cryotubes at - 80 °C for 48 hours, then transferred to liquid nitrogen for long-term storage.

8.2.3.2. Thawing

When required, cells stored in liquid nitrogen were retrieved and thawed in a 37 °C water bath. The 1 ml cell suspension was added to a 12 ml Falcon tube containing 5 ml complete DMEM. The suspension was centrifuged at 4000 rpm (1541 ×g) for 3 minutes. The supernatant was removed, the cells were re-suspended in 5 ml complete DMEM and then transferred to a 100 mm dish containing 10 ml complete DMEM. The cells were incubated at 37 °C, with a medium change after 24 hours.

8.2.3.3. Plating and splitting

When the plates were 80 % confluent, the cells were split. For the splitting procedure, the medium was removed and cells were rinsed with 5 ml PBS (pH 7.5) (See Appendix for preparation) and incubated at 37 °C with 3 ml trypsin for 2 minutes to detach the cells. The detached cells were transferred to a 12 ml tube containing 4 ml complete DMEM. The suspended cells were centrifuged at 4000 rpm (1541 ×g) for 3 minutes. Thereafter, the supernatant was removed and the cells were re-suspended in 5 ml complete DMEM. The suspended cells were plated in a 100 mm dish containing 10 ml complete DMEM and incubated at 37 °C. Thereafter, the medium was changed every 2-3 days.

8.2.4. Cell count

To determine the number of cells, 10 µL re-suspended cells were stained with 10 µL Trypan blue (Molecular Probes®) of which 10 µl was pipetted into a Countess glass slide (Molecular Probes®) and cells were counted using the Countess cell counter (Molecular Probes®). To determine the volume of cells needed, the following formula was used:

$$Volume\ cells\ required\ (ml) = \frac{Number\ of\ cells\ required \times Total\ volume\ of\ cells}{Total\ number\ of\ cells}$$

8.3. Cell Morphology

A change in cellular morphology may indicate cellular stress that may be induced by treatment with drug. For the analysis, 5×10^4 cells were seeded per well into 6 well-plates and allowed to settle and attach for 24 hours at 37 °C. Thereafter, cells were treated with either 2 × 48-hour IC_{50} of **t-PMB** and **200**, or 0.1 % DMSO as a solvent control. Images were then captured at t = 0, 24 and 48 hours at random regions on the plate using an Olympus SC30 digital camera at 10 × magnification and the computer software, Analysis getIT.

8.4. Cell viability (MTT assay)

8.4.1. Cell culturing

The MTT assay quantifies cell proliferation and viability. It is based on the cleavage of yellow tetrazolium salt to purple formazan crystals by metabolically active cells. This reaction involves the pyrimidine nucleotide co-factors; nicotinamide adenine dinucleotide (NADH) and nicotinamide adenine dinucleotide phosphate (NADPH). The formazan crystals formed by metabolically active cells are solubilised and the resulting colour is quantified using a scanning multi-well spectrophotometer. The assay is therefore useful to determine the viability of the WHCO1 cells treated with the various organosulfur compounds (OSC) to test their effect on the viability of the cells.

For the MTT assay, cells were seeded in 96-well plates, at 2500 cells per well suspended in 90 µl complete DMEM. Cells were allowed to attach and recover for 24 hours, and thereafter treated with 10 µl compound at concentrations and times specified below.

The thiosulfonates and disulfides, which were synthesised by Dr. Nashia Stellenboom in the Chemistry department, were stored at - 80 °C until use. 200 mM Stock solutions of each compound were prepared in high purity 99.9% DMSO, with the exception of t-benzyl which was dissolved in ethanol due to its insolubility in DMSO. The solutions were sonicated for 10 minutes at 37 °C to ensure complete dissolution. Thereafter, the stock solutions were further diluted in DMSO (with the exception of t-benzyl, which was diluted in ethanol) to generate a range of concentrations at 2-fold dilutions *i.e.* 200, 100, 50, 25, 12.5, 6.25, 3.13, 1.56, 0.78 and 0.39 mM in a 96-well plate. These solutions were further diluted 100-fold into complete DMEM. Thereafter, the cells were treated with 10 µl compound in DMEM to give a final compound concentration in the cells of 200, 100, 50, 25, 12.5, 6.25, 3.13, 1.56, 0.78 and 0.39 µM. All experiments were performed in quadruplicate. The negative controls for these experiments were always cells treated with 0.1% DMSO in medium, and the background reading was media with MTT with solubilisation solution alone.

To test for cell viability, the MTT reagent (Sigma®) (See Appendix for preparation) was used and prepared according to the protocol described by Roche, with the exception that 10 % SLS (Sodium lauryl sulphate) (See Appendix for preparation) was used instead of 10 % SDS (Sodium dodecyl sulphate). After the 24- or 48-hour treatment with each compound, the cells were incubated at 37 °C with MTT at a final concentration of 0.5 mg/ml for 4 hours.

Thereafter, solubilisation reagent (10 % SLS) was added to a final concentration of 5% and further incubated at 37 °C for 24 hours.

The relative viability of cells was determined spectrophotometrically using the Multiskan FC multi-well reader (Thermo Scientific) at 595 nm. The data for each compound was analysed using PRISM (GraphPad Software, Inc.) and fitted using a non-linear regression with a sigmoidal dose-response curve (variable slope). The proliferation-IC_{50} and 95 % confidence interval for each compound was obtained in triplicate experiments

8.5. Cell proliferation assay (BrdU assay)

To determine the anti-proliferative effects of **t-PMB** and **200**, the BrdU assay was performed using the Cell Proliferation ELISA, BrdU (chemiluminescence) kit (Roche). For the assay, 2500 WHCO1 cells were seeded in complete DMEM in black 96-well plates, with clear-bottoms. Cells were allowed to attach and recover for 24 hours, and thereafter treated with either **t-PMB** or **200** at twice their respective 48-hour IC_{50}'s.

From their stock solutions, compound **200** and **t-PMB** was diluted in DMSO to 20 mM and 30 mM respectively. The compounds were then further diluted 100-fold in media to 200 μM for compound **200** and 300 μM for **t-PMB**. WHCO1 cells were then treated at a final concentration of either 30 μM **t-PMB** or 20 μM **200** in 0.1 % DMSO in quadruplicate, and incubated (37 °C, 5 % CO_2, 91 % humidity) for 20 hours. The solvent controls for these experiments were cells treated with 0.1 % DMSO in media or media alone.

8.5.1. Treating cells with BrdU-labelling reagent and BrdU antibody

Cells treated with compound for 48 hours were incubated at 37 °C with 10 μl BrdU labelling solution for 4 hours. Thereafter, the labelling reagent was removed and the cells were treated with 100 μl FixDenat (to fix and denature the DNA) for 30 minutes at room temperature. The FixDenat solution was removed through inverting and tapping the 96-well plate. The cells were then treated with 100 μl anti-BrdU-POD working solution for 90 minutes at room temperature. After removing the anti-BrdU-POD, the cells were washed thrice with 100 μl washing solution. Thereafter, the peroxidase (POD) substrate solution was added to the cells followed by incubation for 3 minutes at room temperature before measuring the chemiluminescence using a Veritas™ microplate luminometer (Promega).

8.6. Cell-cycle analysis by fluorescence activated cell sorting (FACS) analysis

For the cell cycle analysis, cells were seeded into a 100 mm dish and allowed to settle for 24 hours in an incubator at 37 °C. Cells were treated with either 2 × IC_{50} **t-PMB** (52 μM), 2 × IC_{50} **200** (40 μM), 0.1 % DMSO in media alone or media alone for 0, 6, 12, or 24 hours.

From their stock solutions, compound **t-PMB** and **200** were diluted in DMSO to 52 mM and 40 mM respectively. The compounds were then further diluted 100-fold in media to 520 μM for compound **t-PMB** and 400 μM for **200**. WHCO1 cells were then treated at a final concentration of either 52 μM **t-PMB** or 40 μM **200** in 0.1 % DMSO in triplicate and incubated at 37 °C with compound for 24 hours. The solvent controls for these experiments were cells treated with 0.1 % DMSO in media or media alone.

Medium from each plate was removed and cells were rinsed with 5 ml PBS (pH 7.5). Both the media and PBS were retained. The washed cells were trypsinised by the addition of 3 ml trypsin, transferred to a 50 ml tube, and centrifuged at 3000 rpm (596 ×g) for 5 minutes at room temperature. The cells were then re-suspended in 2 ml PBS (pH 7.5), and counted, followed by treatment with ice-cold 70 % ethanol to give a total volume of 10 ml, and stored at -20 °C (this can be stored for up to 2 weeks).

The cells were suspended in 8 ml 70 % ethanol, centrifuged at 1000 rpm (97 × g) for 5 minutes at room temperature, and the supernatant was removed, with 1 ml remaining, which was transferred to a 1 ml eppendorf, spun in a bench top centrifuge for 1 minute and the remaining supernatant removed. The cells were washed twice with 1 ml PBS (pH 7.5) in a bench-top centrifuge for 1 minute. RNase A was diluted in PBS (pH 7.5) to a final concentration of 10 mg/ml, and added in a ratio of 100 μl RNase A per 1 × 10^6 cells. The propidium iodide (PI) staining solution (See Appendix for preparation) was added at a volume 9 times that of the RNase A to yield a final concentration of 1 × 10^6 cells/ml 20 minutes prior to FACS analysis. The FACS analysis was performed in the FACSCalibur® flow cytometer.

8.7. Histone-association DNA fragmentation assay

To determine whether our compounds induce apoptosis, the histone association assay was performed using the Cell Death Detection ELISA^{PLUS} kit from Roche. The assay is based on a quantitative sandwich-enzyme-immunoassay-principle, using mouse monoclonal antibodies

directed against DNA and histones respectively. This allows the specific determination of mono- and oligonucleosomes in the cytoplasmic fraction of cell lysates.

For the assay, WHCO1 cells were seeded in 96-well plates at 2500 cells per well, and were allowed to settle for 24 hours in an incubator at 37 °C.

WHCO1 cells were treated with either **t-PMB** or **200** at two-fold, one-fold or ½-fold their respective 24-hour IC_{50} concentrations or 0.1 % DMSO alone for 24 hours. The 96-well plate was then centrifuged for 10 minutes at 997 rpm (200 ×g) at room temperature, and 50 µl of the supernatant was removed. The cells were treated with 200 µl lysis buffer for 30 minutes at room temperature.

8.7.1. ELISA assay

After the cells were lysed, 20 µl lysate was transferred to the streptavidin multi-plate and incubated with 80 µl immune-reagent per well. The multi-plate was covered with adhesive foil and incubated, while shaking (200 rpm), for 2 hours at room temperature. The lysate was removed by inverting and tapping the plate, and thereafter washed thrice with 250 µl incubation buffer per well. Each well was treated with 100 µl ABTS solution, and incubated by shaking at 200 rpm until colour development was sufficient for photometric analysis. To stop the reaction, 100 µl ABTS stop solution was added per well and measurements were taken at 405 nm against ABTS stop solution.

8.8. ROS assay

The accumulation of ROS, which is coupled with increased oxidative stress, has been implicated in the pathogenesis of many diseases, including cancer. For the detection of ROS, the cell-permeable fluorogenic probe 2', 7' –dichlorodihydroflouroscin diacetate (DCFH-DA) was used, which diffuses into the cell and is deacetylated by cellular esterases to form the non-fluorescent 2', 7' –Dichlorodihydroflouroscin, which is rapidly oxidised to highly fluorescent 7' –Dichlorodihydroflouroscin diacetate (DCF) by ROS. The fluorescence intensity is proportional to the ROS present in the cell cytosol. The relative florescence intensity of DCF is measured at an excitation wavelength of 480 nm and an emission wavelength of 530 nm.

For the assay, WHCO1 cells were seeded in five sterile white 96-well plates at 10 000 cells/ well in complete DMEM, and allowed to settle and recover for 24 hours in an incubator at 37 °C.

8.8.1 Treating with DCFH-DA and OSC

After the cells were allowed to settle and recover, the media was removed, cells were rinsed twice with 1 × PBS (pH 7.5) and then re-suspended in Krebs' Ringer Buffer (KRB) supplemented with 10 μM DCFH-DA (Sigma). The cells were then treated with either **200** or **t-PMB** at doses ranging from 2-fold, 1-fold or ½-fold of each compounds respective IC_{50}, and control cells were treated with 0.1 % DMSO or media alone in quadruplicate. As a positive control, cells were treated with 5 μM doxorubicin. To account for background DCFH-DA and/or OSC fluorescence, wells with no cells were treated with DCFH-DA, OSC or DCFH-DA and OSC in KRB, and these fluorescence values were subtracted from their corresponding wells with cells. One 96-well plate was used per fluorescence reading, with readings taken at 0, 1, 2, 3 and 6 hours post-treatment at an excitation of 480 nm and an emission of 530 nm using a Cary Eclipse fluorescence spectrophotometer (Varian).

8.8.2. ROS inhibition

WHCO1 cells were seeded in a sterile white 96-well plate at 10 000 cells per well in DMEM, and allowed to settle and recover for 24 hours in an incubator at 37 °C. The medium was removed, cells were washed twice with 1 × PBS (pH 7.5) and then re-suspended in KRB. Cells were then treated with ROS inhibitors; 7.5 mM *N*-acetyl-L-cysteine (NAC) (Sigma), 50 μM L-Ascorbic acid (ascorbate) (Sigma) or 12.5 μM *6-Hydroxy-2,5,7,8-tetramethylchroman-2-carboxylic Acid* (TROLOX) (Calbiochem®) and incubated at 37 °C for 30 minutes. Thereafter cells were treated with 10 μM DCFH-DA and incubated for an additional 30 minutes. Finally, cells were treated with either **t-PMB** or **200** at their respective 24 hour IC_{50} concentrations, and control cells were treated with either 0.1 % DMSO or media alone in quadruplicate. To account for background DCFH-DA and/or OSC fluorescence, wells with no cells were incubated with DCFH-DA, OSC or DCFH-DA and OSC in KRB, and the fluorescence values were subtracted from their corresponding wells with cells. Fluorescence readings were taken 3 hours post-treatment with OSC at an excitation of 480 nm and an emission of 530 nm using a Cary Eclipse fluorescence spectrophotometer (Varian).

8.8.3. NMR on NAC and t-PMB reaction product

A solution of **t-PMB** (150 mg, 0.486 mmol) in THF (5 mL) was added to *N*-acetyl cysteine (40 mg, 0.243 mmol), dissolved in THF (0.5 mL) at room temperature under nitrogen. The reaction was allowed to proceed at room temperature (26 °C) overnight (16 hours). The mixture was then evaporated under reduced pressure and the residue purified by silica gel chromatography to afford the product (53.6 mg, 0.188 mmol) in a 78% yield.

8.9. Tumour growth in nude mice

8.9.1. Preparing WHCO1 oesophageal and A375 melanoma cancer cell-lines

The animal study was approved by the Animal Ethics Committee (AEC), protocol number: 0.12/003). The WHCO1 oesophageal and A375 human melanoma cancer cells were seeded in a 100 mm dish in complete DMEM, and allowed to settle and recover for 24 hours. Thereafter, cells were rinsed with 1 × PBS (pH 7.5) and incubated at 37 °C with trypsin until the cells detached. The cells in trypsin were then transferred to a 12 ml tube, and the plate was washed with complete DMEM and then transferred to the 12 ml tube. Cells were then collected by centrifugation at 4000 rpm (1541 ×g). Thereafter, the trypsin was removed and the cells were re-suspended in complete DMEM. Each mouse was subcutaneously injected with 5×10^6 WHCO1 oesophageal or A375 human melanoma cells in a volume of 100 µl on the right side of the lower back. Immediately following the inoculations, mice with the A375 melanoma xenografts were treated with either **t-PMB** or **200**, whereas mice with the WHCO1 oesophageal cancer xenograft was treated with **200** three days after tumour inoculation.

8.9.2. Preparing OSC

The **t-PMB** or **200** was prepared immediately before treating the mice each day. Briefly, **t-PMB** or **200** was diluted in PEG (Sigma), vortexed and then sonicated for 10 minutes at 37°C. Thereafter chondroitin was added to the solution at a final concentration of 2.5 %, and the solution was vortexed. DMSO was then added to the solution to a final concentration of 10 %, whereafter vortexing and sonication was repeated, and the solution sterilized through filtration. The nude mice were then treated by intraperitoneal (IP) injection of 100 µl **t-PMB** or **200** at a final concentration of 30 mg/kg or 25 mg/kg (50 mg/kg for the first 4 days) respectively in nude mice with the A375 xenograft. Nude mice with the WHCO1 xenograft were treated with 20 mg/kg **200** for the first 6 days, where after the dose was decreased to 10 mg/kg **200**, once a day. Control mice were treated with 50 % PEG, 10 % DMSO and 2.5 %

chondtroitin only. Treatment continued every day until the largest tumour size was almost 200 mm (the animal ethics protocol does not allow a tumour width greater than 20 mm).

8.9.3. Pharmacokinetic data on 200

Pharmacokinetic analysis, done at the Pharmacology department of UCT by Ms. Carmen de Kock, was performed on the blood samples from mice treated with **200** to determine its concentrations in the blood. For the analysis, mice with the WHCO1 xenograft from the treated group received 10 mg/kg **200**, and whole blood was collected in heparin coated tubes 1 hour after treatment. The blood samples of the **200**-treated mice were stored for 2 months at - 80 °C before the analysis was performed.

A calibration curve for **200** ranging from 15.6 – 1000 ng/ml was prepared in mouse plasma, and quality control (QC) samples were prepared at two concentrations namely 400 ng/ml (QC1) and 800 ng/ml (QC2). The standards for the calibration curve and the quality control samples were extracted in duplicate. For the extraction procedure of **200** from the blood of mice, 10 µl blood was mixed with 100 µl acetonitrile, vortexed for 1 minute and then sonicated for 1 minute. Thereafter, the sample was centrifuged at 5750 ×g for 5 minutes and 80 µl of the supernatant was transferred to the mass spectrometer (MS) vials for Liquid Chromatography Mass Spectrometry (LC/MS/MS) which was performed on the API 200 (AB Sciex) LC/MS/MS instrument. The (MS) conditions are depicted in Table 8.3 and 8.4.

Table 8.3. Electro spray ionisation settings for mass spectrometry analysis of **200** samples.

Nebuliser gas (Gas 1) (arbitrary unit)	50
Turbo gas (Gas 2) (arbitrary unit)	60
CUR (curtain gas) (arbitrary unit)	20
CAD (collision gas) (arbitrary unit)	6
TEM (Source Temperature) (°C)	450
IS (Ion Spray Voltage) (V)	5500

The analytical column used was Luna PFP 3 µm, 50 x 2.0 mm (Phenomenex). The mobile phase consisted of acetonitrile and 10 mM ammonium acetate which ran isocratically for 6 minutes, with a flow rate of 300 µl/min. The calibration curves fits quadratic (weighted by 1/concentration) regressions over the ranges 15.6 - 1000 ng/ml, based on peak areas. The

lower limit of quantification was set at 15.6 ng/ml. The system suitability test is done before the batch, a SYS sample (a mid-level extracted sample) is injected 6 times and the acceptance criteria is that the peak area of the samples should be below 5%.

Table 8.4. Mass spectrometry settings for mass spectrometry analysis of **200** samples.

Protonated molecular ion mass (m/z) [M+H]+	185.9
Product ion mass (m/z) Quantifier	111.1
Product ion mass (m/z) Qualifier	144.1
Dwell time (ms)	150
Declustering potential (V)	26.0
Entrance potential (V)	6.5
Collision energy (eV)	35
Collision cell exit potential (V)	6.0

8.10. Protein Disulfide Isomerase (PDI)

8.10.1. Detection of PDI in various cell-lines

To determine the levels of PDI expressed in different cancer cell-lines, protein lysate was collected to detect PDI by western blot analysis, and quantified using densiometric analysis. The cancer cell-lines used to detect PDI levels were HeLa, KYSE-180, PC-3, SiHa, A375, MDA-MB-231 and WHCO1. All apparatus used for the western blot were purchased from Biorad®, unless otherwise stated. For the assay, cells were grown to 90 % confluence, thereafter the media was removed, and cells were rinsed twice with 1 × PBS. The cells were treated with 1 × RIPA buffer (Cell signalling) supplemented with 1 × protease inhibitor (Roche®), for 5 minutes. The lysed cells were freeze-thawed thrice at - 80 °C/37 °C, and sonicated for ~ 2 seconds. The lysate was centrifuged at 14 000 rpm for 15 minutes at 4 °C. Thereafter, the supernatant was retained, and the pellet discarded, and the relative protein concentration in each sample was quantified using the Pierce® BCA Protein Assay Kit according to the manufacturer's instructions.

After protein quantification, 60 µg protein was mixed with 1 × protein loading buffer (See Appendix for preparation) to a final volume of 40 µl, and heated at 95 °C for 10 minutes. Thereafter, the lysate was centrifuged on a bench top centrifuge for 1 minute. The samples were loaded on a polyacrylamide gel containing a 4 % stacking gel (See Appendix for

preparation) and an 8 % separating gel (See Appendix for preparation), where the protein separation took place in running buffer (See Appendix for preparation). The initial voltage was set to 100 V until the dye front reached the separating gel, at which stage the voltage was increased to 200 V until the bromophenol blue was 0.5 cm from the bottom of the gel.

Once the SDS-PAGE was completed, the proteins were transferred to a nitrocellulose membrane (BioTrace™) at 100 V for 1.5 hours in ice-cold transfer buffer (See Appendix for preparation). Once the protein was transferred to the nitrocellulose membrane, the membrane was incubated with Ponseau stain (See Appendix for preparation) for 5 minutes to stain the proteins on the membrane. Thereafter, the membrane was washed with water to remove excess ponseau and an image of the membrane was taken using the CanonScan 4400F scanner (Canon).

After the transfer, the nitrocellulose membrane was blocked by gentle shaking in 5 % fat-free powder milk diluted in TBST (See Appendix for preparation) at room temperature for 1 hour. Thereafter, the membrane was treated with rabbit anti-PDI (Enzo®) (1:1000) antibody at 4 °C overnight. Once labelled with the primary antibody, the nitrocellulose membrane was washed thrice with TBST (See Appendix for preparation), with each wash lasting 10 minutes. The nitrocellulose membrane was then incubated with the goat-anti-rabbit (Biorad) secondary antibody for 1 hour at room temperature with gentle shaking. Once labelled with the secondary antibody, the nitrocellulose membrane was washed thrice with TBST, with each wash lasting 10 minutes. The membrane was treated with LumiGLO Reserve™ chemiluminescence substrate (KPL) for 30 seconds and the relative chemiluminescence was detected using the UVP Biospectrum™ 500 Imaging System.

To measure GAPDH as a loading control, the nitrocellulose membrane was stripped by incubating with glycine (pH 2.5) alternate stripping buffer (See Appendix for preparation) for 10 minutes at room temperature while shaking. Thereafter, 1 M Tris-acetate (pH 7.5) (See appendix for preparation) was added to the stripping buffer to neutralise the solution. Thereafter the protocol for detecting GAPDH on the nitrocellulose membrane is the same as for anti-PDI.

The relative quantities of PDI from each cell-line were detected by normalising with GAPDH as a loading control, which was measured through densiometric analysis using the UVP Vision Works™LS Acquisition and Analysis Software Version 6.8.

8.10.2. Immunohistochemistry

8.10.2.1. Cell culturing

To investigate the localisation of PDI and **DP**, 50 000 KYSE-180 cells were seeded onto a glass coverslip in a 6 well-plate in complete DMEM. The cells were incubated at 37 °C and allowed to settle and recover for 24 hours. The cells were then treated with 9 μM **DP** (IC_{50}) in 0.1 % DMSO or 0.1 % DMSO in media alone for 24 hours.

Once cells had settled and recovered, the coverslips were washed with pre-warmed 1 × PBS (pH 7.5). The cells were then fixed and permeabilised by adding ice-cold absolute methanol and incubating at - 20 °C for 5 minutes. Thereafter, the cells were fixed with 4 % paraformaldehyde in 1 × PBS (pH 7.5) for 5 minutes at room temperature.

Once the cells were fixed, the coverslips were blocked using 1 % bovine serum albumin (BSA) (Sigma) supplemented with 0.1 % Triton X-100 (Sigma) in 1 × PBS (pH 7.5) for 1 hour at room temperature. Thereafter, the cells were treated with the rabbit anti-PDI (1:50 in blocking solution) antibody. The coverslips were sealed in a humidified chamber and incubated at 4 °C overnight. Once labelled with primary antibody, the cells were washed thrice with 1 × PBS, 10 minutes per wash. Thereafter, the coverslips were mounted with MOWIOL® 4-88 (See Appendix for preparation) to a glass slide, and incubated at room temperature overnight to allow the MOWIOL® 4-88 to set. Fluorescence was detected using the Olympus IX81F-3 fluorescence microscope where **DP** was detected with the NU filter (blue) and PDI was detected with the NG filter (red).

8.10.3. PDI enzyme assay

To determine whether OSC inhibit PDI enzyme activity; DTNB, a known PDI inhibitor, **t-PMB**, **200** and **DP** were used in a PDI enzyme assay, which is based on the oxidative renaturation of reduced RNase A by PDI. The renatured RNase A activity was assessed by its ability to hydrolyse cytidine 2',3'-cyclic monophosphate (cCMP), where the hydrolysed product can be detected spectrophotometrically at 296 nm.

RNase A from bovine pancreas was denatured overnight in 6 M guanidine hydrochloride (Sigma®), 0.14 M DL-Dithiothreitol (DTT) (Sigma®) and 2 mM EDTA disodium salt (univAR®) (See Appendix for prepration) in 0.1 M Tris-acetate (pH 8.0) (See Appendix for preparation). Immediately before use, the reduced RNase A was separated from excess DTT,

guanidine hydrochloride and EDTA through centrifugal filtration (14 000 rpm) using a 3000 molecular weight cut off VIVASPIN 500 (satorius stedim) filter unit. To confirm that PDIs isomerase activity on RNase A leads to the renaturation of reduced (denatured) RNase A, and the subsequent hydrolysis of cCMP, a cocktail mixture of Tris-acetate buffer (pH 8.0) with 4.5 mM cCMP (Sigma®), 1 mM reduced L-glutathione (GSH) (Sigma®), 0.2 mM L-glutathione oxidised disodium salt (GSSG) (Sigma®) and 1.4 μM bovine PDI (Sigma®) was initiated by the addition of the 8.4 μM reduced RNase A. The hydrolysis of cCMP, which results from the gain in RNase A activity, was recorded at 296 nm 35 minutes after the initiation of the reaction using the Cary Eclipse UV spectrophotometer. To confirm the inhibitory activity of DTNB, and assess whether **t-PMB**, **200** and **DP** display inhibitory activity against PDI, PDI was treated with 100 μM DTNB, 20 μM **t-PMB**, 20 μM **200** or 20 μM **DP** 10 minutes prior to its addition to the reaction cocktail. Again, 8.4 μM reduced RNase A was added to initiate the reaction. As a background control, 8.4 μM denatured RNAse A was added to Tris-acetate buffer (pH 8.0), 4.5 mM cCMP, 1 mM GSH (Sigma®) and 0.2 mM GSSG (Sigma®).

References

Ankri, S. & Mirelman, D., 1999. Antimicrobial properties of allicin from garlic. *Microbes and infection*, 1, pp.125-129.

Arunkumar, A. *et al*., 2006. Garlic compound, diallyl disulfide induces cell cycle arrest in prostate cancer cell line PC-3. *Molecular and cellular biochemistry*, 288, pp.107-113.

Bai, X. *et al*., 2003. Honokiol, a small molecular weight natural compound, inhibits angiogenesis *in vitro* and tumor growth *in vivo*. *The journal of biological chemistry*, 278, pp. 35501-35507.

Bargagna-Mohan, P. *et al*., 2007. The tumor inhibitor and antiangiogenic agent withaferin A targets the intermediate filament protein vimentin. *Chemistry and Biology*, 14, 623-634.

Block, E. *et al*., 1992. *Allium* chemistry: HPLC analysis of thiosulfinates from onion, garlic, wild garlic (ramsoms), leeks, scallion, shallot, elephant (great headed) garlic, chive and Chinese chive. Uniquely high allyl to methyl ratios in some garlic samples. *Journal of agricultural and food chemistry*, 40, pp.2418-2430.

Borek, C., 2006. Garlic reduced dementia and heart risk. *The journal of nutrition*, 136, pp.810S-812S.

Bourougaa, K. *et al*., 2010. Endoplasmic reticulum stress induces G2 cell-cycle arrest via mRNA translation of the p53 isoform p53/47. *Molecular cell*, 38, pp.78-88.

Brigger, I., Dubernet, C. & Couvreur, P., 2012. Nanoparticles in cancer therapy and diagnosis. *Advanced drug delivery reviews*, 64, pp.24-36.

Buiatti, E. *et al*., 1989. A case-control study of gastric cancer and diet in Italy. *International journal of cancer*, 44, pp.611-616.

Chen, M. *et al*., 2012. Effect of diallyl trisulfide derivatives on the induction of apoptosis in human prostate cancer PC-3 cells. *Molecular and cellular biochemistry*, 363, pp.75-84.

Chivers P.T., Labossiere, M.C. & Raines, R.T., 1996. The CXXC motif: imperatives for the formation of native disulfide bonds in the cell. *The EMBO journal*, 15, pp.2659-2667.

Coussens, L.M. & Werb, Z., 2002. Inflammation and cancer. *Nature*, 420, pp.860-867.

Cragg, G.M. & Newman, D.J., 2005. Plants as a source of anti-cancer agents. *Journal of ethnopharmacology*, 100, pp.72-79.

Cragg, G.M., Newman, D.J. & Snader, K.M., 1997. Natural products in drug discovery and development. *Journal of natural products*, 60, pp.52-60.

Darby, N.J., Freedaman, R.B. & Creighton, T.E., 1994. Dissecting the mechanism of protein disulfide isomerase: catalysis of disulfide bond formation in a model peptide. *Biochemistry*, 33, pp.7937-7947.

Das, A., Banik, N.L. & Ray, S.K., 2007. Garlic compounds generate reactive oxygen species leading to activation of stress kinases and cysteine proteases for apoptosis in human glioblastoma T98G and U87MG cells. *Cancer*, 110, pp.1083-1095.

Davis, S.R., 2005. An overview of the antifungal properties of allicin and its breakdown products-the possibility of a safe and effective antifungal prophylactic. *Mycoses*, 48, pp.95-100.

Dickerhof, N. *et al*., 2011. Bacitracin inhibits the reductive activity of protein disulfide isomerase by disulfide bond formation with free cysteines in the substrate binding domain. *The FEBS journal*, 278, pp.2034-2043.

Dirsch, V.M., 2002. Ajoene, an experimental anti-leukemic drug: mechanism of cell death. *Leukemia*, 16, pp.74-83.

Dirsch, V.M., Gerbes, A.L. & Vollmar, A.M., 1998. Ajoene, a compound of garlic, induces apoptosis in human promyeloleukemic cells, accompanied by the generation of reactive oxygen species and activation of nuclear factor kappaB. *Molecular pharmacology*, 53, pp.402-407.

Enzinger, P.C. & Mayer, R.J., 2003. Esophageal cancer. *The New England journal of medicine*, 349, pp.2241-2252.

Fearnhead, N.S., Wilding, J.L. & Bodmer, W.F., 2002. Genetics of colorectal cancer: hereditary aspects and overview of colorectal tumorigenesis. *British medical bulletin*, 64, pp.27-43.

Ferrari, D.M. *et al*., 1998. ERp28, a human endoplasmic-reticulum-lumenal protein, is a member of the protein disulfide isomerase family but lacks the CXXC thioredoxin-box motif. *European journal of biochemistry*, 255, pp.570-579.

Filomeni, G., Aquilano, K. & Rotilio, G., 2003. Reactive oxygen species-dependent c-Jun NH2-terminal kinase/c-Jun signalling cascade mediates neuroblastoma cell death induced by diallyl disulfide. *Cancer research*, 1, pp.5940-5949.

Fleischauer, A. & Arab, L., 2001. Garlic and cancer: A critical review of the epidemiological literature. *Journal of nutrition*, 131, pp.1032S-1040S.

Freedman, R.B., Hirst, T.R. & Tuite, M.F., 1994. Protein disulfide-isomerase-building bridges in protein folding. *Trends in biochemical science*, 19, pp.331-336.

Gallwitz, H. *et al*, 1999. Ajoene is an inhibitor and subversive substrate of human glutathion reductase and Trypanosoma cruzi trypanothione reductase: Crystallographic, kinetic and spectroscopic studies. *Journal of medical chemistry*, 42, pp.364-372.

Goldberger, R.F., Epstein, C.J. & Anfinsen, C.B., 1963. Acceleration of reactivation of reduced bovine pancreatic ribonuclease by a microsomal system from rat liver. *Journal of biological chemistry*, 238, pp.628-635.

Graham, J.G. *et al*., 2000. Plants used against cancer-an extension of the work of Jonathan Hartwell. *Journal of ethnopharmacology*, 73, pp.347-377.

Hamano, R., Miyata, H. & Yamasaki, M., 2011. Overexpression of miR-200c induces chemoresistance in esophageal cancer mediated through activation of Akt signalling pathway. *Clinical cancer research*, 17, pp.3029-3038.

Hanahan, D. & Weinberg R.A, 2011. Hallmarkrs of cancer: the next generation. *Cell*, 144, pp.646-674.

Hanahan, D., Weinberg, R.A. & Francisco S., 2000. The hallmarks of cancer review. *Cell*, 100, pp. 57-70.

Hawkins, H.C., Blackburn, E.C. & Freedman, R.B., 1991. Comparison of the activities of disulfide isomerase and thioredoxin in catalysing disulphide isomerization in a protein substrate. *The biochemical journal*, 275, pp.349-353.

Herman-antosiewics, A., Powolny, A.A. & Singh, S.V., 2007. Molecular targets of cancer chemoprevention by garlic-derived organosulfides. *Acta* Pharmacologica *Sinica*, 28, pp.1355-1364.

Hosono, T. *et al*., 2005. Diallyl trisulfide suppresses the proliferation and induces apoptosis of human colon cancer cells through oxidative modification of beta-tubulin. *The journal of biological chemistry*, 280, pp. 41487-41493.

Hunter, R, *et al*., 2008. Substituted ajoenes as novel anti-cancer agents. *Bioorganic and medicinal chemistry letters*, 10, pp.5277-5279.

Hwang, C., Sinskey, A.J. & Lodish, H.F., 1992. Oxidised redox state of glutathione in the endoplasmic reticulum. *Science*, 257, pp.1496-1502.

Ilson, D.H. & Kelson, D.P., 1993. Chemotherapy in esophageal cancer. *Anti-cancer drugs*, 4, pp.287-299.

Islami, F., *et al*., 2009a. High-temperature beverages and foods and esophageal cancer risk-a systemic review. *International journal of cancer*, 125, pp.491-524.

Islami, F., *et al*., 2009b. Socio-economic status and oesophageal cancer: results from a population based case-control study in a high-risk area. *International journal of epidemiology*, 38, pp.978-988.

Jain, S., McGinnes, L.W. & Morrison, T.G., 2007. Thiol/disulfide exchange is required for membrane fusion directed by Newcastle disease virus fusion protein. *Journal of virology*, 81, pp.2328-2339.

Jemal, A., Bray, F. & Center, M., 2011. Global cancer statistics. *CA: a cancer journal*, 61, 69-90.

Kaschula, C.H. *et al*., 2011. Anti-proliferative activity of synthetic ajoene analogues on cancer cel-lines. *Anti-cancer agents in medicinal chemistry*, 11, pp.260-266.

Kaschula, C.H. *et al*., 2012. Structure-activity studies on the anti-proliferation activity of ajoene analogues in WHCO1 oesophageal cancer cells. *European journal of medicinal biochemistry*, 50, pp.235-254.

Kawamori, T. *et al*., 1995. Chemoprevention of azoxymethane-induced colon carcinogenesis by dietary feeding of S-methyl methane thiosulfonate in male F344 rats. *Cancer research*, 55, pp.4053-4058.

Kelkel, M. *et al*., 2012. ROS-independent JNK activation and multisite phosphorylation of Bcl-2 link diallyl tetrasulfide-induced mitotic arrest to apoptosis. *Carcinogenesis*, 33, pp.2162-2171.

Kemmink, J. *et al*., 1997. The folding catalyst protein disulfide isomerase is constructed of active and inactive theoredoxin molecules. *Current biology*, 7, pp.239-245.

Kim, S.Y. *et al*., 2008. Thiosulfinates form allium tuberosum L. induce apoptosis via caspase-dependent and –independent pathways in PC-3 human prostate cancer cells. *Bioorganic and medicinal chemistry letters*, 18, pp.199-204.

Kim, Y.A. *et al*, 2007. Mitochondria-mediated apoptosis by diallyl trisulfide in human prostate cancer cells is associated with generation of reactive oxygen species and regulated by Bax/Bak. *Molecular cancer chemotherapeutics*, 6, pp.1599-1609.

Kimbaris, A.C. *et al.*, 2006. Comparison of distillation and ultrasound-assisted extraction methods for the isolation of sensitive aroma compounds from garlic (*Allium sativum*). *Ultrasonics Sonochemistry*, 13, pp.56-60.

Kingston, D.G.I., Bane, S. & Snyder, J.P., 2005. The taxol pharmacophore and the t-taxol bridging principle. *Cell cycle*, 4, pp.279-289.

Klappa, P. *et al*., 1998. The b' domain provides the principle peptide-binding site of protein disulfide isomerase but all domains contribute to binding to misfolded proteins. *The EMBO Journal*, 17, pp.927-935.

Kortemme, T., Darby N.J. & Creighton, T.E., 1996. Electrostatic interactions in the active site of the N-terminal thioredoxin-like domain of protein disulfide isomerase. *Biochemitry*, 35, pp.14503-14511.

Krauth-Siegel, R.L. *et al*., 1996. Glutathione reductase and glutamate dehydrogenase of Plasmodium falciparum, the causative agent of tropical malaria. *European journal of biochemtry*, 235, pp.345-350.

Kwon, K.B. *et al*., 2002. Induction of apoptosis by diallyl disulfide through activation of caspase-3 in human leukemia HL-60 cells. *Biochemical pharmacology*, 63, pp.41-47.

Laakso, I. *et al.*, 1989. Volatile garlic odor components: gas phase and adsorbed exhaled air analysed by headspace gas chromatography-mass spectrometry. *Planta medica*, 55, pp.257-261.

Lara, H.H. *et al*., 2011. Antiviral properties of 5,5'-dithiobis-2-nitrobenzoic acid and bacitracin against T-tropic human immunodeficiency virus type 1. *Virology jounal*, 8, p137.

Lawson, L.D. & Gardner, C.D., 2005. Composition, stability, and bioavailability of garlic products used in a clinical trial. *Journal of agricultural and food chemistry*, 53, pp.6254-6261.

Lawson, L.D. & Wang Z.J., 1993. Pre-hepatic fate of the organosulfur compounds derived from garlic (*Allium sativum*). *Planta Medica*, 59, pp.688-689.

Lee, S.N., Kim, N.S. & Lee, D.S. Comparative study of extraction techniques for the determination of garlic flavour components by gas chromatography-mass spectrometry. *Analytical and bioanalytical chemistry*, 377, pp.749-756.

Li, M. *et al*., 2002. Anti-tumour activity of *Z*-ajoene, a natural compound purified form garlic: anti-mitotic and microtubule-interaction properties. *Carcinogenesis*, 23, pp.573-578.

Liao, Q.J. *et al*., 2007. Inhibitory effects of diallyl disulfide on proliferation of human colon cancer cell line SW480 in nude mice. *Ai Zheng*, 26, pp.828-832.

Lowe, S.W. *et al*., 1994. p53 status and the efficacy of cancer therapy *in vivo*. *Science*, 266, 807-810.

Lyles, M.M. & Gilbert, H.F., 1991. Catalysis of the oxidative folding of ribonuclease A by protein disulfide isomerase: dependence of the rate on the composition of the redox buffer. *Biochemistry*, 30, pp.613-619.

Mandel, R. *et al*., 1993. Inhibition of a reductive function of the plasma membrane by bacitracin and antibodies against protein disulfide-isomerase. *Proceedings of the national academy of Sciences of the United States of America*, 90, pp.4112-4116.

Murakami, A. *et al*., 2002. Zerumbone, a Southeast Asia ginger sesquiterpene, markedly supresses free radical generation, proinflammatory protein production, and cancer cell proliferation

accompanied by apoptosis: a α,β-unsaturated carbonyl group is a prerequisite. *Carinogenesis*, 23, pp.795-802.

Matejcic, M. *et al*., 2011. Association of a deletion of GSTT2B with an altered risk of oesophageal squamous cell carcinoma in a South Afican population: a case control study. *PloS one*, 6, pp.1-8.

Miller, A.B. *et al*., 1981. Reporting results of cancer treatment. *Cancer*, 47, pp.207-214.

Naznin, M. *et al*., 2008. Characterization of *E*- and *Z*-ajoene obtained from different varieties of garlics. *Food chemistry*, 106, pp.1113-1119.

Nishikawa, T. *et al*., 2002. Inhibition by ajoene of skin-tumour promotion in mice. *Bioscience, biotechnology and biochemistry*, 66, pp.2221-2223.

Nobili, S. *et al*., 2009. Natural compounds for cancer treatment and prevention. *Pharmacology research*, 59, pp.365-378.

Noiva, R., 1999. Protein disulfide isomerase: the multifunctional redox chaperone of the endoplasmic reticulum. *Seminars in cell & developmental biology*, 10, pp.481-493.

Noiva, R., Freedman, R.B. & Lennarz, W.J., 1993. Peptide binding to protein disulfide isomerase occurs at a site distinct form active sites. *The journal of biological chemistry*, 268, pp.19210-19217.

Peer, D. *et al*., 2007. Nanocarriers as an emerging platform for cancer therapy. *Nature nanotechnology*, 2, pp.751-760.

Pelicano, H., Carney, D. & Huang, P., 2004. ROS stress in cancer cells and therapeutic implications. *Drug resistance updates: reviews and commentaries in antimicrobial and anticancer chemotherapy*, 7, pp.97-100.

Reddy, B.S. *et al*., 1999. Chemopreventative effect of *S*-methylmethane thiosulfonate and sulindac administered together during the promotion/progression stages of colon carcinogenesis. *Carcinogenesis*, 20, pp.1645-1648.

Reinhart, K.M. *et al*., 2008. Effects of garlic on blood pressure in patients with and without systolic hypertension: A meta-analysis. *The annals of pharmacotherapy*, 42, pp.1766-1771.

van Rensberg, S.J., 1981. Epidemiologic and dietary evidence for a specific nutritional predisposition to oesophageal cancer. *Journal of the natural cancer institute*, 67, pp.243-251.

van Rensburg, S.J. *et al*., 1985. Oesophageal cancer in Zulu men, South Africa: a case-control study. *British journal of cancer*, 51, pp.399-504.

Ried, K. *et al*., 2008. Effects of garlic on blood pressure: a systemic review and meta-analysis. *BMC cardiovascular disorders*, 8, pp.13.

Rose, E.F. & McGlashan, N.D., 1975. The spatial distribution of oesophageal carcinoma in the Transkei, South Africa. *British journal of cancer*, 31, pp.197-206.

Santos, C.X.C. *et al*., 2009. Protein disulfide isomerase (PDI) associates with NADPH oxidase and is required for phagocytosis of Leishmania chagasi promastigotes by macrophages. *Journal of leukocyte biology*, 86, pp.989-998.

Scharfenberg, K., Wagner, R. & Wagner, K.G., 1990. The cytotoxic effects of ajoene, a natural product from garlic, investigated with different cell-lines. *Cancer letters*, 53, pp.103-108.

Scherer, W.F. & Syverton, J.T., 1952. Studies on the propagation *in vitro* of poliomyelitis virus. III. The propagation of poliomyelitis virus in tissue cultures devoid of nerve cells. *The journal of experimental medicine*, 96, pp.389-400.

Semenza, G.L., 2003. Targeting HIF-1 for cancer therapy. *Nature reviews Cancer*, 3, pp.721-732.

Shaaban, A.M. *et al*., 2012. A comprehensive biomarker study of 514 matched cases of male and female breast cancer reveals gender-specific biological differences. *Breast cancer research and treatment*, 133, pp.949-958.

Shukla, Y. & Kalra, N., 2007. Cancer chemoprevention with garlic and its constituents. *Cancer Letters*, 247, pp.167-181.

Stellenboom, N., Hunter, R., Caira M.R., 2010. One-pot synthesis of unsymmetrical disulfides using 1-chlorobenzotrizole as oxidant: Interception of the sulfenyl chloride intermediate. *Tetrahedron*, 66, pp.3228-3241.

Sumiyoshi, H. & Wargovich, J., 1990. Chemoprevention of 1,2-dimethylhydrazine-induced colon cancer in mice by naturally occurring organosulfur compounds. *Cancer research*, 50, pp.5084-5087.

Sundaram, S.G. & Milner, J.A., 1996a. Diallyl disulfide inhibits the proliferation of human tumour cells in culture. *Biochemica et biophysica acta*, 1315, pp.15-20.

Sundaram, S.G. & Milner, J.A., 1996b. Dially disulfide suppresses the growth of human colon tumor cell xenografts in athymic nude mice. *The journal of nutrition*, 126, pp.1355-1361.

Sundaram S.G. & Milner J.A, 1996c. Diallyl disulfide induces apoptosis of human colon tumour cells. *Carcinogenesis*, 17, pp.669-673.

Surh, Y.J., 2003. Cancer chemoprevention and dietary phytochemicals. *Nature reviews*, 3, pp.768-780.

Taylor, P. *et al*., 2006. Ajoene inhibits both primary tumor growth and metastasis of B16/BL6 melanoma cells in C57BL/6 mice. *Cancer letters*, 239, pp.117-123.

Tilli, C.M.L.J. *et al*., 2003. The garlic-derived organosulfur component ajoene decreases basal cell carcinoma tumor size by inducing apoptosis. *Archives for dermatological research*, 295, pp.117-123.

Toyojuni, S. *et al*., 1995. Persistent oxidative stress in cancer. *FEBS letters*, 358, pp1-3.

Tsang, W.P. *et al*., 2003. Reactive oxygen species mediate doxorubicin-induced p53-independent apoptosis. *Life Sciences*, 73, pp.2047-2058.

Veale, R.B. & Thornly, A.L, 1989. Increased single class low-affinity EGF receptors expressed by human oesophageal squamous carcinoma cell lines. *South African journal of science*, 85, 375-379.

Vermorken, J.B. *et al*., 2007. Cisplatin, fluorouracil, and docetaxel in unresectable head and neck cancer. *The New England journal of medicine*, 357, pp.1695-1705.

Vuori, K. *et al*., 1992. Expression and site-directed mutagenesis of human protein disulfide isomerase in *Escherichia coli*. This multifunctional polypeptide has two independently acting catalytic sites for the isomerase activity. *The Journal of biological chemistry*, 267, pp.7211-7214.

Wang, M. *et al*., 1996. Lipid peroxidation-induced putative malondialdehyde-DNA adducts in human breast tissues. *Cancer epidemiology, biomarkers and prevention*, 5, pp.705-710.

Wang, S. *et al*., 2004. Doxorubicin induces apoptosis in normal and tumor cells via distinctly different mechanisms. *The journal of biological chemistry*, 279, pp25535-25543.

Wattenberg, L.W., Sparnins, V.L & Barany, G., 1989. Inhibition of *N*-nitrosodiethylamine carcinogenesis in mice by naturally occurring organosulfur compounds and monoterpenes. *Cancer research*, 49, pp.2689-2692.

Wu, M. *et al*., 2009. Green tea drinking, high tea temperature and esophageal cancer in high and low risk areas of Jiangsu Province, China: a population-based control-study. *International journal of cancer*, 124, pp.1907-1913.

Wu, X.J., Kassie, F. & Mersch-Sundermann, V., 2005. The role of reactive oxygen species (ROS) production on diallyl disulfide (DADS) induces apoptosis and cell cycle arrest in human A549 ling carcinoma cells. *Mutation research*, 579, pp.115-124.

Wunderlich, M. *et al*., 1995. Efficient catalysis of disulfide formation during protein folding with a single active-site cysteine. *Journal of molecular biology*, 247, pp.28-33.

Xiao D. *et al*., 2004. Diallyl trisulfide induced apoptosis in human prostate cancer cells involves c-Jun N-terminal kinase and extracellular-signal regulated kinase-mediated phosphorylation of Bcl-2. *Oncogene*, 23, pp.5594-5606.

Xiao D. *et al*., 2005. Diallyl trisulfide-induced G(2)-M phase cell cycle arrest in human prostate cancer cells is caused by reactive oxygen species-dependent destruction and hyperphosphorylation of Cdc 25 C. *Oncogene*, 24, pp.6256-6268.

Xiao, D. *et al*., 2005. Effects of a series of organosulfur compounds on mitotic arrest in human and induction of apoptosis in colon cancer cells. *Molecular cancer therapeutics*, 4, pp1388-1398.

Xiao, D. *et al*., 2009. Diallyl trisulfide selectively causes Bax- and Bak-mediated apoptosis in human lung cancer cells. *Environmental and molecular mutagenesis*, 50, pp.201-212.

Yang, J. *et al*, 2006. Diallyl disulfide inhibits WEHI-3 leukemia cells *in vivo*. *Anticancer research*, 26, pp.219-226.

Yang, J.S. *et al*., 2009. Diallyl disulfide induces apoptosis in human colon cancer cell-line (COLO 205) through the induction of reactive oxygen species, endoplasmic reticulum stress, caspase cascade and mitochondrial-dependent pathways. *Food and chemical toxicology*, 47, pp.171-179.

You , W.C. *et al*., 1989. Allium vegetables and reduced risk of cancer. *Journal of the national cancer institute*, 81, pp.162-164.

Zapun, A. *et al*., 1992. Folding *in vitro* of bovine pancreatic trypsin inhibitor in the presence of proteins of the endoplasmic reticulum. *Proteins*, 14, pp.10-15.

Zbar, B. *et al*., 1995. Hereditary papillary renal cell carcinoma: clinical studies in 10 families. *The journal of urology*, 153, pp.907-912.

Appendix: Reagent Contents

Acrylamide/bisacrylamide stock solution (30 %) (29:1):

For the acrylamide/bisacrylamide stock solution, 29 g Acrylamine and 1 g bisacrylamide was diluted in 100 ml double distilled water and stored in the dark at 4 °C.

Alternate stripping solution:

1 M Glycine at pH 2.5.

10 % Ammonium persulfate (APS):

100 mg APS was dissolved in 1 ml double-distilled water, and stored at 4 °C.

Coomassie staining solution:

For the preprataion of coomassie staining solution, 0.5 g Coomassie BB was diluted in 200 ml methanol, 100 ml acetic acid and 400 ml double-distilled water.

Destaining solution:

Destaining solution included 100 ml acetic acid, 100 ml methanol and 800 ml double-distilled water and stored at room temperature.

Dulbecco's minimal eagle media (DMEM):

The DMEM is made from DMEM Powder, catalogue number 12800-017, and is made according to the manufacturer's instructions.

0.5 M EDTA (pH 8.0):

37.22 g $Na_2EDTA{\cdot}2H_2O$ was added to 140 ml double distilled water. The pH was adjusted to 8.0 with NaOH, where after double-distilled water was added to a final volume of 200 ml, and the solution autoclaved and stored at room temperature.

MOWIOL® 4-88 mounting medium:

75 g MOWIOL 4-88 ® (Calbiochem) mounting medium was diluted in 300 ml 1× PBS and stirred for 16 hours at room temperature. Thereafter, 150 ml glycerol was added, and the solution was stirred for a further 16 hours at room temperature and centrifuged for 15 minutes at 4000 rpm in 50 ml Falcon tubes where after the pH of the solution was adjusted to 8. The supernatant was stored in aliquots at -20 °C, supplemented with n-Propylgallate.

5 % Non-fat blocking solution:

2.5 mg non-fat milk powder was dissolved in 30 ml TBST, which was dissolved to a final volume of 50 ml with double-distilled water.

5 mg/ml 3-[4,5-dimethylthiazol]-2,5-diphenyltetrazolium bromide (MTT):

100 mg MTT (3-[4,5-dimethylthiazol]-2,5-diphenyltetrazolium bromide) (Sigma) was transferred to a 50 ml conical tube. Under sterile conditions, 20 ml 1 × PBS (pH 7.5) was transferred to the 50 ml conical tube. The mixture was then vortexed and incubated in a water bath for 15 minutes. The conical tube was then wrapped in foil, stored at 4 °C, and used within a month.

Penicillin G/Streptomycinsulfate:

For the preparation of the penicillin G/streptomycinsulfate solution, 604 mg (999620 IU) penicillin G and 1316 mg (1000160 IU) streptomycinsulfate was dissolved in 100 ml double-distilled water, and filter sterilised.

10 × Phosphate Buffer Saline (PBS) (pH 7.5):

For a 10 × PBS preparation NaCl (Merck), KCl (Merck), Na_2HPO_4 (Merck) and KH_2PO_4 (Merck) powders were diluted in double distilled water to 1.37 M , 27 mM, 43 mM and 14 mM respectively, and finally calibrated to a final pH of 7.5.

Ponseau staining soluntion:

The Ponseau ($usb_®$) staining solution was prepared by diluting Ponseau powder and acetic acid in double-distilled water to 0.2 % and 5 % respectively.

Propidium iodide (PI) staining solution:

Stocks of 100% Triton X-100, 1 M $MgCl_2$, 1 M NaCl, 0.1 M PIPES and 1 mg/ml PI were diluted in 20 ml double-distilled water to give a final concentration of 0.1 % Triton X-100, 2 mM $MgCl_2$, 0.1 M NaCl, 10 mM PIPES and 0.01 mg/ml PI. The solution was stored in a 50 ml Falcon tube and covered with foil as it is sensitive to light.

4 × Protein loading buffer:

2.5 ml 1 M Tris at pH 6.8, 4 ml 20 % SDS, 0.2 ml 0.1 % bromophenol blue and 4 ml glycerol were mixed. 50 µl bromophenol blue (Merck) was added after the solution was diluted to a 1 × concentration.

10 × Running buffer:

Tris, glycine and SDS were diluted in double distilled water to a final concentration of 240 mM, 1.92 M and 35 mM respectively.

10 % Sodium dodecyl sulphate (SDS):

10 g SDS was dissolved in 80 ml double-distilled water, then made to a final volume of 100 ml with double-distilled water.

10 % Solubilisation reagent: Sodium Lauryl Sulfate (SLS):

5 ml 1 M HCl was added to 50 g SLS (MERCK). The solution was further diluted with double distilled water to a final volume of 500 ml.

4 % Stacking gel:

0.63 ml 1 M Tris (Merck) at pH 6.8, 0.65 ml 30 % acrylamide/bisacrylamide (Sigma®) and 50 µl 10 % SDS (Merck) was diluted in 3.65 ml double-distilled water. Immediately before adding to the gel tray, 25 µl 10 % ammonium persulfate (APS) (MERCK) and 5 µl TEMED (Sigma) was added to the solution.

8 % Stacking gel:

For the preparation of 8 % stacking gel, 3.75 ml 1 M Tris at pH 8.8, 2.7 ml 30 % acrylamide/bisacrylamide and 100 µl 10 % SDS was diluted in 3.39 ml double-distilled water. Immediately before adding to the gel tray, 50 µl 10 % ammonium persulfate (APS) and 5 µl TEMED was added to the solution.

TBST (TBS-tween):

To make up TBST, 50 ml 1 M tris-base, 20 ml 5 M NaCl and 250 µl Tween-20 was dissolved in 100 ml double-distilled water, and stored at room temperature.

10 × Transfer buffer:

3.03 Tris and 14.5 glycine (Merck) were diluted to a final concentration of 24 mM and 193 mM respectively in 1 L double distilled water.

Tris-buffered saline (TBS):

3.03 g Tris (pH 7.5) and 9 g NaCl was added to final concentrations of 25 mM and 0.9 % (w/v) respectively in 1 L double-distilled water.

1 M Tris pH 6.8 (per litre):

Add 121 g Tris base to 800 ml double-distilled water, adjust the pH to 6.8, and add double distilled water to 1 L, then autoclave.

1 M Tris pH 7.5 (per litre):

Add 121 g Tris base to 800 ml double-distilled water, adjust the pH to 7.5, and add double distilled water to 1 L, then autoclave.

1 M Tris pH 8.0 (per litre):

Add 121 g Tris base to 800 ml double-distilled water, adjust the pH to 8.0, and add double distilled water to 1 L, then autoclave.

1 M Tris pH 8.8 (per litre):

Add 121 g Tris base to 800 ml double-distilled water, adjust the pH to 8.8, and add double distilled water to 1 L, then autoclave.

Trypsin:

Trypsin is made up by adding 0.5 g trypsin powder to 0.2 g EDTA powder, and making up to a total volume of 1 L with PBS buffer. The pH of the solution was adjusted to 7.4 and the solution was filter sterilised.